UCGE Reports

Number 20386

Department of Geomatics Engineering

WiFi-Based Fine Timing Assistance for GPS Acquisition

by

Mahsa Shafiee

September 2013

UNIVERSITY OF CALGARY

WiFi-based Fine Timing Assistance for GPS Acquisition

by

Mahsa Shafiee

A THESIS

SUBMITTED TO THE FACULTY OF GRADUATE STUDIES

IN PARTIAL FULFILMENT OF THE REQUIREMENTS FOR THE

DEGREE OF DOCTOR OF PHILOSOPHY

DEPARTMENT OF GEOMATICS ENGINEERING

CALGARY, ALBERTA

SEPTEMBER, 2013

Abstract

Emerging applications of location-based services have led to a growing interest in the use of positioning systems. Performance of the satellite-based GPS as the most popular positioning technique is degraded in indoor and urban environments due to visibility limits and multipath fading. Due to ever-growing coverage of WLAN networks, especially in indoor and metropolitan areas, integrating Wi-Fi and GPS has drawn attention, in academic research and industry, as a promising approach to solving problems encountered by precise indoor GPS positioning such as severe multipath.

This thesis investigates effective methods to integrate 802.11g WLAN signals with GPS in order to develop a seamless and robust positioning system especially in indoor environments. Towards this goal, the research presented in this thesis is first focused on the integration of WiFi and GPS in a context-aware framework for navigation filter adaption. A new two-layer multiple model adaptive estimation (MMAE) Kalman filtering algorithm is proposed where the parameters are adapted based on identified contexts using WiFi signals. The performance of the algorithm is assessed using real data to demonstrate positioning accuracy improvements. Secondly, this thesis investigates WiFi and GPS integration at the receiver level. To this end, a collaborative WiFi-based A-GPS scheme is proposed where 802.11g OFDM signals are used to provide fine time assistance for a reduced search space and a faster acquisition in challenging environments. The proposed scheme is primarily developed and tested for a controlled LOS environment using low complexity time domain OFDM timing techniques. The performance of the developed structure is subsequently evaluated in NLOS multipath environments. In order to improve the timing accuracy and robustness of the system in indoor multipath environments, an OFDM timing

estimation method is proposed based on constrained Gaussian mixture modeling of the correlator output. The algorithm is tested for different multipath environments and the results demonstrate considerable performance improvements in terms of timing accuracy. It is shown that using the proposed timing method, the system is able to maintain its robustness in multipath environments under non-dominant direct path condition and for low SNR values.

Acknowledgements

I wish to express my sincere gratitude to my supervisor, Professor Gérard Lachapelle, for all his invaluable guidance, encouragement and continuous support during my PhD studies and research. I would like to thank him for all the things that I have learned from him and for all his precious advice and insights towards my academic and professional growth. I would also like to acknowledge his honesty, positive attitude and sharing his vast knowledge and experience all along the way.

I would like to express my deep appreciation to my co-supervisor, Professor Kyle O'Keefe as well. I would like to thank him for all the guidance and support, all the insightful discussions throughout my research and for everything I have learned from him. Working with him has always been a very pleasurable experience for me; thanks to his talent of simplifying the seemingly complicated material and his ability of keeping perfect balance between freedom and flexibility in research on one side, and giving motivations and directions when it was most needed, on the other side.

I would also like to acknowledge my friends and colleagues in the Position, Location And Navigation (PLAN) group for their help and instructive discussions. Special thanks to Dr. James Curran, Dr. Aiden Morrison, Anup Dhital, Billy Chan, Bernhard Aumayer, Srinivas Bhaskar, Mohammad Mozaffari, Dr. Fatemeh Ghafoori, Erin Kahr and Bo Li. I also thank all my wonderful UofC friends (either from inside or outside of the PLAN group), for all the fun and memorable times we shared together.

Finally, my thanks to my parents are beyond words for their endless love and support. I would specially like to thank them and my lovely sister for all their encouragement, patience and understanding along the way.

Dedication

To my parents Mojgan and Nasrollah

Table of Contents

List of Tables

List of Figures and Illustrations

List of Symbols

Symbol	Definition
D	OFDM data vector
U	Transmitted OFDM data block
M	Total number of OFDM blocks
$h(t)$	Channel impulse response
$\upsilon(t)$	Noise
$y(t)$	Received OFDM signal
ε	Frequency Offset Error
$\tau(t)$	Propagation delay
$\alpha(t)$	Attenuation factor
σ	Signal standard deviation
$I_0(.)$	Zero order modified Bessel function
f_s	Sampling frequency
τ_{rms}	RMS delay spread
σ_v	Standard deviation of noise
$\mathrm{R}(\tau, \mathrm{F}_d)$	Cross-ambiguity function
$r(t)$	Received GPS signal
$\eta(t)$	GPS Antenna noise
d	Navigation message
c	PRN code
f_d	Doppler frequency
f_{IF}	IF frequency
φ	Carrier phase
C	Received power
e_{true}, e_{est}	Line-of-sight unit vector
H_{Error}	Horizontal error
V_{Error}	Vertical error
El	Elevation angle
x_k	State vector
z_k	Measurement vector
H	Design matrix
P	Covariance matrix of estimation error
v_k	Innovation Sequence
R_k	Covariance matrix of observations
Q_k	Process noise matrix
$\Phi_{k,k+1}$	Transition matrix
$\mathbf{C}_{\mathbf{v_k}}$	Covariance matrix of innovation sequence
bel	Belief function

P_{corr}	Probability of correct decision
T_{GPS}	GPS time
$T_{GPS}^{'}$	Estimated GPS time
$\partial t_{WiFi/GPS}$	Time offset between WiFi and GPS
∂t_{WiFi}	Time offset between WiFi users
$A[\delta]$	Correlation sequence
$B[\delta]$	Received energy sequence
δ	Sample delay
L	CP length
N	OFDM data block length
$\Lambda(\delta, \varepsilon)$	Log likelihood function
$f(.)$	Probability density function
$\boldsymbol{F}$	Fisher information matrix
$s(t)$	Pulse shape
α_p	Attenuation factor
μ_p	Mean of Gaussian function
$\sum_p$	Width of Gaussian function
ω_p	Weight of Gaussian function

List of Abbreviations

Symbol	Definition
ACK	Acknowledge
A-GPS	Assisted GPS
AM	Amplitude Modulation
AOA	Angle Of Arrival
AP	Access Point
AWGN	Additive White Gaussian Noise
BER	Bit Error Rate
BPSK	Binary Phase Shift Keying
CAF	Cross-Ambiguity Function
CCK	Complementary Code Keying
CDMA	Code Division Multiple Access
CF-End	Contention Free End
CI	Cell Identity
CP	Cyclic Prefix
CRC	Cyclic redundancy code
CRLB	Cramer-Rao Lower Bound
CTS	Clear to send
DDP	Dominant Direct Path
DP	Direct Path
DS	Distribution System
DSM	Downhill Simplex Method
DSSS	Direct Sequence Spread Spectrum
DST	Dempster-Shafer Theory
EGPRS	Enhanced General Packet Radio Service
EM	Expectation Maximization
EPRS	Enhanced Packet Radio Service
FCC	Federal Communications Commission
FCS	Forward check sequence
FFT	Fast Fourier Transform
FHSS	Frequency Hopping Spread Spectrum
FM	Frequency Modulated
GI	Guard Interval
GLRT	General Likelihood Ratio Test
GM	Gaussian Mixture
GNSS	Global Navigation Satellite System
GPS	Global Positioning System
GSM	Global System for Mobile communication
IAE	Innovation-based Adaptive Estimation
ICI	Inter Carrier Interference
IDFT	Inverse Discrete Fourier Transform
IF	Intermediate Frequency
IFFT	Inverse Fast Fourier Transform
IMM	Individual Model Method

IMU	Inertial Measurement Unit
INS	Inertial Navigation System
ISI	Inter Symbol Interference
KF	Kalman Filter
LOS	Line Of Sight
LTS	Long Training Sequence
MA	Moving Average
MAC	Medium Access Control
MDP	Markov Decision Process
MIMO	Multiple-Input Multiple-Output)
ML	Maximum Likelihood
MMAE	Multiple Model Adaptive Estimation
MPDU	MAC protocol data unit
MS	Mobile Station
NDDP	Non-Dominant Direct Path
NLOS	Non Line Of Sight
OFDM	Orthogonal Frequency Division Multiplexing
OSI	Open System Interconnection
PLCP	Physical layer convergence protocol
PPDU	PLCP protocol data unit
PRN	Pseudo Random Noise
PS-Poll	Power Save Poll
ROC	Receiver Operating Characteristics
RSS	Received Signal Strength
RSSI	Received Signal Strength Indicaion
RTLS	Real Time Location Systems
RTS	Request to send
RTT	Round Trip Time
RWP	Random Walk Position
RWV	Random Walk Velocity
Rx	Receiver
SISO	Single-Input Single-Output)
SNR	Signal to Noise Ratio
STS	Short Training Sequence
S-V	Saleh-Valenzuela
TDMA	Time Division Multiple Access
TDOA	Time Difference Of Arrival
TOA	Time Of Arrival
TTFF	Time To First Fix
UDP	Undetected Direct Path
WCDMA	Wideband Code Division Multiple Access
WLAN	Wireless Local Area Network
WPS	Wireless Positioning System

CHAPTER 1: INTRODUCTION

Emerging location-based applications, ranging from E911 emergency services to vehicle navigation, network optimization and advertisement, require the use of positioning systems. A leading wireless positioning technology, the Global Positioning System (GPS) is a satellite-based navigation system that provides instantaneous three-dimensional position, velocity and precise time information worldwide. However, the position accuracy is limited by several error sources and varies from centimetre to metre level depending on the conditions (Conley et al 1996, Lachapelle 2010, Misra & Enge 2011). The performance of GPS is degraded in urban and indoor environments due to poor geometry, weak satellite signal reception, fading and severe multipath conditions (Parkinson et al 1996, Braasch 1996, Mora-Castro et al 1998). This limits the availability and accuracy of GPS solution especially in indoor environments (Misra et al 2006). Thus, using other positioning systems and signals of opportunity in environments with poor GPS signals in order to provide a seamless localization service has drawn attention in the literature (Bensky 2008, Pahlavan et al 2010, Eggert 2004, Kim 2006, Zheng & Zhang 2011). In accordance with increasing interest in research, recent industry market studies also report that the substantial demand for indoor positioning is driving growth in investment into indoor positioning systems, which augment or replace Global Navigation Satellite System (GNSS) in challenging environments (Inside GNSS 2013, Andrea Bottino et al 2013).

There are several different categories of non-GPS positioning techniques (e.g. Mautz 2012). As examples of such positioning systems that can provide accurate short-term navigation solutions, Inertial Navigation Systems (Qi & Moore 2002) and Attitude and Heading Reference System (Hayward 1997) can be named. However, such systems have unbounded positioning errors in the absence of coordinate

updates from other information sources such as GPS or other wireless measurements (Sahinoglu et al 2008).

As other alternatives, terrestrial wireless positioning methods can also be used to determine the user location. These methods use radio frequency signals to determine the position of the receiver (Kaveh et al 2000). Examples are the use of broadcast single carrier systems such as Amplitude Modulated (AM) and Frequency Modulated (FM) radio signals, cellular communication systems, or broadcast multicarrier systems for positioning applications (Bensky 2008, Carey 1998, McEllroy 2006).

1.1 Thesis Motivations

Among terrestrial networks, Wireless Local Area Network (WLAN) has drawn a growing attention as an option to estimate the receiver location indoors based on several techniques. Defined by the IEEE 802.11 standards, WLAN is implanted in 2.4, 3.6 and 5 GHz frequency bands. Depending on the protocol, Direct Sequence Spread Spectrum (DSSS), Frequency-Hopping Spread Spectrum (FHSS), or Orthogonal Frequency Division Multiplexing (OFDM) waveform is used as the signaling technique in 802.11 standards. The wide-spread coverage of access points within public and urban areas, particularly in indoor environments, makes WiFi a good candidate as a complementary positioning technology for GPS navigation applications. This has driven the rapid development of WiFi positioning techniques in recent years (Au et al 2013, Pahlavan 2010, Bagosi & Baruch 2011, Addesso et al 2010, Lassab et al 2009, Nuno-Barrau & Paez-Borrallo 2006, Roos et al 2002).

Pattern matching is a popular technique, which is used in two major categories of WiFi positioning methods i.e. RSS (Received Signal Strength)-based and model-based methods. RSS-based methods are

based on collecting a database of observed RSS from available Wi-Fi access points and then applying pattern recognition algorithms to define an unknown position with regard to AP positions. Therefore, these methods require fingerprinting the network coverage and populating the database, which implies additional time and financial cost. Also, since the accuracy of the WiFi access point databases tends to decrease over time, these systems should frequently update the database, which is an expensive process (Pahlavan et al 2010). On the other hand, model-based methods suffer from lack of knowledge for modeling signal propagation especially in indoor environments and under multipath conditions (Leo & Chen 2007, Xiang et al 2004, Hatami & Pahlavan 2006).

Other main WiFi-based positioning methods include TOA, two-way TOA, TDOA and AOA techniques (Bensky 2008, Zekavat & Buehrer 2012), which use different signal characteristics for a position solution. Each has specific advantages and drawbacks. These methods will be discussed in more detail in Chapter 2.

As stand-alone positioning systems, terrestrial wireless networks could not provide the accuracy of GPS (while operating in good signal conditions). Some of these methods also suffer from short range of communication and lack of outdoor coverage. One recent example is the NextNav indoor solution. It was released as a GPS-independent system with the ultimate goal of emerging to become the next generation E911 system (FCC Report 2013). NextNav uses a deployment of an overlay network of wide area beacon transmitters for outdoor/indoor positioning. The broadcast beacons are precisely synchronized, encrypted and sent on a licensed spectrum band and with a broad range. This system shows improved performance in terms of accuracy, however with the cost of deployment of the required infrastructure and the beacon transmitters (CSRIC III Report 2012). The system has a limited coverage

so far and at the time with 15 beacon transmitters are operating within the San Francisco Bay area, California.

This motivates research to investigate approaches to most effectively exploit the advantages of widely-deployed signals of opportunity, such as WiFi, in order to enhance GPS towards robust and accurate positioning performance in challenging environments.

1.2 Related Research and Prior Work

One class of solutions to overcome the problems encountered by GPS in harsh situations is known as hybrid positioning systems. Such systems integrate other methods in order to enhance the availability and robustness of positioning solutions (Papandrea et al 2009). In other words, non-GPS technologies can be employed as augmentation or back-up in GPS-denied environments. Moreover GPS can complete with the other techniques through its high availably and accuracy in outdoor environments and by providing global position and time reference estimates. Depending on the amount of interaction and shared information, this integration can be in a loose or a tight manner. In loose integration, the GNSS solution is merged with the other available solutions to form the final result, while in a tight integration the combination occurs at a deeper level (such as integration of raw observations) and mostly through various filtering techniques.

Different non-GNSS methods can be integrated to GPS towards a hybrid positioning system. INS as a self-contained system with high short-term accuracy has been widely studied in the literature to be integrated with GNSS (El-Sheimy et al 1995, Grejner-Brzezinska et al 1998, Petovello 2003, Shin 2005, Godha 2006). Furthermore many hybrid positioning systems have been developed using terrestrial

wireless networks (Sun et al 2005). Tight integration of GPS and CDMA-based cellular networks has been addressed in Reza (2000) where the hybrid system proves to result in increased accuracy and reduced hardware complexity, memory allocation and computational load. Hyung et al (2003) integrates GPS pseudorange observations with cellular TDOA measurements when the number of visible satellites is not sufficient to achieve a position fix. Also in Ma (2002), adaptive data fusion techniques are used to integrate cellular networks and GPS. As an already deployed cellular-based example, E-GNSS is a loose hybrid architecture to enhance positioning performance by using GSM TDOA techniques when GNSS signals are not available (Samama 2008).

Due to wide indoor deployment of WiFi and its complementary availability to GPS, these two can also be used in an integrated framework as a promising approach to obtain a continuous and robust positioning service (Mok 2006, Singh et al 2004, Cavalieri 2007, Cipriani et al 2010).

Recently several algorithms have been developed and products have been released to integrate WiFi with GPS in a hybrid system. The first commercial application was in real time location systems (RTLS) which is an RSS-based indoor tracking system using WiFi signals and WiFi localization tags are integrated with GPS chipset in a loose manner for a more complete coverage (Pahlavan et al 2010). Wireless Positioning System (WPS) is another system that combines GPS and WiFi for metropolitan positioning coverage (Pahlavan et al 2010).

As an industry product Skyhook released Loki in 2006, which used WiFi signal sniffing for obtaining the MAC address fingerprints of APs. This data was then associated with location estimates provided by GPS for a better accuracy indoors.

Since existing methods are mostly implemented using WiFi RSS for direct integration with GPS in the navigation domain, they still suffer from the drawbacks of fingerprinting and database generation as explained earlier.

With hybrid positioning systems, the integration is mostly performed in the navigation domain to achieve a higher-accuracy and a more robust position estimate. Another approach to enhance performance in challenging environments is to integrate signals of opportunity at the receiver level. As one of these receiver-level solutions to improve GPS performance indoors, assisted GPS (A-GPS) technique rose in the literature and rapidly became commercially available (Carver 2005, Sun et al 2005, Van Diggelen 2009, Goran & Richton 2001).

The basic concept of an A-GPS system is to provide assistance information from an external source in order to reduce acquisition time and improve positioning performance in difficult environments. Assistance information mainly includes approximate user receiver position, almanac and ephemeris data, frequency aiding and also time assistance i.e. coarse-time assistance (with poorer than a millisecond timing accuracy) and fine-time assistance (with accuracy of better than a millisecond). Furthermore, navigation data bit assistance can also be used to allow for faster time to first fix and increased coherent integration times exceeding the length of a navigation data bit.

There are two common approaches towards A-GPS acquisition, namely Mobile Station (MS)-Assisted and Mobile Station (MS)-Based approaches. In MS-assisted GPS the receiver acquires signals from satellites in view and sends the measurements to the server to compute the receiver position. In MS-based GPS acquisition, the acquisition and positioning are both performed in the receiver (Van Diggelen

2009). Previous work in A-GPS has typically focused on obtaining assistance data via cell phone networks; A-GPS systems using cellular networks have already been deployed in industry (Zandbergen 2009, Carver 2005, Van Diggelen 2009).

Precise timing is available in CDMA-based cellular A-GPS systems due to the protocol in use and synchronous nodes. The TIA/IS-801-1 standard has been developed for A-GPS messaging between the users in such systems.

Duffet & Hansen (2005) proposed to provide precise time information as assistance data in an asynchronous communication network such as a Global System for Mobile communication (GSM) or a Wideband Code Division Multiple Access (WCDMA) network. However, a fixed GPS station is used to provide the precise timing information while relative timing of the received signals is just used to approximate the user position. This provides a network synchronization map in order to use the precise timing from the fixed GPS reference in shielded areas. The above authors also discussed the accurate time assistance with microsecond level accuracy using GSM mobile synchronization.

Carlson & Koorapaty (2006) employ the Enhanced Packet Radio Service (EPRS) to provide assistance information over GSM and Time Division Multiple Access (TDMA) cell phone systems via a packet control channel. The method includes performing the position fixed based on the received assistance data.

Although research has been dedicated to accomplish A-GPS systems using assistance information from wireless networks (such as cellular networks), to the best of author's knowledge, no scheme has yet been investigated to use the 802.11 WLAN signal structure to provide complete assistance information. So

far, the use of WiFi networks has been mostly confined to providing position information in assisted GPS acquisition algorithms (Weyn & Schrooyen 2008, Amidi 2010, Bhattacharya 2006).

In Loomis (2007), a radio positioning system is proposed which uses the determined times of arrival at several locations in order to approximate the time and position of the receiver. This information is then used as assistance data for a fast acquisition algorithm in A-GPS. A GPS reference server is used to provide reference time in this scheme and yet the matters of fine-time assistance and coarse-time assistance have not been discussed. In addition, specific considerations for the radio network, which is used to carry out the proposed idea, has not been investigated or suggested by the author.

In Sundaramurthy (2011), the assistance data consists of coarse location, which is determined by IP addresses and WLAN MAC addresses similar to the cell-ID positioning method. However, the work mostly considers implementation of an assisted GPS structure by augmenting the conventional GPS simulators for technology testing purposes. WiFi is used to provide position assistance for implementing A-GPS support.

WiFi signals are also proposed by Monnerat (2007) to be used in a hybrid positioning system in order to accelerate GPS acquisition algorithm. The position of the user receiver, which is approximated by short-range communication systems such as WiFi networks, is used to predict the satellites to be acquired. The WiFi receiver is then synchronized to GPS and signal acquisition is accelerated while moving from indoors to outdoors. However, a cartographic representation of the building should be available in this method in order to determine the satellites that can be acquired by the receiver from where it is located in the building.

Recently Deric (2011) addressed the fine-time assistance using WiFi signals. However, this research assumes that fine-time information is available to a WiFi-enabled device. Thus, the method uses IEEE 802.11v protocol to synchronize WiFi receivers and mostly investigates approaches to communicate assistance data within a cooperative WiFi network in the access layer.

Hence, as mentioned earlier, the ever-growing coverage of WiFi network and its availability in GPS-denied environments in addition to the lack of existing research, result in the need for an in-depth study on possible approaches to integrate WLAN networks and GPS.

1.3 Research Goals and Summary of Contributions

According to the motivations described in the previous section, this research aims to develop an effective WLAN/GPS structure that optimally uses WLAN signals of opportunity in order to improve the performance of existing positioning algorithms, especially in indoor environments.

Possible ways are investigated to develop an integrated structure for WiFi-assisted GPS in order to enhance the availability of position solution and improve the performance in both the position estimates and receiver operation. The integration can be considered in two different domains as follows:

1. *Integration of WiFi with GPS at the position solution level and in the navigation domain*

2. *Integration of WiFi with GPS to assist acquisition at the receiver level & in the signal domain*

Towards the first approach, this research explores different ways that WiFi signals can be used indirectly in the navigation domain. In other words, instead of using Wi-Fi data directly for localization, the information obtained by observing WiFi signals (WiFi features) are used as side information so that

GPS can modify its behavior according to changes in the environment (static/kinematic and indoors/outdoors). The use of external information in a context-aware programming framework to improve GPS positioning performance within the navigation solution is investigated. The performance of the positioning algorithms (Kalman filtering) and the optimality of the Kalman filter are closely related to the a priori knowledge of the model and the process noise and the measurement noise. Insufficient a priori information reduces the precision of estimated states and may even result in the divergence of the filter and in the poor estimation of the weak observable states. As a solution many research reports address the problem of adaptive KF (Mehra 1970, Mohammed & Schwarz 1999, Moreno & Pigazo 2009, Lee et al 2012). In Chapter 3, a new WiFi-based two-layer adaptive extended Kalman filter positioning algorithm is proposed based on multiple model adaptive estimation. Each individual Kalman filter, matched to a different dynamic model, has an IAE (Innovation-based Adaptive Estimation) structure and the external information is used as context to adjust the adaptive parameters based on different situations, i.e. environmental contexts like indoor/outdoor and motion context like static/kinematic. More specifically, the motion contexts are used to weight multiple models while the indoor/outdoor contexts are used to adapt the statistical information through the measurement covariance matrix or the process noise. The weighted sum of all individual estimates is used as the adaptive optimal estimate of the states. Afterward for an enhanced accuracy and robustness of the proposed method, the concept of combining multiple identifiers is addressed as a promising approach to improve the probability of correct context identification. An algorithm based on the Dempster-Shafer theory is proposed to fuse decision sequences of several identifiers, which may or may not use the same source of external information. The algorithm is then modified to deal with high conflict situations and

correlative decisions. Furthermore to improve the robustness of the proposed context-aware algorithm a control block based on finite state Markov Decision Process (MDP) is implemented.

For the second approach, this thesis focuses on the concept of WiFi-based A-GPS for receiver-level integration of WiFi and GPS. A method of WiFi-based A-GPS is proposed by monitoring 802.11g signal characteristics at the physical layer within collaborative users. The proposed system can be deployed in places where WiFi coverage is available and where there is no or limited access to other synchronized systems based on the existing infrastructure. Examples include WiFi-enabled mobile devices deployed on university campuses, hospitals and shopping malls, or tablet computers being used on public WiFi networks.

Considering the parameters of the existing WLAN infrastructures, coarse-time and fine-time estimation techniques are discussed in order to provide acquisition assistance data to the A-GPS structure. Due to the growing popularity of 802.11g/n protocols for implementing next generation WiFi networks, herein the goal is to extract assistance data from OFDM signals. Hence, in order to implement the proposed method, several practical OFDM timing estimation techniques are developed to enable an effective and complete WiFi-based A-GPS. The algorithm is primarily realized and tested in a LOS controlled environment using low-complexity time estimation methods. Correlation-based time domain estimation techniques are then combined for an improved timing accuracy in multipath conditions. Afterwards the system is extended to operate in challenging indoor environments. In order to achieve a more robust performance and improve timing accuracy in challenging NLOS multipath environments with low SNR, novel time estimation algorithms with higher complexity are developed based on channel estimation

techniques. Performance of the developed algorithm is then evaluated in the proposed A-GPS structure and is compared for various environments through the collection of real data.

1.4 Thesis Outline

Chapter 2 provides an overview on the background material. Physical and MAC layer characteristics of WLAN 802.11g standard and OFDM signal structure are reviewed, different WLAN cannel models are introduced and basic 802.11g receiver structure is described. Then this chapter provides an overview on the existing indoor positioning methods based on WLAN 802.11g. Afterwards, GPS signal characteristics and acquisition are explained and A-GPS schemes and different kinds of assistance data are introduced and discussed.

Chapter 3 presents WiFi/GPS integration in a context-aware framework. First the concept of adaptive filtering for navigation is introduced. Then the structure of the proposed algorithm is described and the performance of the proposed algorithm is analyzed using real data. The problem of context identification based on WiFi signals is then discussed and the structure of the DST-based decision fusion block and MDP control block are explained. Finally, the performance of the proposed algorithm replacing the bank of Kalman filters with a single constraint-based Kalman filter is analyzed and conclusions and suggestions for further development are proposed.

Chapter 4 focuses on receiver-level integration of WiFi and GPS and describes the basic system model of the proposed collaborative WiFi-based A-GPS system. In order to develop the proposed method, several practical time-domain correlation-based methods are presented to estimate the time offset between users with microsecond accuracy. The system is implemented and the performance is tested

primarily in controlled LOS environments. Then the performance of low-complexity correlation-based timing methods is analyzed under different multipath conditions and an algorithm is introduced for time offset estimation in multipath indoor environments. Finally, performance of the proposed method is evaluated using real data and the results are presented and compared to existing A-GPS solutions. Results lead to the next chapter where novel timing methods are developed to achieve higher accuracy and a more robust performance in NLOS multipath environments under low SNR condition.

Chapter 5 aims to improve the performance of the proposed method in terms of robustness and accuracy under NLOS multipath condition. To this end, novel OFDM timing algorithms are developed and the performance is theoretically analyzed and also tested in real world situations. The performance of the proposed WiFi-based A-GPS method is then evaluated in several challenging environments using the new timing algorithms and the results are compared to the ones achieved by low-complexity correlation-based methods.

Chapter 6 summarizes the thesis and draw conclusions from the work presented in earlier chapters.

Contributions

The work described in this thesis has been presented and published in the following papers:

Shafiee M., K. O'Keefe, G. Lachapelle (2013), "Symbol Timing Acquisition for Collaborative OFDM WLAN-based A-GPS", International Journal of Wireless Information Networks (IJWIN), July 2013, DOI 10.1007/s10776-013-0214-8, http://link.springer.com/article/10.1007/s10776-013-0214-8

Shafiee M., K. O'Keefe, G. Lachapelle (2012), "OFDM Symbol Timing Acquisition for Collaborative WLAN-based Assisted GPS in Weak Signal Environments", ION GNSS 2012, September 19-22, Nashville, Tennessee, USA, 13 pages.

Shafiee M., K. O'Keefe, G. Lachapelle (2011), "Context-aware Adaptive Extended Kalman Filtering Using Wi-Fi Signals for GPS Navigation", ION GNSS 2011, September 20-23, Portland, OR, USA, 14 pages.

CHAPTER 2: BACKGROUND

2.1 Overview on WLAN IEEE 802.11g standard

WiFi is a trade name for devices using the IEEE 802.11 standard for wireless communication. The 802.11 wireless local area network (WLAN) physical and medium access control layers were originally established in June 1997. The original data rates were 1 Mbps and 2 Mbps using frequency hopping spread spectrum (FHSS) and direct sequence spread spectrum (DSSS) techniques (IEEE 802.11b 1999). The data rates rose to 5.5 Mbps and 11 Mbps with introduction of IEEE Standard 802.11b in 1999. This standard uses DSSS and complementary code keying (CCK) and is compatible with earlier versions. IEEE Standard 802.11a was also approved in 1999, as a high speed protocol for unlicensed national information infrastructure bands at 5 GHz. Using the Orthogonal Frequency Division Multiplexing (OFDM) technique the 802.11a version supports data rates up to 54 Mbps (IEEE 802.11a 1999). IEEE Standard 802.11g evolved as an extension of WLAN standard in June 2003 to provide high data rates (up to 54 Mbps) in the 2.4 GHz band by using OFDM. 802.11 MAC (Medium Access Control) and Physical layers are shown in the Open System Interconnection (OSI) reference model in Figure 2.1. OSI is a conceptual model for characterization and standardization of connections between internal functions within a communication system, where these functions are represented as different layers (ISO/IEC standard 1994).

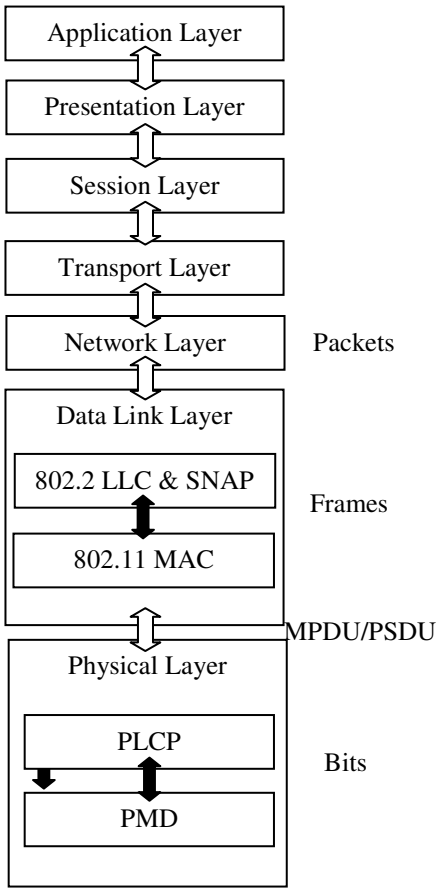

Figure 2.1: 802.11 MAC and Physical layers in OSI model

2.1.1 Frame Structure

The output frame from medium access control layer is called the MAC protocol data unit (MPDU) and arrives as the input data at the physical layer as the physical layer convergence protocol (PLCP). MDPU contains the header information and 32 bit cyclic redundancy code (CRC) as forward check sequence (FCS) and, to support infrared transmissions within the protocol, has a maximum length of 2346 bytes. This consists of a maximum of 2312 bytes of data as the frame body, 30 bytes of header and 4 bytes of CRC. Figure 2.2 shows the 802.11g frame formation through the MAC and Physical layers and Figure 2.3 shows the MDPU frame format.

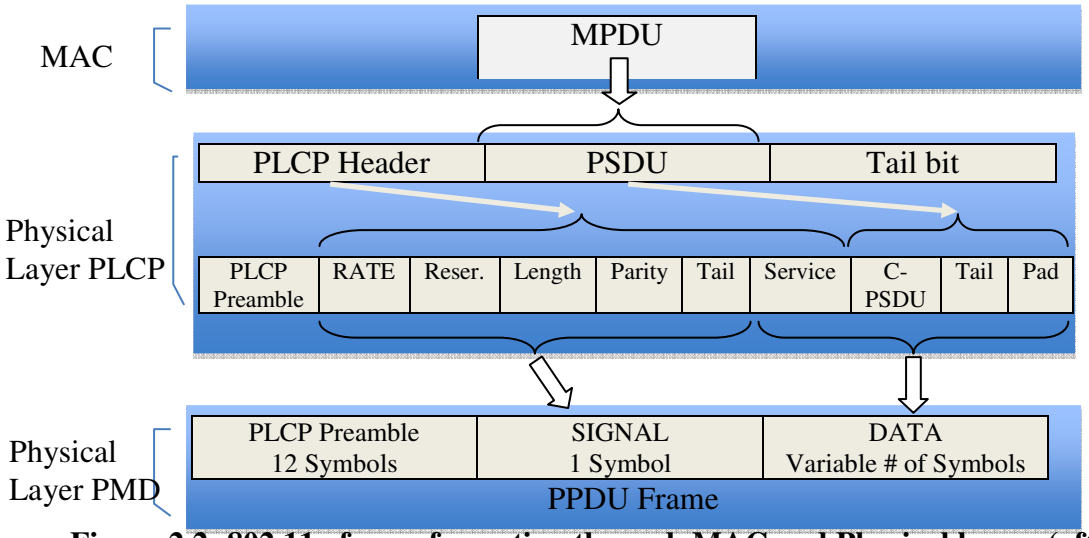

Figure 2.2: 802.11g frame formation through MAC and Physical layers (after IEEE 802.11g standard 2003)

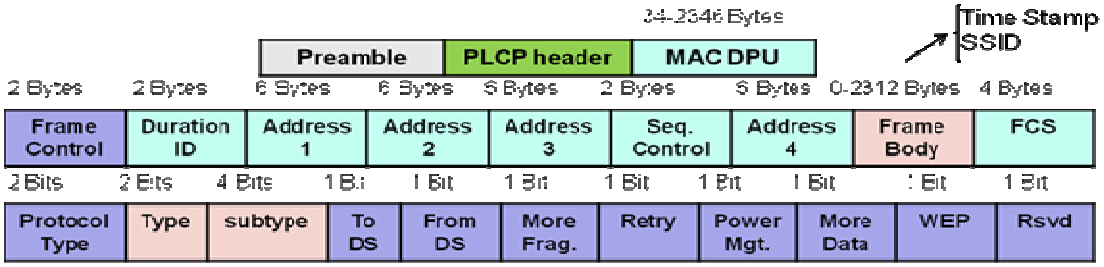

Figure 2.3: 802.11 MDPU frame format (after IEEE 80211g standard 2003)

Frame control specifies the version of the protocol used along with the type of the frame transmitted. The fields To DS and From DS within the Frame Control indicate whether the transmission is designated for Distribution System or is from Distribution System. Duration ID carries information on the duration the medium is expected to remain busy. Address fields contain destination MAC address, source MAC address, also BSSID for a specific transmission. Sequence Control includes sequence number and fragment number and FCS is the frame check sequence.

In the IEEE 802.11g standard, there are three types of frames, namely data, management and control. The type of frame is defined by the Type and Subtype fields within the Frame Control part in MDPU. Management frames are used to define authentication, association and privacy of the system, control frames contain delivery specifications such as information on the protocol used, the type of frame, number of data fragments and duration of the transmitted data. There are six types of control frames among which the most important ones are RTS (request to send), CTS (clear to send) and ACK (acknowledge) frames. The other three are Power Save Poll (PS-Poll), Contention Free End (CF-End) and CF-End plus ACK (CF-End Ack). RTS and CTS control frames are sent for coordination between the nodes in a specific service set. In 802.11, medium access is controlled by the carrier sensing multiple access with collision avoidance (CSMA/CA) algorithm through the exchange of RTS and CTS frames among the nodes within a service set. RTS and CTS frames carry information on the required duration of channel reservation for transmitting the data by a node and receiving the ACK (acknowledge) frame. As such, all the other nodes within the range of a specific transmission (any node that is able to hear the RTS sent by the transmitter or CTS sent by the receiver) will back off while the media is reserved in order to avoid collision between packets.

Management frames allow the nodes to establish and maintain communication within a service set. Common management frames include beacon frames, probe request and response frames, authentication frames, de-authentication frames, association request and response frames, re-association request and response frames and de-association request and response frames. When a station requests to join a service set, by exchanging the management frames, it goes through the association process to be associated to an AP in the range and authentication process where a node is identified as an AP.

Beacon frames are a sub-type of management frame identified by a Type value of 00 and Subtype value of 1000 that carry network management and synchronization information such as supported rates and security settings. The 802.11g standard requires all the access points to periodically transmit beacon frames with a default interval of 102.4 ms between transmissions. The beacon frame fields are shown in Figure 2.4.

Frame Control	Duration ID	Addr 1	Addr 2	Addr 3	Sequence Control	Addr 4	Frame Body	FCS

Timestamp	Beacon Interval	Capability Info	SSID	Supported Rates	FH Parameters	DS Parameters	CF Parameters	IBSS Parameters	TIM

Figure 2.4: 802.11g Beacon frame fields

The Frame Body field of a beacon frame contains a timestamp field. The timestamp indicates the time at which the frame is transmitted, as established by the access point's clock, with microsecond precision. Thus, by passive scanning of the beacon frames transmitted by the AP and decoding the timestamp, microsecond-level timing can be estimated and achieved at WiFi receivers. This can then be used to resolve the ambiguities between the WiFi symbols received by different users from one access point (as described in Section 4.1).

2.1.2 Physical Layer Signal Structure

The IEEE 802.11g standard uses Orthogonal Frequency Division Multiplexing (OFDM) over the frequency band of 2.401 GHz to 2.495 GHz. Overall, 14 channels are defined in the 802.11g spectrum but not all the channels are used in every country. As an example, in North America mostly three non-overlapping channels 1, 6 and 11 are used (Figure 2.5).

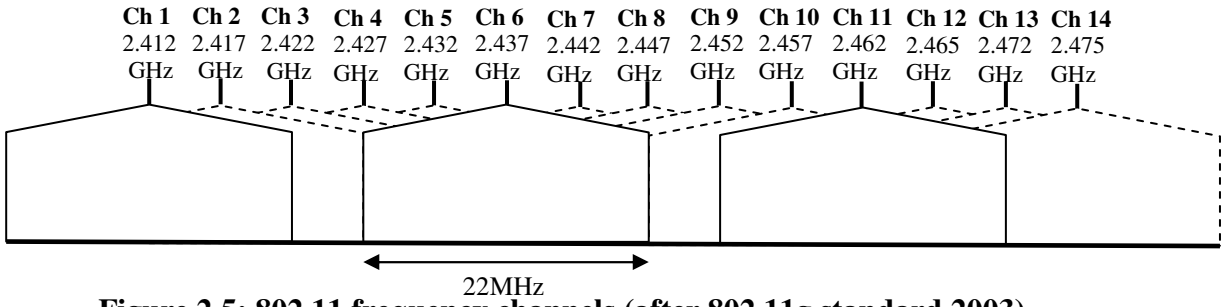

Figure 2.5: 802.11 frequency channels (after 802.11g standard 2003)

OFDM is a multi-carrier parallel communication technique, which allows for high data rates and reduces the transmission bandwidth by using orthogonal sub-carriers. Orthogonality of the sub-channels eliminates the effects of Inter Carrier Interference (ICI) and allows for improved spectral efficiency. However, in real OFDM implementations there are several factors that lead to loss in orthogonality and thus create ICI. Furthermore, by using a time-domain guard interval, OFDM will be resistant to Inter Symbol Interference (ISI) effects caused by multipath delay spread. By making the guard interval a cyclic extension of the OFDM symbol, ICI can also be avoided. IEEE 802.11g uses OFDM with a Cyclic Prefix (CP) of length 16 (Figure 2.6). This means that the last 16 samples of an OFDM data symbol are copied to the beginning of the same symbol as a guard interval to reduce ISI. If the length of CP is more than the length of channel impulse response or multipath delay spread, ISI can be eliminated. CPs also introduce correlation and redundancy into transmitted OFDM symbols which can be used for fine symbol start time estimation purposes.

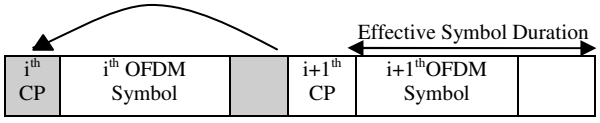

Figure 2.6: Cyclic Prefix (CP) in 802.11g signaling

OFDM transmission is more sensitive to carrier frequency offset, oscillator phase noise and sampling clock mismatch in comparison to single carrier techniques. To combat this problem, pilot subcarrier symbols and known training sequences are incorporated in the transmitted OFDM symbols, which allow for estimation and correction of carrier frequency and clock offsets.

Basically, in OFDM the data stream is divided into several parallel streams and then modulated onto individual orthogonal subcarriers. Then all the orthogonal subcarriers are transmitted simultaneously. Figure 2.7 demonstrates a basic block diagram of OFDM modulation.

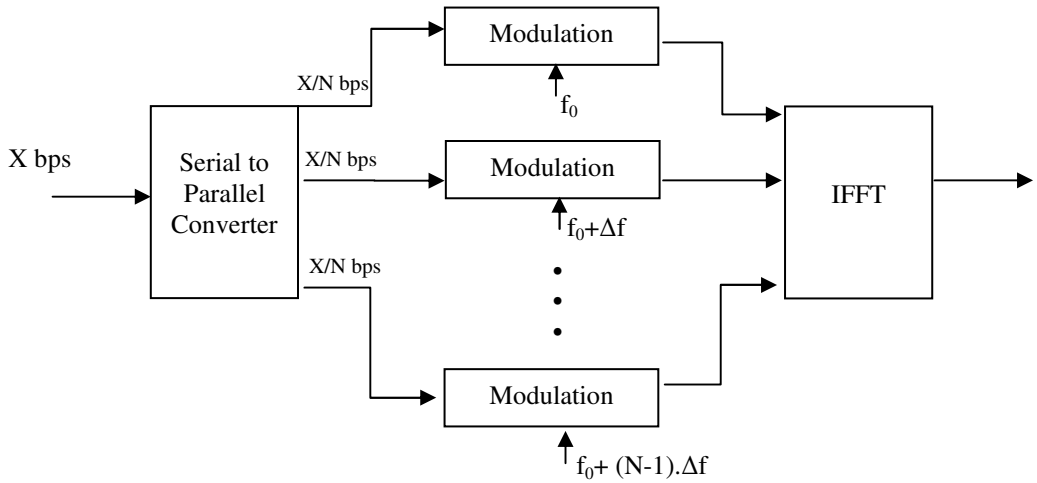

Figure 2.7: Basic block diagram of OFDM modulation

The transmitted baseband OFDM signal can be represented in the continuous and discrete time domains respectively as follows (Goldsmith 2005):

$$u_i(t) = \sum_{i=0}^{\infty} \sum_{k=0}^{N-1} d_i[k] e^{2\pi f_k (t-iT)} \tag{2.1}$$

$$u_i[n] = \sum_{k=0}^{N-1} d_i[k] e^{j2\pi kn/N} \qquad n = 0,1,2,...,N-1 \tag{2.2}$$

where $D_i = \{d_i[0] d_i[1] \ldots d_i[N-1]\}$ is the i^{th} data vector and d represent data samples. $U_i = \{u_i[0] u_i[1] \ldots u_i[N-1]\}$ is the i^{th} OFDM data block and by appending CP samples of length L, extends to $U_{i\_CP} = \{u_i[N-L] \ldots u_i[N-1] u_i[0] u_i[1] \ldots u_i[N-1]\}$.

As shown in Equation 2.2, the transmitted OFDM signal can be considered as the Inverse Discrete Fourier Transform (IDFT) of the modulated data symbols. The discrete time base-band complex transmitted signal can then be represented by $\{U_{1\_CP} U_{2\_CP} \ldots U_{M\_CP}\}$, where M is the total number of OFDM blocks transmitted. Assuming a channel impulse response of $h_i(t)$, the i^{th} continuous-time received signal can be written as

$$y_i(t) = u_{i\_CP}(t) * h_i(t) + \upsilon_i(t) \tag{2.3}$$

where $\upsilon_i(t)$ is additive white Gaussian noise. Thus, the corresponding discrete form of the received symbol is given as

$$y_i[n] = u_i[n] * h_i[n] + \upsilon[n] = \sum_{m=0}^{\infty} h_i[m] u_i[n-m] + \upsilon[n] \tag{2.4}$$

By assuming a flat fading channel, the discrete time complex baseband received signal for a single path and frequency offset error of ε can be written as

$$y[n] = u[n] \exp[j 2\pi \varepsilon n] + \upsilon[n] \tag{2.5}$$

As can also be seen in Equation 2.1, for subcarriers to be orthogonal, the minimum required spacing is $1/T$ where T is the symbol duration. In other words the distance between two adjacent subcarriers should be an integer multiple of the inverse of the OFDM symbol duration. The spectral peak of each carrier then coincides with the spectral zero crossings of all the other subcarriers. Figure 2.8 shows the concept

of orthogonality for five subcarriers. A typical schematic view of the 802.11 OFDM transmitter is shown in Figure 2.9.

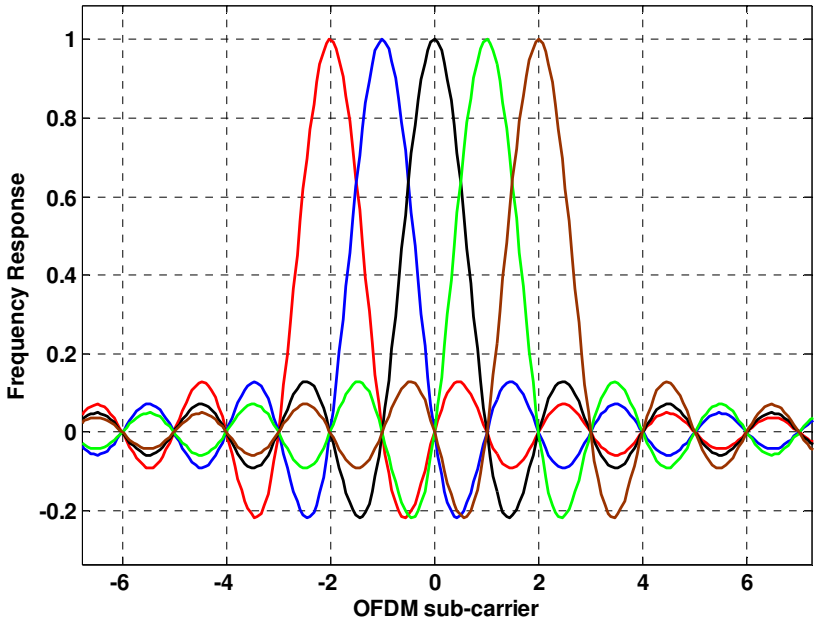

Figure 2.8: OFDM orthogonality concept for five subcarriers

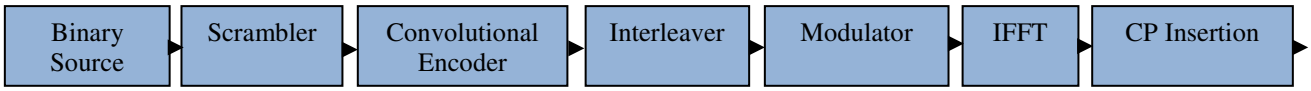

Figure 2.9: Basic blocks in an OFDM transmitter

The input data to the transmitter is the PLCP protocol data (PPDU) packet, which is the PLCP along with a preamble, header, tail bits and pad bits as shown in Figure 2.2. The preamble field consists of two parts, namely the Short Training Sequence (STS) and the Long training Sequence (LTS) with a total length of 16 μs. The 10 short training symbols are modulated with the elements of a known sequence using 12 subcarriers, while two long training symbols, consisting of 52 subcarriers, are also modulated with an a priori known sequence (IEEE standard 802.11g 2003). For generating the STS, the 12 subcarriers are modulated by the elements of a normalized known sequence as given below:

$$STS\_Seq = \sqrt{\frac{13}{6}}\{0,0,1+j,0,0,0,-1-j,0,0,0,1+j,0,0,0,-1-\mathrm{j},0,0,0,-1-\mathrm{j},$$
$$0,0,0,1+j,0,0,0,0,0,0,0,-1-\mathrm{j},0,0,0,-1-j,0,0,0,1+j,0,0,0,1+j,0,0,0 \quad (2.6)$$
$$1+j,0,0,0,1+j,0,0\}$$

The LTS known sequence is:

$$\text{LTS\_Seq}=\{1,1,\ -1,\ -1,1,1,\ -1,1,\ -1,1,1,1,1,1,1,1,\ -1,\ -1,1,1,\ -1,1,\ -1,1,1,1,1,1,0,$$
$$1,\ -1,\ -1,1,1,\ -1,1,\ -1,1,\ -1,\ -1,\ -1,\ -1,\ -1,1,1,\ -1,\ -1,1,\ -1,1,\ -1,1,1,1,1\}. \quad (2.7)$$

The STS and LTS are used for packet detection and synchronization applications and to estimate the time and frequency offsets between a WiFi receiver and transmitter (Bhattacharya 2006). The header field contains transmission specifications such as rate of PSDU, length of PSDU and initialization bits. The header is then followed by the data field, which includes a service field for data scrambler initialization, the PSDU, six tail bits for resetting the convolutional encoder and finally the pad bits. The number of pad bits is selected such that the total length of the packet is an integer multiple of required coded bits for each OFDM symbol i.e. 48 samples. The header is modulated using the BPSK (binary phase-shift keying) with code rate of 1/2. The code rate for transmitting data samples depends on the modulation used and the data rate and can be found in Table 2.1.

Table 2.1: 802.11g code rates

Data Rate (Mb/s)	Modulation	Code Rate	Coded bits per OFDM symbol
6	BPSK	½	48
9	BPSK	¾	48
12	QPSK	½	96
18	QPSK	¾	96
24	16-QAM	½	192
36	16-QAM	¾	192
48	64-QAM	2/3	288
54	64-QAM	¾	288

The PSDU packet with the service field is encoded using a convolutional encoder with length seven and rate 1/2. Other coding rates can be generated using a puncturing procedure. Puncturing is the process of deleting some of the coded bits while keeping the code dimension (number of data bits) fixed and thus results in an increased code rate. Afterwards, the coded data passes through a two-stage block interleaver for a more robust performance in the presence of channel noise bursts. The data is interleaved by mapping the adjacent coded bits into non-adjacent subcarriers and then, mapping the coded bits into less and more significant bits of the modulation constellation (i.e. in the two-dimensional scatter representation of the signal in the complex plane at sampling time instants). The second mapping step randomizes the distance between the symbols and is obviously only performed for modulations schemes with a constellation size of more than two bits. The constellation mapping uses the Gray-coding standard and is normalized to maintain the same average power for all mappings.

After the mapping procedure, data bits are divided into groups of 48 samples and along with four pilot symbols pass through the IFFT block with a common size 64 (i.e. the first power of two above 52). Finally the CP is added to the output OFDM symbols from the IFFT block. Windowing and wave shaping is performed for a better performance and the data is transmitted through the media.

Figure 2.10 shows the basic structure of the 802.11g OFDM signal and its Physical Layer Convergence Protocol (PLCP) preamble (IEEE standard 802.11g 2003).

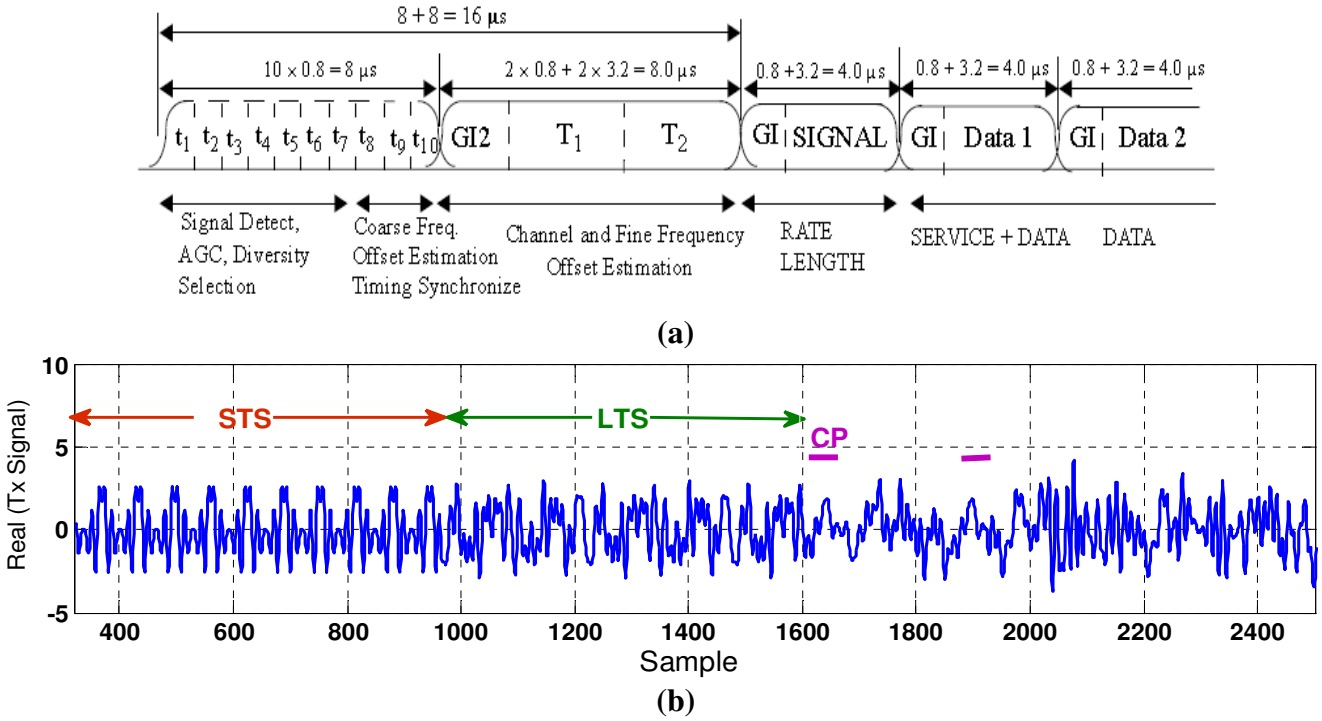

Figure 2.10: (a) IEEE 802.11g OFDM Signal Structure (from IEEE standard 802.11g 2003) (b) 802.11g transmitted signal

2.1.3WLAN Channels Models

Herein we discuss the most common and basic channel models used for 802.11 WLAN communications to model the multipath effects. Generally the channel impulse response of a time-varying wireless channel can be modeled as an FIR filter with independent complex Gaussian taps so that the impulse of the channel at time t can be written as (Goldsmith 2005)

$$h(\tau;t)=\sum_{p=1}^{P}\alpha_p(t)e^{-j2\pi f_c\tau_p(t)}\delta[t-\tau_p(t)] \tag{2.8}$$

where $\alpha_p(t)$is the attenuation factor for path *p* at the time instant *t*, $\tau_p(t)$ is the propagation delay for path *p* at time *t* and *P* is the total number of paths between the receiver and the transmitter.

In WLAN, the channel is generally assumed to have time-invariant properties over the duration of a packet i.e. the channel is assumed to be quasi-stationary. Thus the channel impulse response can be written as

$$h(\tau)=\sum_{p=1}^{P}\alpha_p e^{-j2\pi f_c\tau_p}\delta[t-\tau_p] \tag{2.9}$$

Furthermore, with a large number of reception paths, according to the central limit theorem, the received signal (equivalent low-pass received signal) can be assumed to follow a complex Gaussian distribution. Hence the impulse response of the channel can be assumed to be a complex Gaussian random process along time.

2.1.3.1 Rayleigh Fading Model

In a Rayleigh fading model, the channel impulse response is considered a zero mean complex Gaussian process so the channel envelope at any time instant follows a Rayleigh distribution as follows (Proakis 2001):

$$f_Y(y) = \frac{y}{\sigma^2} e^{-\frac{y^2}{2\sigma^2}} \tag{2.10}$$

with y > 0 and σ is the received signal standard deviation.

The Rayleigh fading channel model implies that there is no direct LOS path between the receiver and the transmitter. This can be considered true, when the relative power delay is significantly lower than the sampling rate and hence the receiver cannot resolve the individual paths. Under a Rayleigh fading channel, the amplitude of the received signal follows a Rayleigh distribution while the phase is considered to be uniformly distributed over the interval [0, 2π]. Furthermore, it should be noted that Rayleigh channel is a frequency non-selective channel model.

In case where there exists a LOS path along with scatter paths due to both fixed and randomly moving objects, the channel is considered to be a Rician fading channel and the envelope follows a Rice distribution as follows (Papoulis 2000):

$$f_Y(y) = \frac{y}{\sigma^2} e^{-\frac{y^2+\zeta^2}{2\sigma^2}} I_0\left(\frac{y\zeta}{\sigma^2}\right) \tag{2.11}$$

where ζ is the bias generated by LOS and fixed scatter paths and $I_0(.)$ is the zero order modified Bessel function.

2.1.3.2. Exponential Channel Model for 802.11

In order to be able compare different WLAN system performances, an exponential model was proposed by the 802.11 task group b as a consistent channel model for the wireless LAN 802.11 standard (Fakatselis 1997). The model is simple to generate and shows good accuracy in real world situations, hence it is an appropriate model especially for performance prediction of WLAN implementations. In this model the average power profile of the channel taps decay exponentially and the taps are zero-mean complex Gaussian distributed random variables:

$$h_i = N(0,\frac{1}{2}\sigma_i^2) + jN(0,\frac{1}{2}\sigma_i^2) \tag{2.12}$$

where $i=1,..,I_{max}$ and $I_{\max} = \lceil 10.f_s.\tau_{rms} \rceil$. σ_i^2 can be expressed as (O'Hara & Patrick 1999):

$$\sigma_i^2 = \frac{1-\beta}{1-\beta^{I_{\max}+1}}\beta^i \tag{2.13}$$

where $\beta = e^{1/f_s\tau_{rms}}$ with f_s and τ_{rms} being the sampling frequency and the RMS delay spread. Delay spread is used as a factor to characterize a multipath channel and represents the difference between the LOS time of arrival and time of arrival of the latest multipath component.

It should be noted that in practical realizations of the channel, the exponential model includes both ISI and flat fading effects.

2.1.3.3 Saleh-Valenzuela Channel Model

The Saleh-Valenzuela (S-V) model has also been proposed for indoor SISO (Single-Input Single-Output) communication links, in multipath environments (Saleh & Valenzuela 1987). Based on extensive experimental channel measurements, the S-V model is proven to be appropriate for modeling indoor multipath channels in SISO 802.11 wireless communications. In this model, multipath is assumed to arrive in multiple clusters including multiple rays where the cluster and ray arrival times are modeled as Poisson processes. In this case the channel impulse response can be given as

$$h(t) = \sum_{m=0}^{\infty} \sum_{n=0}^{\infty} \lambda_{n,m} e^{j\theta_{n,m}} \delta(t - T_m - \tau_{n,m}) \tag{2.14}$$

where $\theta_{n,m}$ is a uniform random variable over [0, 2π] and $\lambda_{n,m}$ follows a Rayleigh distribution:

$$f_{\lambda_{n,m}}(\lambda_{n,m}) = \frac{2\lambda_{n,m}}{\overline{\lambda}^2_{n,m}} e^{-\lambda^2_{n,m} / \overline{\lambda}^2_{n,m}} \tag{2.15}$$

where $\overline{\lambda}^2_{n,m}$ is the average power of the n^{th} ray in the m^{th} cluster.

Figure 2.11 depicts the distribution of ray and cluster arrival times in this model and compares theoretical results to monte-carlo simulation results for channel realizations. A sample generation of the channel impulse response using 1000 random realizations of an S-V channel model is shown in Figure 2.12. The RMS value of the cluster arrival time is 50 ns.

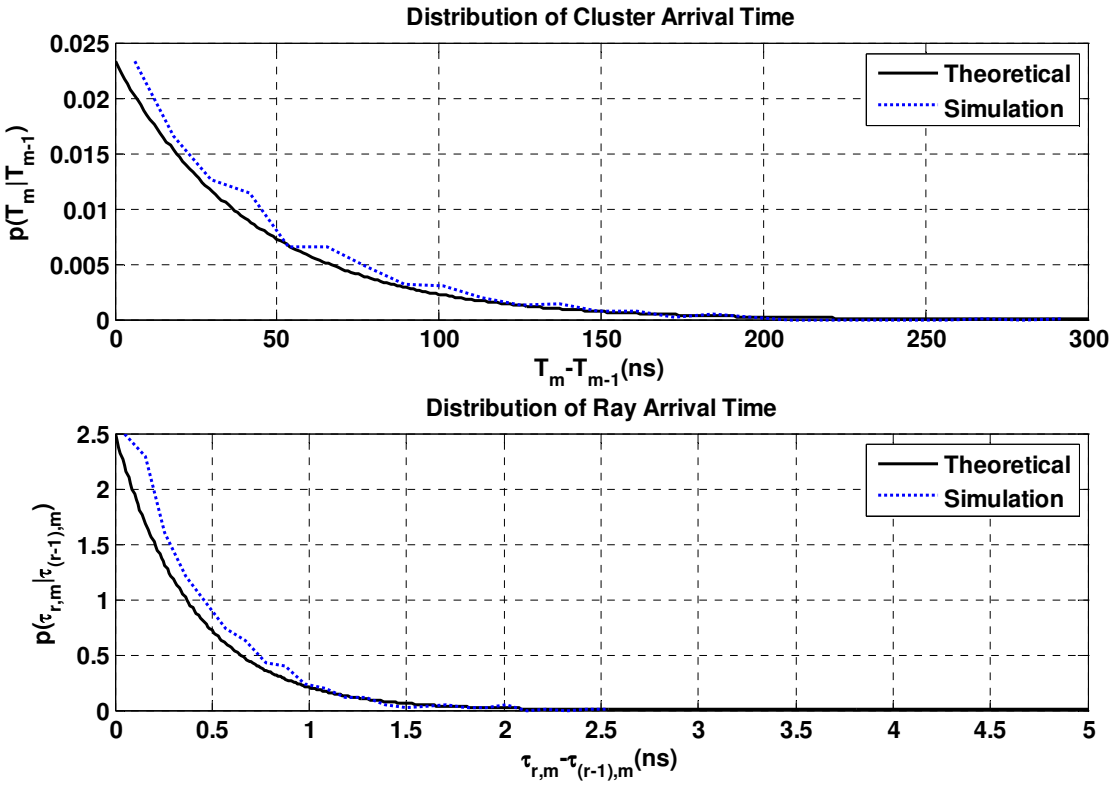

Figure 2.11: Distributions of ray and cluster arrival times in an S-V channel model

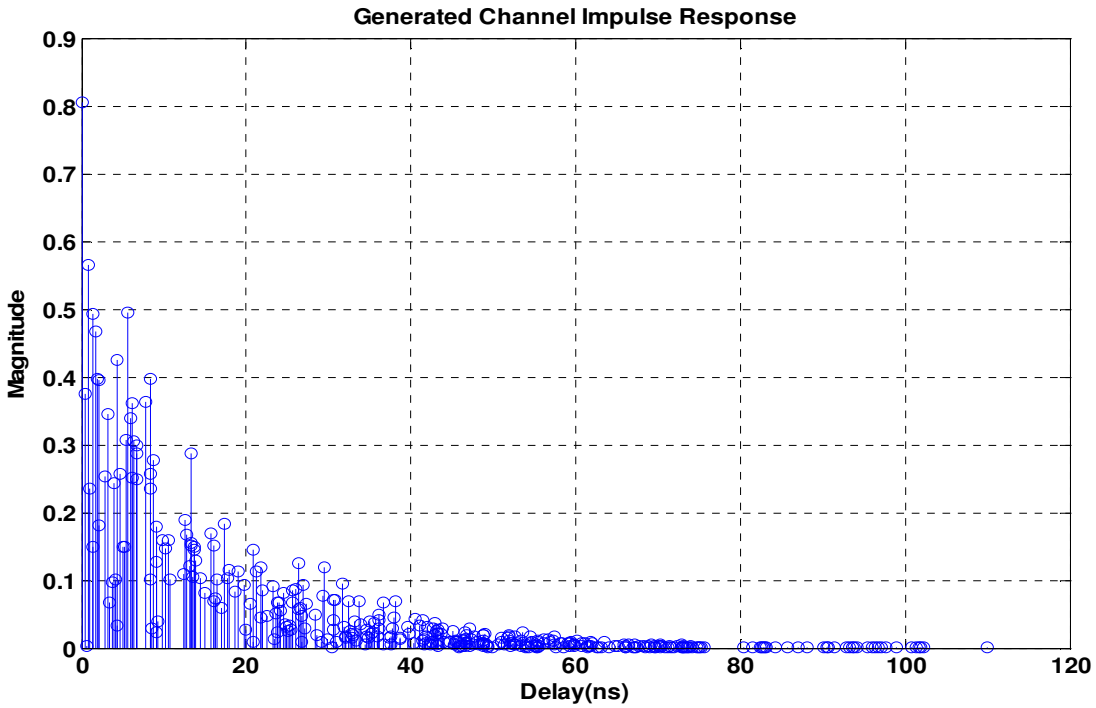

Figure 2.12: A realization of channel impulse response for S-V channel model

2.1.4 802.11g OFDM Receiver Structure

The general structure of a WiFi software receiver to decode IEEE 802.11g signals is shown in Figure 2.13. First, using the 802.11g Short Training Sequence (STS) which consists of 10 repetitions of a 0.8 μs signal, a primary estimate of time and frequency offset is computed using a delay and correlation approach (Dick& Harris 2003). Then the Long Training Sequence (LTS) is used for a higher-accuracy estimation of the time and frequency offset which allows for packet tuning. The estimation technique is based on the correlation of the received LTS with the known LTS signal for 802.11g standard as described in Schmidl & Cox (1997).

After performing frequency and time synchronization on the received signal to estimate and compensate for time and frequency offset, the basic functions of the OFDM receiver are discarding the guard data and Cyclic Prefix (CP), transforming samples into the frequency domain using the FFT block, demodulating the symbols, de-interleaving and finally decoding the signal to extract and recover the original data bits.

Hard-decision demodulation is performed to map the in-phase and quadrature data into the same constellation as used in the transmitter. Equalization and phase rotation are done using the estimated channel frequency response.

After converting the data into binary digits, the samples are de-interleaved using the interleaving matrix of the OFDM transmitter. Here, the maximum distance pattern is used to interleave the samples in the transmitter and the receiver de-interleaver block simply reverses the transmitter interleaver block to reorder the samples.

A soft decision Viterbi decoder block is used to process and decode the convolutionally encoded data. For the 802.11g standard, the default decoder block has a constraint length of 7 and generating polynomials 133 and 171 in octal representation (IEEE 802.11g 2003).

According to the modulation method and code rate used in the transmitter, additional blocks may need to be added to the general structure to de-puncture and de-scramble the data as appropriate (Guffeyet al 2007).

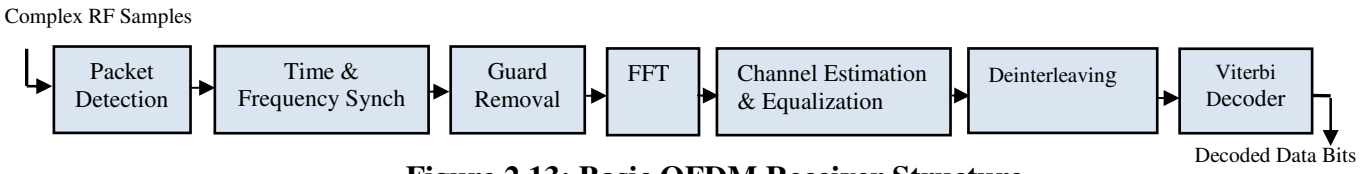

Figure 2.13: Basic OFDM Receiver Structure

Figure 2.14 shows the BER performance of the 802.11g receiver assuming a non-dispersive multipath Rayleigh fading channel with additive white Gaussian noise. A maximum distance pattern is used to interleave the data and the code rate is set to ¼ . The result is compared to the theoretical Bit Error Rate (BER) for 4 fading paths as given below (Proakis 2001):

$$BER_f = \frac{1}{2^P}\left(1-\sqrt{\frac{1}{1+\sigma_v^2}}\right)\sum_{i=0}^{P}\binom{P-1+i}{i}\frac{1}{2^i}\left(1+\sqrt{\frac{1}{1+\sigma_v^2}}\right) \tag{2.16}$$

where P is the number of fading paths and σ_v^2 is the noise variance.

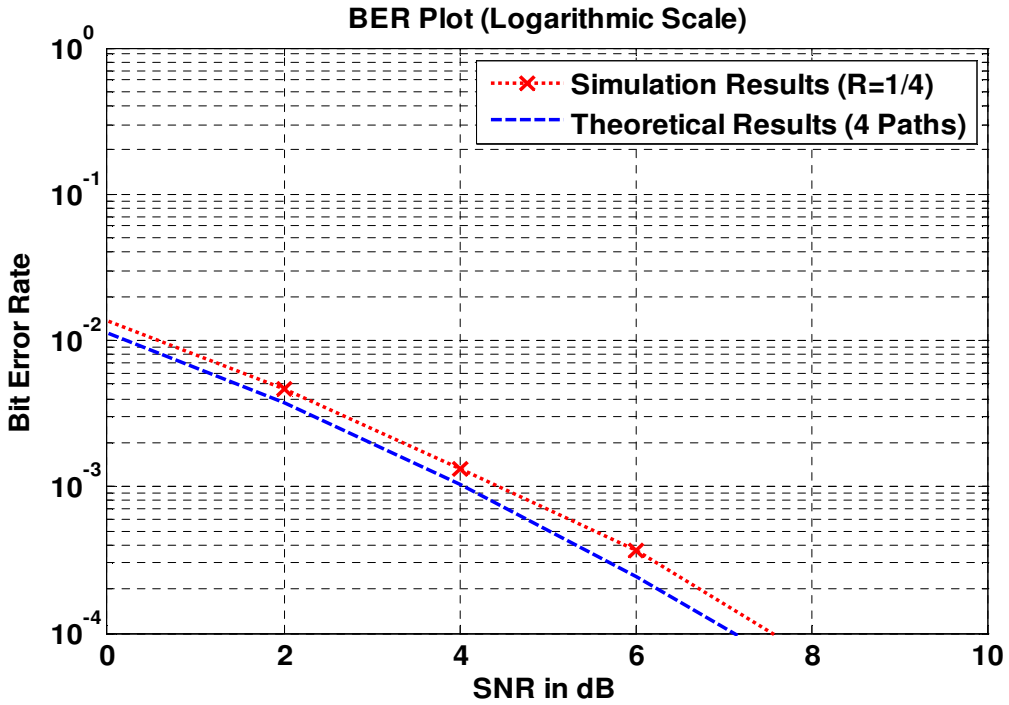

Figure 2.14: BER Performance of the 802.11g software receiver

2.2 Indoor Positioning Methods based on WLAN 802.11g (WiFi)

Due to indoor and urban coverage, Wireless LAN technology is considered an important candidate to determine the position of a mobile user in these environments. Thus, indoor positioning using WiFi signals has been addressed extensively in existing literature. Different properties of wireless signals can be used to obtain an estimated position for indoor location-based applications.

Several methods have been proposed in the literature to perform WiFi positioning and they are described as follows:

Angle of Arrival (AOA) refers to the method where the directions of incoming signals, from transmitters with known locations, are used to approximate the receiver position. The triangulation technique is used in this case to compute the location of the mobile device and a special antenna array is required to measure the angle (Lim et al 2007).

Cell Identity (CI) is another method that makes use of the radio coverage of an identified cell to indicate the location of a mobile device. The location of the identified cell at the time of detection must be available. The main drawback of this method is its accuracy since usually the coverage area of a cell is wide. Moreover, the presence of many stationary points and reflectors in an indoor setting makes this method inaccurate due to multipath propagation (Kotanen et al 2003).

Time of Arrival (TOA) measures the round-trip time (RTT) of a signal (Golden 2007). After estimating the distances from a mobile device to three stationary devices, using the trilateration method, the position of the mobile device with respect to the stationary devices can be determined. TOA requires very accurate and also synchronized clocks since 1.0 μs error corresponds to a 300 m error in the

distance estimate. Thus, inaccuracy in measuring time differences should stay within tens of nanoseconds (Bagdonas 2008). Different approaches have been followed in this case. In Cheung et al (2004), the authors propose a model-based TOA method for opportunistic indoor navigation using 802.11 a/g WLAN signals, while in Ciurana et al (2007), a TOA-based ranging technique is proposed using 802.11b data frames based on time of flight estimation with the cost of additional hardware. Wibowo et al (2009) propose time of flight estimation using 802.11b tags and claim that no additional hardware is required, however it assumes that the processing time at nodes are known and time invariant. Most recently, two-way TOA estimation between users in a cooperative network has been proposed in Oguz-Ekim et al (2013), where processing times are assumed unknown and estimated throughout the network. In practice, accurate TOA and time of flight methods are not easy to implement for WLAN systems due to hardware requirements, timing resolution of mainstream network adaptors for off-the-shelf products and also time invariant network parameters (Muthukrishnan et al 2006, Bagdonas & Borre 2008).

Time Difference Of Arrival (TDOA) is similar to the Time Of Arrival method but uses the measured time differences of arrival. While the synchronization requirement of the user clock is eliminated in this method, the transmitters must still be synchronized and high-precision time difference measurements must still be made by mobile users if an accurate user position is to be achieved. For example, in order to stay within a position accuracy requirement of ±150 m, implied by the FCC (Federal Communications Commission) E911 Phase 2 specifications, time differences should be measured with a precision of the order of microsecond for 90% of the cases (Jami et al 1999, Sayed et al 2005, Ho & Chan 1993).

Received Signal Strength (RSS) methods use the received power along with knowledge of the transmitted power and signal attenuation properties of radio wave propagation to estimate the position of the mobile device. One common approach consists of surveying signal strength in a specific location in order to form a database, which describes an RSS "fingerprinting" map of that area. The database is subsequently used to determine the location of a mobile device through the use of pattern recognition algorithms (Kaemarungsi & Krishnamurthy 2004). This method requires the use of time consuming and costly survey procedures. Another approach that uses the signal strength of received signals is the path-loss modeling approach to estimate the relationship between signal strength and distance from transmitters. The estimated distances from three or more transmitters are used to trilaterate the position of the mobile device (di Flora & Hermersdorf 2008, Cook et al 2005).

The most common WiFi positioning methods use either an off-line database of RSS (Received Signal Strength) map or a path loss model to convert RSS to distance values. RSS-mapping methods are based on collecting a database of observed RSS from available WiFi access points and then applying pattern recognition algorithms to define an unknown position with regard to AP positions. Therefore, these methods require fingerprinting the network coverage and populating the database, which implies additional time and financial costs. Also, since the accuracy of the WiFi access point data bases generally decrease over time (as changes are made by the access point operators without updating the databases), these systems require frequent and expensive updates (Pahlavan et al 2010, Bahl & Padmanbhan 2000). On the other hand, model-based methods suffer from lack of knowledge for modeling signal propagation especially in indoor environments and under multipath conditions (Lee & Chen 2007, Xiang et al 2004).

Different methods of WiFi positioning are compared in Table 2.2. Each method requirements and drawbacks are also shown. In general, existing WiFi positioning algorithms give typical average position accuracy of 1 to 4 m indoors and 10 to 40 m outdoors (Mok & Retscher 2007), depending on the method used, the geometry of transmitters, and in the case of fingerprinting, on the density of the database observations.

Table 2.2: Comparison between different WiFi localization methods along with the drawbacks

	Principle of the method	Technique used	Draw-backs
Angle of Arrival (AOA)	**Direction of incoming signals**	**triangulation**	**Deployment of array antenna**
Cell Identity (CI)	**Radio coverage of an identified cell**	**Identifying the cell**	**Wide coverage Vulnerability to multipath**
TOA	**RTT of a signal OFDM signal structure**	**trilateration**	**Needs accurate clocks Hardware Requirements**
TDOA	**RTT of a signal OFDM signal structure**	**trilateration**	**Needs accurate time difference (tens of nano-seconds)**
Fingerprinting Method	**Signal attenuation of radio wave**	**Fingerprinting**	**Time-consuming survey procedure**
Path-Loss Modeling Method	**Signal attenuation of radio wave**	**Path-loss modeling**	**Lack of an accurate indoor model**

Any of the above methods can be used, either as an independent positioning system or as a complementary and back-up positioning system, in order to solve problems encountered by GPS indoors such as severe multipath and signal attenuation (Pahlavan et al 2010, Jami et al 2009, Cavalieri 2007). For instance, in Papandrea et al (2009), an indoor localization technique is implemented, based on WiFi positioning methods only, in order to locate the user receiver. In contrast, Cacopardi et al (2010), for

example, proposed to integrate WiFi access point position information with GPS solutions in order to extend positioning performance into environments with limited satellite visibility. In this case, WiFi access points are treated as virtual satellites in places where only three GPS satellites are visible. The geo-referenced positions of access points are supposed to be obtained from broadcasted WiFi beacons. Once this information is available, APs can be used as virtual satellites to fix the user receiver position by trilateration while the receiver acquires signals from only three GPS satellites.

As the primary step to WiFi and GPS integration, this thesis focuses on new approaches where WiFi features can be used indirectly to improve GPS performance in the navigation domain, as discussed in the next chapter. Then as the next step, the signal domain integration of WiFi and GPS is considered in an Assisted-GPS (A-GPS) scheme as explained in the following section.

2.3 GPS and A-GPS Systems

2.3.1 Overview of GPS Signals

GPS uses Code Division Multiple Access (CDMA) with all the satellites transmitting on the same frequencies using different Pseudo Random Noise (PRN) codes. PRN codes are deterministic binary signals with similar spectrum characteristics of random sequences (Ward et al 2006). By comparing received PRN code and the generated replica in a GPS receiver, the propagation time of the transmitted signal can be estimated. GPS mainly uses two carrier frequencies of L1 (1575.42 MHz) and L2 (1227.60 MHz) and is under modernization since 2000 for broadcast of new signals for civil and military uses including L2C civil signal, L5 frequency (1176.45 MHz), L1C signal and military code M (Ward et al 2006). The carriers are modulated using two types of PRN codes. The Coarse Acquisition (C/A) code is

used in civil applications and has a duration of 1 millisecond with a 1.023 MHz chip rate and is available on L1. Precise (P) code is used for military applications and has a period of seven days with a 10.23 MHz chip rate and is available on both L1 and L2. The carriers are also modulated by a 50 Hz navigation message, which includes information on satellite location and clock errors.

2.3.2 GPS Acquisition Overview

Before a GPS receiver can perform any satellite tracking or positioning, the satellite signals must be detected and acquired by estimating the correct frequency for each of the satellites in view and the code delays. After acquisition of the satellites, a conventional GPS receiver will decode the broadcast time of week, clock model and the satellite orbit information from ephemeris data.

Basically, the GPS acquisition steps can be represented as shown in the flowchart of Figure 2.15.

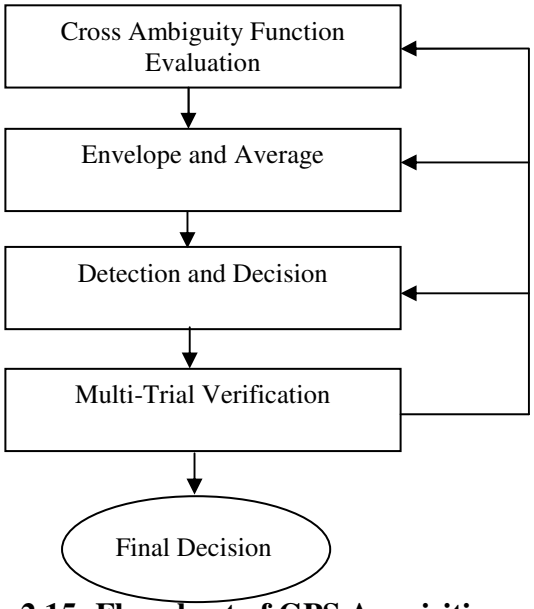

Figure 2.15: Flowchart of GPS Acquisition

First, a generalization of the standard correlation is computed and evaluated for the received signal. The square modulus of this correlation function is then obtained through an envelope and averaging procedure to form the decision statistics and the final decision (on the absence or presence of the signal) is made after multi trial verification of these statistics.

Typical GPS satellite detection strategies are based on a two-hypothesis criteria function for absence H_0 or presence H_1 of the signal as

$$\begin{cases} H_1: & r(n) = y(n) + \eta(n) \\ H_0: & r(n) = \eta(n) \end{cases} \tag{2.17}$$

where *r(n)* is the received signal and $\eta(\mathrm{n})$ is the Gaussian zero mean noise collected by the antenna as

$$r(n) = \sqrt{2C}\, d(nT_s - \tau) c(nT_s - \tau) \cos(2\pi(f_{IF} + f_d) nT_s + \varphi) + \eta(n) \tag{2.18}$$

$$\eta(n) \sim \mathrm{N}(0, \sigma_{IF}^2) \tag{2.19}$$

with d being the navigation message, c the PRN code, τ the code delay, f_d the Doppler frequency, f_{IF} the IF frequency, φ the carrier phase and C the received power.

The decision statistics, based on General Likelihood Ratio Test (GLRT) can be written as

$$\Lambda = \arg\max_{\tau, \mathrm{F}_d, \varphi} \Re[\mathrm{R}(\tau, \mathrm{F}_d) \exp\{-\mathrm{j}\varphi\}] \tag{2.20}$$

where $F_d = f_d + f_{IF}$ and $\mathrm{R}(\tau, \mathrm{F}_d)$ is the cross-ambiguity function (CAF) and is written as

$$\mathrm{R}(\tau, \mathrm{F}_d) = \frac{1}{N} \sum_{n=0}^{N-1} r(\mathrm{n})\, \mathrm{c}^*(\mathrm{nT}_s - \tau) \exp\{-\mathrm{j}2\pi \mathrm{F}_d \mathrm{nT}_s\} \tag{2.21}$$

In fact, CAF is a correlation function representing signal similarities along time and frequency.

The maximization of the amplitude of CAF should be performed with respect to the variables τ and F_d. This creates a two-dimensional acquisition search space as a function of frequency and code delay as shown in Figure 2.16.

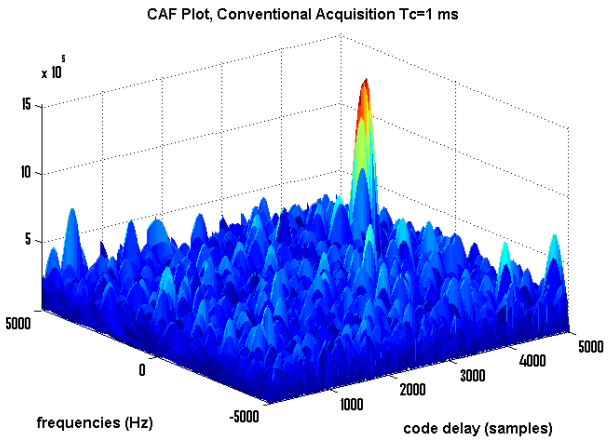

Figure 2.16: Two dimensional GPS acquisition search space in a sample CAF plot

In general, satellite motion, receiver motion, local oscillator uncertainty and clock drift are the main factors contributing to frequency search, which normally ranges from -5kHz to 5kHz.

The code delay search space has a length of 1023 chips, which is the number of chips in the C/A code.

Figure 2.17 depicts a basic structure of GPS acquisition. This structure represents the first two blocks in the flowchart of Figure 2.15, which occurs at the cell domain and outputs the decision statistic to the decision domain (i.e. the last two blocks in Figure 2.15). The decision statistic is the square modulus of the CAF.

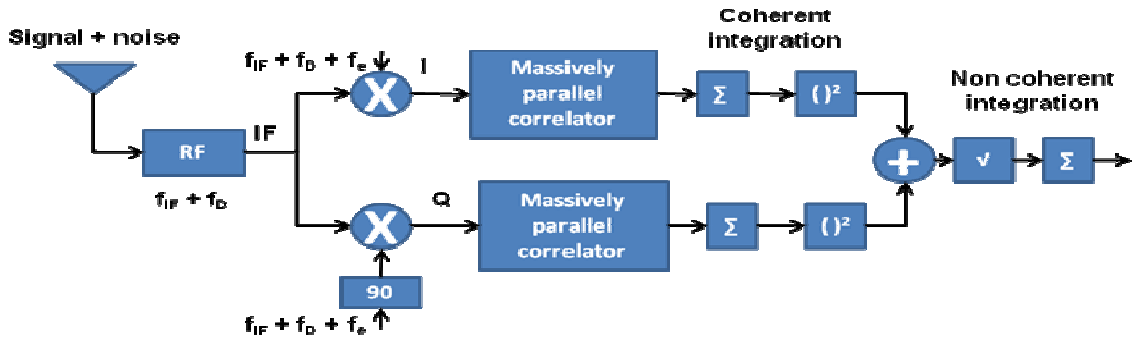

Figure 2.17: A schematic view of basic GPS receiver acquisition blocks

2.3.3 A-GPS Schemes

A conventional GPS receiver with a cold start (i.e. no a priori information is available) could take approximately 1 minute to compute the position and perform the first fix when operating in ideal conditions (Van Diggelen 2009). Typically, in this condition, the receiver should search a two-dimensional frequency/code delay space of size 20×1023 to 50 ×1023, which takes at least 20 s. To decode the ephemeris data and do a first fix the receiver should wait for at least about another 30 s (Van Diggelen 2009). If there is any data bit errors due to weak signal or multipath conditions, it is normal for the receiver to take several minutes for a first fix. Any a priori information will result in considerable reduction in the acquisition time and time to first fix. To this end, assisted GPS (A-GPS) has been proposed as a method to improve the performance of standard GPS acquisition algorithms (Van Diggelen 2009, Goran & Richton 2001).

As mentioned in the previous section, acquisition of the satellites in view can be considered as the first step in GPS-based positioning and the A-GPS method makes use of assistance data from alternative sources (such as communication networks) to aid acquisition of GNSS signals. Assuming different acquisition strategies, the type of assistance data that can be employed will be different. In general, this

assistance information includes time, reference time, reference frequency, receiver position, almanac and/or ephemeris, expected satellite Doppler, Doppler rate and navigation data bits (Van Diggelen 2009, Progri 2010, Monnerat 2007). Most of the assistance data allow the receiver to reduce and limit the frequency/code-delay search space during acquisition. This translates in reduced time to first fix. Navigation data bit assistance additionally allows for longer integration times in the acquisition, which is limited to 20 ms in conventional GPS due to the 50 bps ephemeris data rate.

There are two common approaches towards A-GPS acquisition, namely Mobile Station (MS)-Assisted and Mobile Station (MS)-Based approaches. In MS-assisted GPS, the receiver acquires signals from satellites in view and sends the measurements to the server to compute the receiver position. In MS-based GPS acquisition, the acquisition and positioning are both performed at the receiver (Van Diggelen 2009).

Assuming different acquisition strategies, the type of assistance data that can be employed will be different. Depending on the accuracy, time information can be applied as fine-time assistance or coarse-time assistance data. Coarse-time assistance has accuracy better than one millisecond and thus can be used to assist frequency search space only, while fine-time has accuracy of microsecond or nanosecond level and can further assist the code-delay search space. Thus having fine-time assistance data will result in considerable reduction in search space. Typically, the acquisition time can be reduced to about 1 s in coarse-time assistance strategy and to tens of milliseconds when fine time assistance is available (Van Diggelen 2009). In the following sub-sections two important types of assistance information, namely position assistance and time assistance, are discussed in more details.

2.3.3.1 A-GPS using Position Assistance information

Position assistance data can reduce the frequency search space by allowing prediction of the expected Doppler frequency. The upper bound for the accuracy of position assistance can be considered to be 300 km since this result in an ambiguity of ±150 km for the expected code delay, which is equal to 1 ms (total length of C/A code). Hence using the wireless networks as an external source of assistance data, the position can always be estimated accurately enough to assist GPS acquisition. As an example, in mobile phones the estimated position from the cell-tower data base has typically an accuracy of 3 km.

For a more detailed discussion on the assistance error analysis due to position inaccuracies it should be noted that the Doppler frequency of each satellite is the dot product of the unit vector from receiver to satellite with the velocity vector. Hence, one can write:

$$\begin{aligned} satellite\ Doppler\ error &\approx v(e_{true} - e_{est}) \\ &\le v \bullet \delta x / range \le |\delta x| \bullet satellite\ speed / range \\ &\le 3.8\times10^{3} \bullet |\delta x| / (2\times10^{7})\ m/s = 0.19\times10^{-3} |\delta x|\ m/s \end{aligned} \tag{2.22}$$

where e_{true}, e_{est} are two line-of-sight unit vectors and a position error introduces a line-of-sight vector error. In the above equation the difference between two unit vectors is written in terms of position error ($|\delta x| / range$) and the worst-case error has been computed. The equation shows that for a position estimate error of 1 km, the maximum satellite Doppler error is approximately 0.19 m/s= 1 Hz. This can be scaled and we can conclude that for each 1 km of position error, a 1 Hz satellite Doppler error is introduced to the search space.

For the code-delay error analysis of position assistance information one can write (Van Diggelen 2009)

$$\left|r_{Error}\right| = \cos(el) \bullet H_{Error} + \sin(el) \bullet V_{Error} \tag{2.23}$$

where *el* is the elevation angle, and H_{Error} and V_{Error} are horizontal and vertical errors respectively. It should be noted that the error contribution computed above is the worst-case error since the direction of the position error is not known.

The error contribution of position assistance data for the frequency and code-delay search is summarized in Table 2.3 for an accuracy of 1 km.

Table 2.3: Error contribution of position assistance for frequency and code delay search space

Contribution to Frequency Search Space Position Error of 1 km	Contribution to Code-delay Search Space Horizontal Position Error of 1 km
± 1 Hz	± cos (el).1 km < ± cos (el).4 chips

2.3.3.2 A-GPS using coarse time assistance information

The time assistance data consists of date and time, which can be provided in the form of GPS week and seconds of the week or in the UTC form. For assisting the frequency search space it is enough for the time assistance information to have an accuracy of few seconds i.e. coarse time assistance. For analyzing the contribution of the time assistance error to the frequency search space it should be noted that the magnitude of rate of change of Doppler frequency is maximum 0.8 Hz/s (Van Diggelen 2009). Thus, an error of 0.8 Hz occurs in the expected Doppler due to an error of 1s in time information.

Also it should be mentioned that, although the accuracy of coarse time does not allow for code delay assistance to acquire the first satellite, the information can still be used to assist the code delay for acquiring other satellites in view. After acquiring the first satellite, the expected pseudorange can be

estimated using the ephemeris and assistance position. Hence the expected code delay of the first satellite can be calculated as the expected pseudorange modulo 1 ms and the receiver clock bias can be worked out by computing the difference between measured and expected code delay values. Using the estimated clock bias, expected code delays for other satellites can be computed. However, due to satellite motion, the code delay search space is still not reduced as much as it can by having fine time assistance information (Van Diggelen 2009).

Time assistance can also be analyzed in terms improvements in receiver performance. For results presented in this section, -1 dB worst-case roll-off is assumed for the receiver structure shown in Figure 2.17. This will be used to solve for coherent integration time T_c as in

$$Max\,roll-off = -1\,dB = 20\log 10\,(\sin(\pi f T_c)/(\pi f T_c)) \tag{2.24}$$

Also squaring loss is defined as

$$squaring\ loss = post\ RSS\ SNR\ /\ coherent\ SNR \tag{2.25}$$

The ratio of variances at the peak and away from the peak is used to derive the probability analysis of the system as (Van Diggelen 2009)

$$ratio\ of\ \text{var}iances\ at\ and\ away\ from\ peak = q$$
$$= \frac{4}{4-\pi}(\gamma + 1 - \frac{\pi}{4}e^{-\gamma}[(1+\gamma)I_0(\gamma/2) + \gamma I_1(\gamma/2)]^2 \tag{2.26}$$

The overall implementation loss is

$$\text{Im } plementation\ Loss = \Delta_{IF} + \Delta_Q + \Delta_F + \Delta_C + \Delta_B \tag{2.27}$$

where Δ_{IF} is the filtering effect on acquisition and is considered to be zero (Van Diggelen 2009). Δ_Q is a 3-bit analog to digital quantization error. Δ_F is the average cross-bin loss, Δ_C is the code alignment loss and Δ_B is the bit alignment error .

In terms of receiver operational performance, having coarse time assistance information will result in a search space reduction, which leads to a higher probability of detection for satellite acquisition. In Figure 2.18 coarse-time WiFi-assisted acquisition has been compared to conventional non-assisted acquisition by plotting the ROC (Receiver Operational Characteristic) for system probability of detection and system probability of false-alarm. As it can be shown reducing the search space by using the coarse-time assistance from WiFi signals will increase the probability of detection for a fix probability of false alarm.

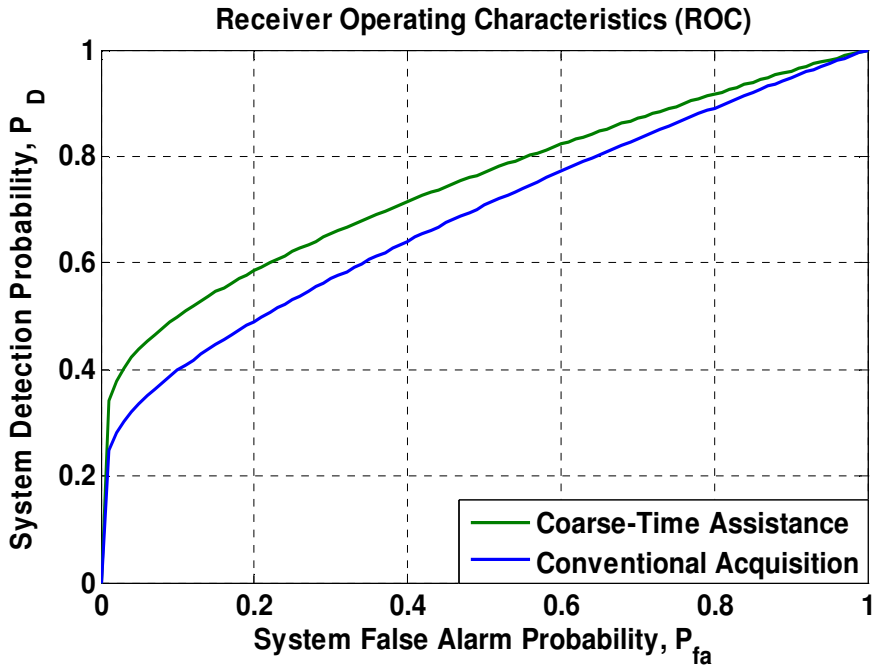

Figure 2.18: System ROC plots for the coarse-time assisted GPS acquisition algorithm and the conventional non-assisted acquisition algorithm

The ROC plot in Figure 2.18 is shown for system probabilities, which can be computed as below from the probability of detection and the false alarm probability for one cell:

$$p_{fa-cell} = Q(\frac{\lambda - \mu_n}{\sigma_n}) \tag{2.28}$$

where Q is the Q-function and μ_n and σ_n are the mean and the standard deviation of the noise and a Gaussian distribution is assumed. For the probability of detection of a cell one has

$$p_{D-cell} = Q(\frac{\lambda - \mu_s}{\sigma_s}) \quad - \tag{2.29}$$

Hence, having a search space of size N (with N being the number of cells) will result in system probabilities of:

$$p_{fa} = 1 - P_{Correct-\text{Re}\,jection} = 1 - \left(1 - p_{fa-cell}\right)^{N} = 1 - \left(1 - Q(\frac{\lambda - \mu_n}{\sigma_n})\right)^{N} \tag{2.30}$$

$$p_{D} = 1 - \left(1 - p_{D-cell}\right)\left(1 - p_{fa-cell}\right)^{N-1} = 1 - \left(1 - Q(\frac{\lambda - \mu_s}{\sigma_s})\right)\left(1 - Q(\frac{\lambda - \mu_n}{\sigma_n})\right)^{N} \tag{2.31}$$

Furthermore, receiver sensitivity can be analyzed when coarse time information is available as assistance data. To this end, coarse-time acquisition sensitivity versus total non-coherent integration time per frequency bin is plotted in Figure 2.19. This plot shows the family of curves for a set of coherent integration times. The curves show the signal strength at which the expected squared root of SNR magnitude equals the false alarm threshold. Any signal stronger than that has a chance of being detected more than 50%. It can be seen that by increasing the coherent time, the sensitivity increases. It should be noted that T_{eff} is considered to be 296 K, while the front-end noise figure is assumed to be 2 dB. The sampling rate is 2 samples/chip and the magnitude ratio of false alarm threshold is set to be 6, which is a ratio representing the design parameter of square root of the SNR (Van Diggelen 2009).

Figure 2.20 represents the signal strength versus coherent integration time for various total integration times. The plot shows the family of curves where each singe curve represents a fixed total integration time for coarse-time acquisition. As it can be seen in this plot, the slopes of the curves are about -1.5 dB per octave, which means that as the coherent interval doubles while the total integration time stays the same, the sensitivity increases by approximately 1.5 dB (Van Diggelen 2009).

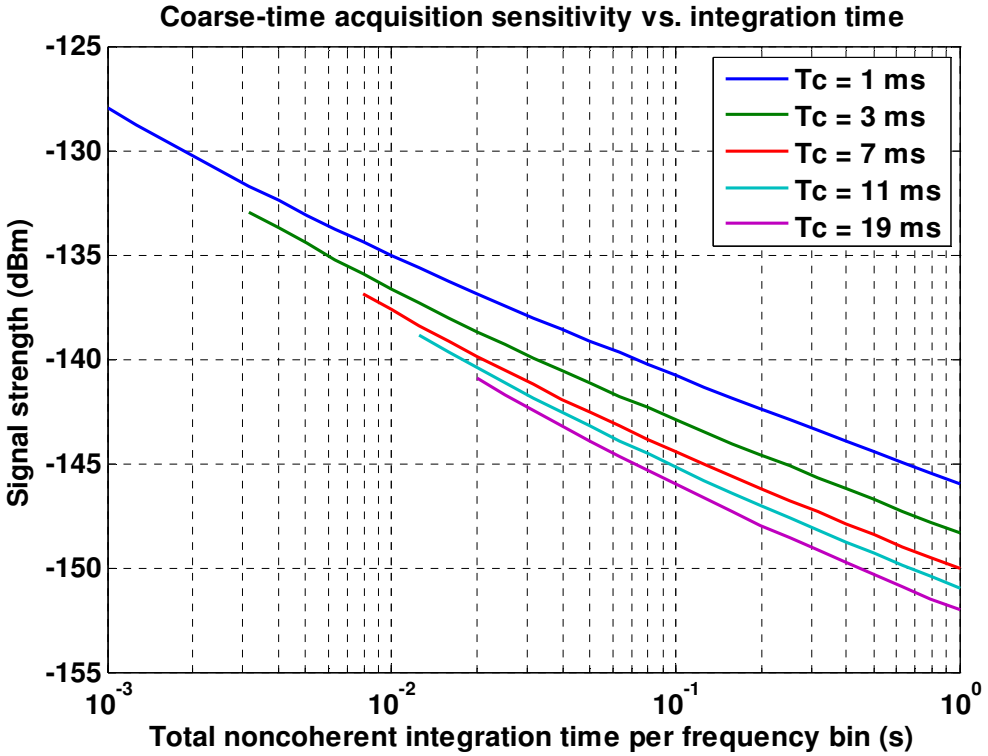

Figure 2.19: Coarse-time acquisition sensitivity (minimum signal strength required for performing acquisition) as a function of total non-coherent integration time for different coherent time intervals (after Van Diggelen (2009))

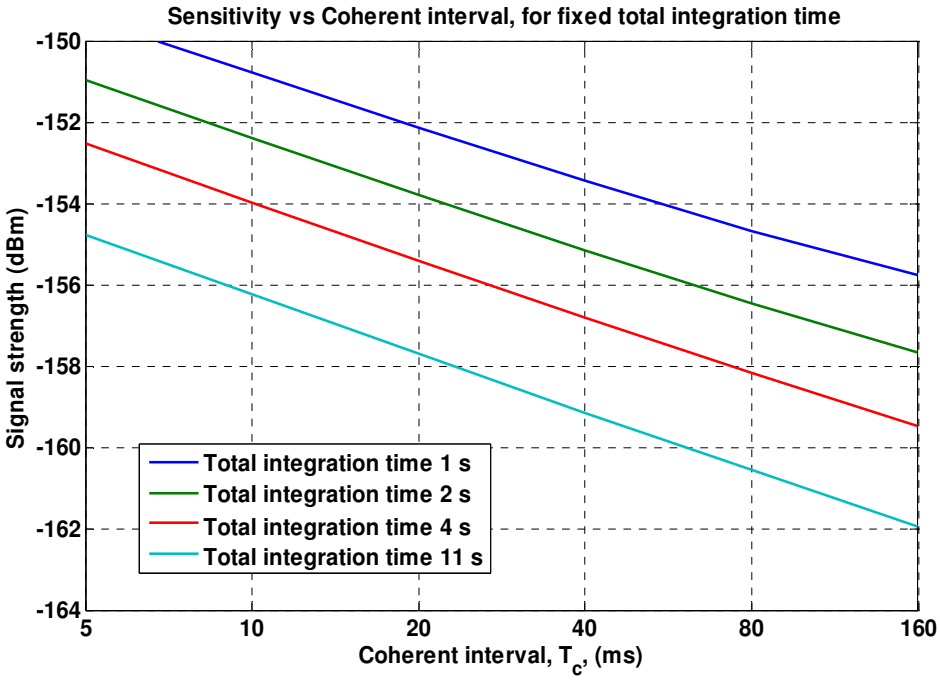

Figure 2.20: Sensitivity for coarse-time acquisition versus coherent integration interval for different total integration times (after Van Diggelen (2009))

2.3.3.3 A-GPS using fine time assistance information

If fine time assistance data is available (i.e. time assistance is known better than 1 ms), the number of chips can be reduced in the code delay search space. This means that time assistance with accuracy of better than 1 μs can be used to estimate the expected correct chip and thus limit the search space to only one chip. The achievable accuracy depends on the limitations of the external source of information (such as wireless networks), communication environment and structure and receiver parameters. As an example, CDMA networks can provide time accuracy in the order of microsecond due to the signal structure and synchronized nodes within the network. On the other hand, GSM, UMTS and WCDMA networks have typically time accuracy in the order of second (mostly one to two seconds) and thus can generally be used as a source of coarse time information.

For code delay assistance error analysis due to fine time, as explained before, there is a direct relationship between time accuracy and code delay error. In other words, since the number of chips per millisecond is 1023, each 1 µs error in the time data will result in a 1.023 chips error.

Table 2.4 presents and compares the contribution of the coarse time assistance error and fine time assistance error in the frequency and code delay search space. In this example, the accuracy of coarse time is assumed to be 1 s and fine time is assumed to be good to 5 µs. It should be noted that the code delay contribution of coarse time assistance is calculated after the first satellite acquisition. The worst-case value in this case happens with expected relative velocity of the satellite being ± 800 m/s (Van Diggelen 2009). Obviously, the error of time assistance is not the only factor contributing to the total search space uncertainty and cannot be considered alone. As was mentioned before the position should be computed with good accuracy in order to make use of the time. An accuracy of ±150 km is sufficient to enable code delay assistance. The error contribution of the position assistance is given in Section 2.3.3.1. In the proposed A-GPS method described in Chapter 4 where the position is computed for two WiFi receivers within the range of the same AP, the position accuracy of better than ± 100 m can be achieved which corresponds to 0.3 µs.

Table 2.4: Error contribution of coarse and fine time assistance for frequency and code delay search space

	Contribution to frequency search space uncertainty	Contribution to code delay search space uncertainty
Coarse time assistance good to ±1 s	±1 s×0.8 Hz/s= ± 0.8 Hz	±1 s× expected relative velocity < ±6 chips
Fine time assistance good to 5 µs	±5 µs ×0.8 Hz/s (insignificant)	±5 µs=±5.23 chips< ±6 chips

In terms of receiver operational performance, the probability of detection for the correct bin can be compared for two cases of coarse-time assisted and fine-time assisted GPS acquisition for different

coherent integration times as shown in Figure 2.21. Typical signal strength at the antenna for outdoor environments is about -130 dBm (about 44 dBHz) while these numbers can be reduced by 20 to 30 dB for weak signal environments and indoors (Van Diggelen 2009). Typical signal levels for coarse-time A-GPS and high sensitivity acquisition is about -150 dBm (around 20-24 dBHz) and the sensitivity can be increased to -160 dBm and beyond with fine-time A-GPS (Van Diggelen 2009). The noise power is assumed to be -109.1 dBm. The effective thermal noise temperature is considered to be T_{eff} = 296.4 K and the signal strength is assumed to be -150 dBm in this case. T_{eff} is the effective noise temperature of the front-end in degrees Kelvin.

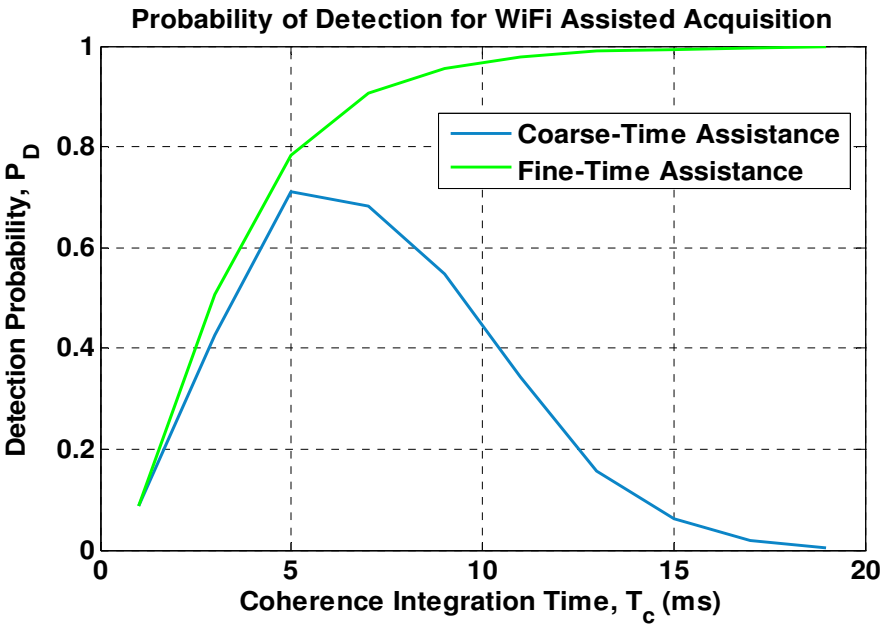

Figure 2.21: Probability of detection for the correct bin vs. Coherence integration time; comparison between fine-time assistance and coarse-time assistance systems

If the assistance data includes only coarse time then the implementation loss includes the bit alignment loss, which depends on the coherent time. As the coherent time increases the bit alignment loss increases as well. Figure 2.22 shows the bit alignment loss as a function of coherent interval (Van Diggelen 2009).

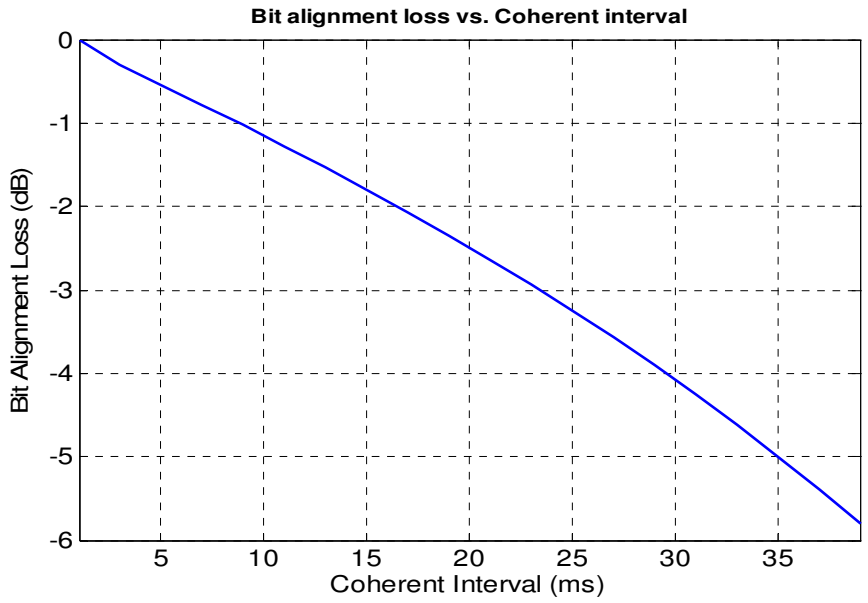

Figure 2.22: relationship between different bit alignment loss values and the coherent integration time (after Van Diggelen (2009))

This explains the behaviour of the probability of detection curve for the coarse time assistance information. In this case there is a trade off between increasing coherent time and introducing bit alignment loss. If fine-data is available no bit alignment loss is introduced to the system, which gives better performance for higher T_c values.

To further compare the performance of the assisted acquisition system in the two cases of the coarse-time and fine-time assistance, another criterion can be considered to be the receiver operating characteristic. A ROC comparison for the correct bin with a fixed coherent interval time of 11 ms, for

fine-time assistance versus coarse-time assistance can also be seen in Figure 2.23. To avoid inconsistency of the performance, with coarse-time assistance and unknown bit alignment, the coherent integration time should be an odd value, which is not dividable into 20 (Van Diggelen 2009). Hence, here the particular value of 11 ms is chosen for performance comparisons. As it can be seen in this plot, if fine-time assistance is available, for a fix probability of the false alarm, a higher probability of detection can be achieved which means better acquisition performance.

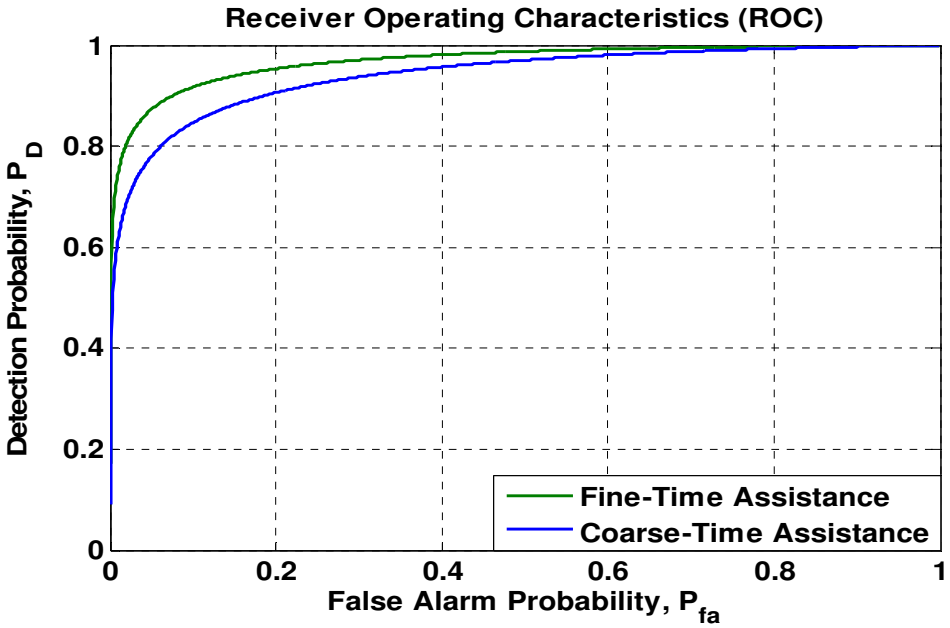

Figure 2.22: The ROC plot for the correct bin; comparison of the system performance in two cases of coarse-time and fine-time assisted acquisition

All this motivates research to explore practical options and new approaches for providing high accuracy time information to assist acquisition of satellites as the primary task of a GPS receiver, especially in challenging and weak signal environments. In the following chapters, this thesis discusses the feasibility and performance of A-GPS using WiFi signals.

CHAPTER 3: WIFI/GPS INTEGRATION FOR CONTEXT IDENTIFICATION AND NAVIGATION FILTER ADAPTATION

In this Chapter, WiFi RSSI observations are used to determine user context so that a GPS position estimator can modify its behaviour according to changes in environment (static/kinematic and indoors/outdoors).

First, the existence of similar patterns in WiFi signal features under similar environmental and/or dynamic conditions is investigated. Results repeatability and consistency using WiFi features as context identifiers and pattern utilization to make assumptions or predictions about the current mode are demonstrated. Some simple effective identification algorithms are proposed based on features such as the number of available APs or the number of APs with RSS exceeding a certain threshold, the mean and the variance of the total RSS from available APs, etc. The performance of these algorithms is then evaluated through field tests under different conditions.

After characterizing different receiver contexts, this additional information is used as the next step to enhance the performance of GPS positioning algorithms. One possible way to take these changes into account is to implement adaptive positioning algorithms. More specifically, WiFi information can be used to adjust the uncertain parameters of an adaptive Kalman filter. This can include both the variance/covariance matrices and the system model. Specifically, the model is adapted based on the user being static or in motion while the observation covariance matrix is adapted based on whether the receiver is indoors or outdoors.

Herein, a new two-layer adaptive extended Kalman filter positioning algorithm is proposed based on multiple model adaptive estimation in which each individual Kalman filter, matched to a different dynamic model, has an IAE (Innovation-based Adaptive Estimation) structure and external information obtained from WiFi signals. The above is then used to adjust the adaptive parameters based on the different situations.

3.1 Kalman Filtering Algorithm

The Kalman filter is widely used in the field of GPS navigation to obtain an optimal estimate of the states in the sense of minimum mean square error (Kalman 1960, Papoulis & Pillai 2002). It takes into account the state vector time variations by adding a dynamics model into the least squares estimation technique (Papoulis & Pillai 2002, Maybeck 2011). As such it relies on the system having an a priori known dynamic process model and a measurement model. The Kalman filtering method has a recursive structure and can be formulated through update and prediction steps in a loop with covariance propagation between the two steps (Petovello 2011).

The update loop derives an optimal estimation of the states using a priori information and a vector of measurements. In the discrete-time model Kalman filter the update processing equations can be written as (Gelb 1974)

$$\hat{x}_k^+ = \hat{x}_k^- + K_k(\mathrm{z}_k - H_k\hat{x}_k^-) \tag{3.1}$$

$$P_k^+ = (\mathrm{I} - K_k\,\mathrm{H}_k)\,\mathrm{P}_k^- \tag{3.2}$$

with Kalman filter gain at epoch k given by

$$K_k = P_k^- H_k^T(\mathrm{H}_k\,P_k^- H_k^T + R_k)^{-1} \tag{3.3}$$

Here, x_k and z_k are the state vector and the measurement vector at epoch k, H is the design matrix, P is the covariance matrix of the estimation error and the superscripts minus and plus are used to show the a priori and updated estimates respectively.

The term $z_k - H_k \hat{x}_k^-$ in Equation 3.1 is the innovation sequence v_k and contains the new information in the measurements. The innovation sequence is generally assumed to be white noise process (Papoulis & Pillai 2002, Petovello 2011) and the covariance matrix of the innovations is given by

$$C_{v_k} = H_k P_k^- H_k^T + R_k \tag{3.4}$$

where R_k is the covariance matrix of observations at epoch *k.* Within the Kalman filter prediction loop, the updated state vector is extrapolated using the state model and the equations can be written as

$$\hat{x}_{k+1}^- = \Phi_{k,k+1} \hat{x}_k^- \tag{3.5}$$

$$P_{k+1}^- = \Phi_{k,k+1} P_k^+ \Phi_{k,k+1}^T + Q_k \tag{3.6}$$

with Q_k being the process noise matrix at epoch k and $\Phi_{k,k+1}$ being the transition matrix from epoch k to epoch k+1. The choice of $\Phi_{k,k+1}$ depends on the dynamics model selected for the system, several examples of which are given in (Brown & Hwang 1996). The procedure to select Q_k, which depends on the uncertainty of the dynamics model when compared to the actual dynamics is described in (Grewal & Andrews 2001). Details of each are given below.

3.1.1 Adaptive Kalman Filtering Algorithm

The performance of the Kalman filter in state estimation is closely related to the accuracy of the a priori knowledge of the dynamic model and measurement noise. However, in many realistic situations, a

precisely known model is not available and the performance is degraded according to the modeling uncertainties. These modeling errors can also lead to divergence problems in the navigational state estimation. Adaptive Kalman filtering has been addressed in the literature (Maybeck 1994, Salychev 1998) as one of the promising strategies to improve the performance under such conditions.

Different adaptive Kalman filtering algorithms have been investigated in the literature. The performance of positioning algorithms and the optimality of the Kalman filter are closely related to the a priori knowledge of the model, the process noise and the measurement noise.

An IAE algorithm approach can be developed by adapting the covariance matrix of measurements or the process noise (Mehra 1970, Mohammed & Schwarz 1999). A second approach is based on introducing fading factors to the covariance matrix of the states (Geng & Wang 2008, Moreno & Pigazo 2009). The fading factor and IAE models are actually following the same procedure of controlling the amount of noise introduced in the dynamic model (or covariance matrix of the observations) to control the performance and assure the convergence of the Kalman filter.

The other approach is to use Multiple Model Adaptive Estimation (MMAE) methods in which the state estimation is achieved by using a weighted sum of the estimates from a series of parallel filters matched to different system models. Both IAE and MMAE methods exploit the new information in the innovation or residual sequence but with different implementations. Recent improvements in processor speed have made the MMAE algorithms one of the major groups of adapting algorithms used in navigation applications such as in integrating INS/GPS data (Mohammed & Schwarz 1999, Moreno & Pigazo 2009). The optimal state estimation is then computed using the weighted combination of the

states from all individual Kalman filters. The weighting scheme is based on the a posteriori probabilities of the hypothesis represented by each of the dynamics models.

As another adaptive method, the Individual Model Method (IMM) algorithm runs several individual model-matched Kalman filters in parallel, which interact and exchange information at each epoch (Tseng et al 2011). The IMM methods use Markov chain state probabilities to weight the input and the output of a bank of parallel Kalman filters and the overall estimate is obtained by a combination of the estimates. IMM algorithm consists of four major steps: interaction, filtering, mode probability calculation (using a Markov chain model) and combination (Tseng et al 2011).

Most adaptive filters use the information in the innovation sequence or residuals to adapt the covariance matrix of measurements or the process noise covariance matrix and are categorized as IAE adaptive Kalman filtering algorithms. A Maximum Likelihood (ML) Innovation-based Adaptive Estimation Kalman filtering can be formulated as follows.

The probability density function of the measurements conditioned on the adaptive parameter $\boldsymbol{\alpha}$ at a specific epoch can be considered as a Gaussian distribution and be written as (Mohammed & Schwarz 1999)

$$P(\mathbf{z} \mid \boldsymbol{\alpha}) = \frac{\mathbf{1}}{\sqrt{(2\pi)^{m} \mid \mathbf{C}_{v_k} \mid}} \mathbf{e}^{-\frac{1}{2} \mathbf{v_k}^{T} \mathbf{C}_{v_k}^{-1} \mathbf{v_k}} \tag{3.7}$$

where *m* is the number of measurements, $\mathbf{v_k}$ is the innovation sequence at epoch k and $\mathbf{C}_{v_k}$ is the covariance matrix of the innovation sequence at epoch k.

The ML condition based on the adaptation parameter is obtained as

$$\ln P(z \mid \alpha)_k = -1/2(m\ln(2\pi) + \ln(\mid C_{v_k} \mid + v_k^T C_{v_k}^{-1} v_k)) \tag{3.8}$$

$$\sum_{j=j_o}^{k} \ln \mid C_{v_j} \mid + \sum_{j=j_o}^{k} v_j^T C_{v_j}^{-1} v_j = \min \tag{3.9}$$

Applying the formula

$$\frac{\partial P}{\partial \boldsymbol{\alpha}} = \mathbf{0} \tag{3.10}$$

results in (Mohammed & Schwarz 1999)

$$\sum_{j=j_o}^{k} [tr(C_{v_j}^{-1} \frac{\partial C_{v_j}}{\partial \alpha_k}) - v_j^T C_{v_j}^{-1} \frac{\partial C_{v_j}}{\partial \alpha_k} C_{v_j}^{-1} v_j] = 0 \tag{3.11}$$

Also by having

$$C_{v_k} = R_k + H_k P_k(-) H_k^T \tag{3.12}$$

$$\frac{\partial C_{v_k}}{\partial \alpha_k} = \frac{\partial R_{v_k}}{\partial \alpha_k} + H_k \frac{\partial P_k(-)}{\partial \alpha_k} H_k^T \tag{3.13}$$

the ML estimation for the adaptive Kalman filter can be obtained as (Mohammed & Schwarz 1999)

$$\sum_{\mathbf{j=j_0}}^{\mathbf{k}} \mathbf{tr}\{[\mathbf{C_{v_j}^{-1} - C_{v_j}^{-1} v_j^T v_j C_{v_j}^{-1}}][\frac{\partial \mathbf{R_j}}{\partial \boldsymbol{\alpha}_\mathbf{k}} + \mathbf{H_j} \frac{\partial \mathbf{Q_{j-1}}}{\partial \boldsymbol{\alpha}_\mathbf{k}} \mathbf{H_j^T}]\} = \mathbf{0} \tag{3.14}$$

where *tr* is the trace matrix operation and $\mathbf{H}$ is the measurement design matrix. This shows how both R and Q can be adapted based on α.

To obtain an explicit expression for *R*, the *Q* matrix is assumed to be completely known and independent from the adaptation parameter $\boldsymbol{\alpha}$. By considering the adaptation parameters to be the diagonal elements of the *R* matrix, the expression for adapting the covariance matrix of the observations can be obtained as

$$\hat{\mathbf{R}}_k = \hat{\mathbf{C}}_{v_k} - \mathbf{H}_k \mathbf{P}_k(-)\mathbf{H}_k^T \tag{3.15}$$

with

$$\hat{\mathbf{C}}_{v_k} = \frac{1}{N}\sum_{j=j_0}^{k} \mathbf{v}_j \mathbf{v}_j^T \tag{3.16}$$

By the same strategy, assuming the *R* matrix to be known, an approximation for the process noise covariance can be achieved as

$$\hat{\mathbf{Q}}_k = \frac{1}{N}\sum_{j=j_0}^{k} \Delta\mathbf{x}_j \Delta\mathbf{x}_j^T + \mathbf{P}_k(+) - \Phi\mathbf{P}_{k-1}(+)\Phi^T \tag{3.17}$$

where the state correction sequence can be computed as

$$\Delta\mathbf{x}_k = \hat{\mathbf{x}}_k(+) - \hat{\mathbf{x}}_k(-) \tag{3.18}$$

Assuming a steady state condition and using the relation

$$\Delta\mathbf{x}_k = \mathbf{K}_k \mathbf{v}_k \tag{3.19}$$

the expression for process noise can be simplified to

$$\hat{\mathbf{Q}}_k = \mathbf{K}_k \hat{\mathbf{C}}_{v_k} \mathbf{K}_k^T \tag{3.20}$$

3.2 Context-aware Adaptive Extended Kalman Filtering Using WiFi

In the proposed MMAE WiFi-based algorithm, a bank of Kalman filters is used to estimate the final states. Each of the Kalman filters is matched to a specific model and the state elements of the Kalman filters are weighted based on the model probabilities and the decision sequence. The DST-based decision block effectively combines N decision sequences coming from N context identifiers and using the correlation coefficients. These parameters can be fed to the system as a priori known information or

can be computed adaptively in an online manner. Each individual Kalman filter has an IAE structure and the external information is used as a context to adjust the adaptive parameters based on the different situations. More specifically, the motion contexts are used to weigh multiple models while the indoors/outdoors contexts are used to adapt the statistical information through the covariance matrix of observations (the choice of the adaptive statistical characteristics which is either R (covariance matrix of observations) or Q (process noise) is made based on identified context). In other words, if the identified context is indoors the R is adapted and if it is outdoors, Q is selected for adaptation. The choice of adapted-R or adapted-Q depending on the identified contexts will be explained more in the following sections. The weighted sum of all individual estimates is used as the adaptive optimal estimate of the states. The weighting scheme is based on the posteriori probabilities for each of the hypothesis. The proposed algorithm has a closed loop structure and the weighted sum is exploited to provide feedback information for both Kalman filters.

Furthermore, in the WiFi-based MMAE algorithm, the KFs other than the KF whose model best matches the current mode perform adaptation on Q so that in the transitions between contexts, the changes are smoother and the algorithm can track the changes more smoothly.

Two methods are proposed, namely a soft and hard combination. In the soft combination the weighting block is developed to deal with abrupt changes in the decision sequences and making the weight of the best-matching KF converge to unity. In the hard combination the weights are simply binary sequence of (0,1). The block diagram of the proposed algorithm is shown in Figure 3.1.

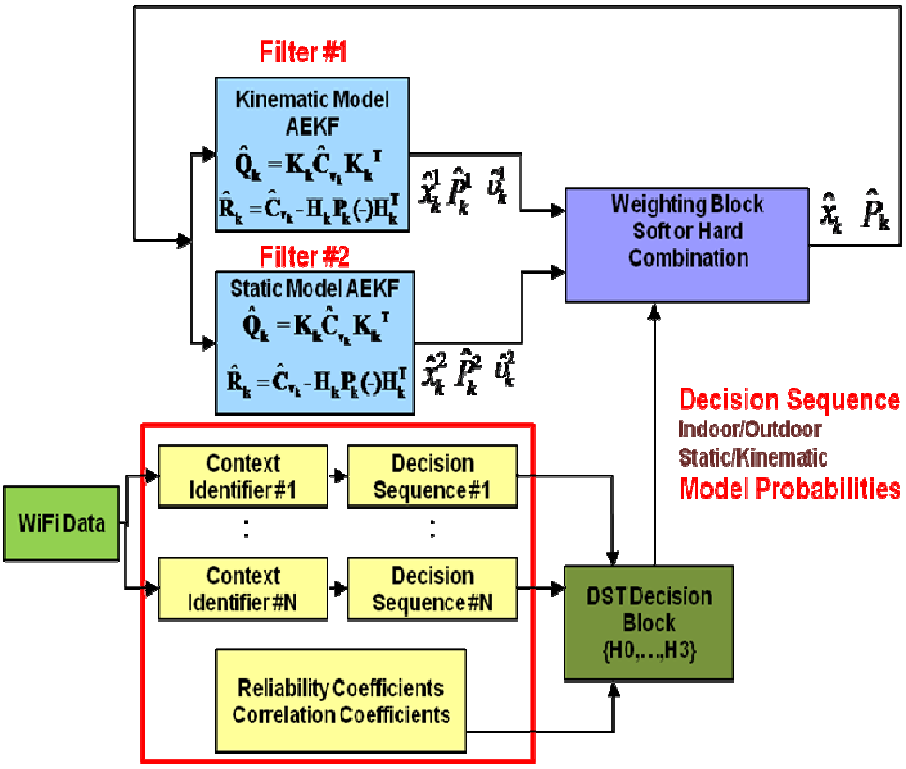

Figure 3.1: Block diagram of the proposed algorithm

As it has been mentioned before, the weighted sum will be fed back to the system (each Kalman filters in the prediction step). Here the bank of Kalman filter consists of two Kalman filters with random walk position and random walk velocity dynamic models. For static data, the dynamic model is a Random Walk Position (RWP)

$$\dot{\mathbf{p}} = \mathbf{w} \tag{3.21}$$

For static data the dynamic model is a Random Walk Velocity (RWV)

$$\dot{\mathbf{v}} = \mathbf{w} \tag{3.22}$$

In the prediction step, the new state vector and state covariance matrix are computed as

$$x_k^{i-} = \Phi x_{k-1}^{i+}$$
$$\mathbf{P}_k^{i-} = \Phi \mathbf{P}_{k-1}^{i} \Phi^T + \mathbf{Q} \tag{3.23}$$

where x_{k-1}^{i+} and $\mathbf{P}_{k-1}^{i}$ are estimated based on the final estimate of the algorithm which has been fed back to each individual Kalman filters. In the update step, the updated state vector and covariance matrix are given as

$$x^{i}{}_{k} = x_k^{i-} + \mathbf{K}^{i}{}_{k} z$$
$$\mathbf{P}^{i}{}_{k} = (\mathbf{I} - \mathbf{K}^{i}{}_{k} \mathbf{H})\, \mathbf{P}_k^{i-} \tag{3.24}$$

where $\mathbf{K}^{i}{}_{k}$ is the Kalman gain for i^{th} dynamic model as

$$\mathbf{K}^{i}{}_{k} = \mathbf{P}_k^{i-} \mathbf{H}^T (\mathbf{H} \mathbf{P}_k^{i-} \mathbf{H}^T + \mathbf{R})^{-1} \tag{3.25}$$

The measurements are weighted according to the reciprocal sine of the satellites elevation angles as (while R is not adaptive)

$$R = \sigma_z^2 \begin{bmatrix} \frac{1}{\sin^2(El_1)} & 0 & & 0 \\ 0 & \frac{1}{\sin^2(El_2)} & & 0 \\ & & \ddots & \\ 0 & 0 & & \frac{1}{\sin^2(El_N)} \end{bmatrix} \tag{3.26}$$

The elevation weighting is used to give lower weights to low elevation satellites. The reason is to weight down the low quality measurements with lower power due to antenna gain roll-off, larger atmospheric errors, and higher multipath effects.

For the clock bias and clock drift the following oscillator model is used (Van Dieredonck et al 1984, Brown & Hwang 1997)

$$\begin{bmatrix} c\dot{dt} \\ c\ddot{dt} \end{bmatrix} = \begin{bmatrix} 0 & 1 \\ 0 & 0 \end{bmatrix} \begin{bmatrix} cdt \\ c\dot{dt} \end{bmatrix} + \begin{bmatrix} w_b \\ w_d \end{bmatrix} \tag{3.27}$$

where w_b and w_d are process noise values for the clock bias and the clock drift respectively. The spectral densities of these process noise values are also respectively given as (Brown & Hwang 1997)

$$q_b = \frac{h_0}{2} c^2,\ q_d = 2\pi^2 h_{-2} c^2 \tag{3.28}$$

where h_0 and h_{-2} are oscillator specific parameters which are assumed to be

$$h_0 = 10^{-21}\ Hz^{-1},\ h_{-2} = 10^{-20}\ s^{-2} Hz^{-1} \tag{3.29}$$

Note that these two terms represent the bias and the drift of the clock as in Equation 3.27. The flicker term (second term in clock error modeling which uses h_{-1}) is ignored in here, which is a common approach for an approximate estimation in the case of GPS receiver clock modeling and gives a sufficiently accurate model for our purpose (Brown & Hwang 1997). Since a specific model is defined for the clock, this model is not modified or affected by the adaptive Kalman filtering. By feeding back the final state estimates of the system to each individual filter, a more accurate prediction is used in the Kalman filter with the non-matching dynamic model. This may delay the divergence of this filter due to implementation of the incorrect model.

In comparison to other adaptive Kalman filtering algorithms, the proposed algorithm has a two layer adaptive scheme, which means that each of the Kalman filters performs IAE adaptive filtering itself. The indoors/outdoors context sequence is used to choose between the adaptation parameter for IAE filtering, namely the adaptation parameters changes from the covariance matrix of the observations (R) to the process noise of the system (Q) when moving from indoors to outdoors.

In indoor environments the adaptation parameter is the R matrix and the covariance matrix of observations is adapted based on the quality of measurements. In outdoor environments the better choice will be to adapt the process noise of the system to reduce the mismatches between the assumed and the actual dynamic models of the system. Results showing the advantage of using this method are discussed in the next section.

3.3 Experiment Design

To analyze the performance of the proposed algorithm, static and kinematic WiFi and GPS data were collected in pedestrian mode inside and outside the MacEwan Student Center of the University of Calgary. This selected location is a four story shopping center-like building with a glass ceiling. This test is done in the navigation domain and the above choice ensures that some GPS position solutions exist in the indoor environment (Figure 3.2). The equipment used is shown in Figure 3.4. A Netstumbler and a wireless D-Link card were used to collect WiFi RSS values. A u-blox receiver was used for GPS data collection. A NovAtel Span-LCI system was to collect IMU data and create GPS/INS reference trajectory shown in Figures 3.2 and 3.3 in blue.

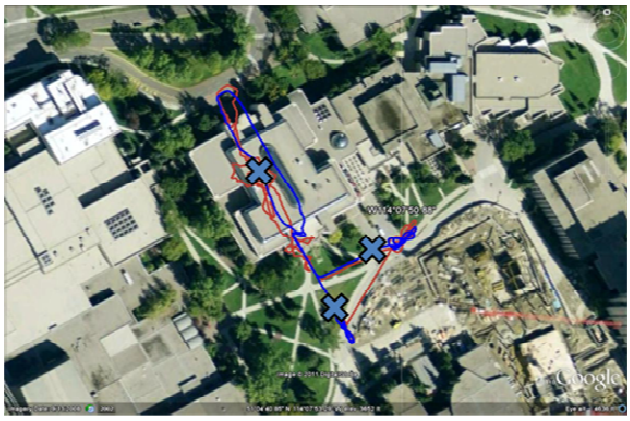

Figure 3.2: Data trajectories (blue line indicates the reference trajectory, red line indicates u-blox trajectory, blue crosses show the static points)

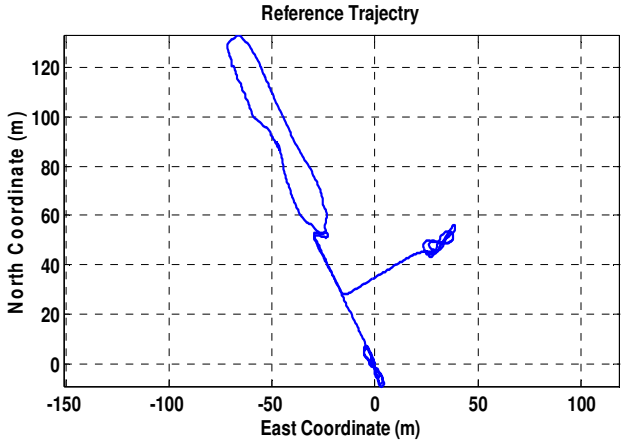

Figure 3.3: Reference trajectory in local level coordinates

A vehicle test with higher velocity will better show the differences between multiple models and the advantage of the proposed algorithm; however the test has been done in pedestrian mode since it is the most common case for the WiFi-enabled hand-held devices like cell phones. The proposed method shows benefits even under minor differences between models. The data collection path is chosen in a way that there exists WiFi coverage along the trajectory.

Figure 3.4: Data collection equipment

The reference trajectory is plotted versus time in the north and east direction in Figure 3.5. The trajectory begins and ends with some figure eight to allow for INS calibration and fine alignment.

There were also several turns along the data collection trajectory that affect the performance of the algorithm in those epochs since the random walk acceleration and constant velocity model is used. The figure eight and turns are circled in Figure 3.5.

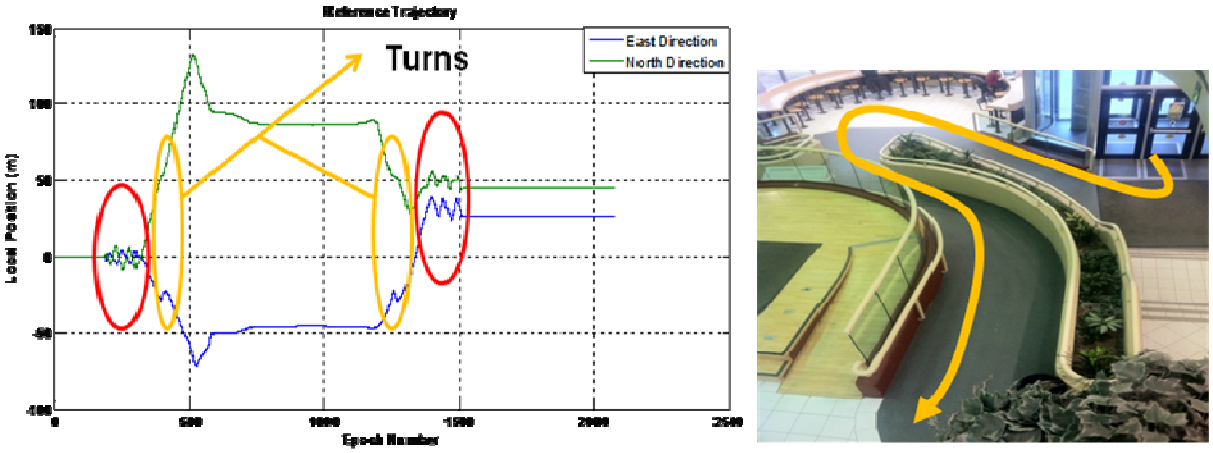

Figure 3.5: Data collection trajectory in north and east direction versus time, turns are circled in yellow color and figure eights are circled in red color; the turn is shown in the right hand picture

The correct contexts as a function of time are shown in Figure 3.6, which has been computed using the reference data and manual time tagging.

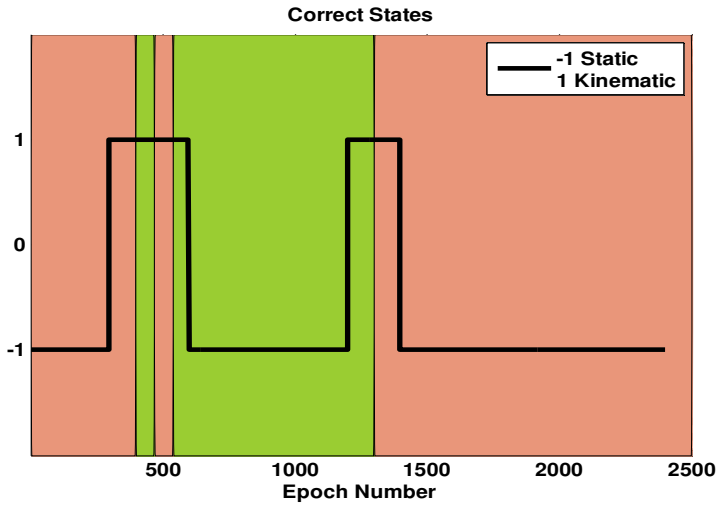

Figure 3.6: Correct sequence of contexts (Pink areas indicate outdoors, green areas indicate indoors)

3.3.1 Performance analysis of the proposed algorithm in the position domain

To analyze the performance of the proposed WiFi-based adaptive MMAE algorithm, first the algorithm is compared to conventional non adaptive Kalman filtering with a kinematic dynamic model. Position errors for both are shown in Figure 3.7.

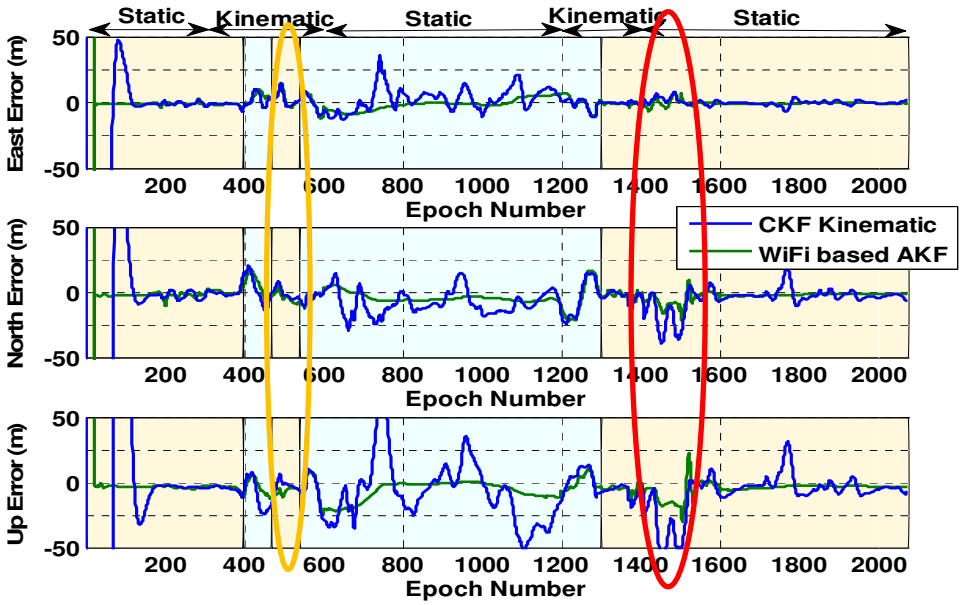

Figure 3.7: Performance comparison of proposed algorithm versus conventional Kalman filtering (CKF) with kinematic model (Yellow oval indicate turn, red oval indicates figure eight; yellow area indicates outdoors, blue area indicates indoors)

Table 3.1: Statistics for performance comparison of the proposed algorithm vs. conventional Kalman filtering with kinematic model

WMMAE CKF	Stat/Outdoor	Kin/Outdoor	Stat/Indoor	Kin/Indoor
RMS E	1.6	3.1	4.0	5.1
(m)	2.1	3.9	9.3	5.4
RMS N	4.4	5.5	5.8	7.1
(m)	9.9	6.8	12.3	11.2
RMS U	6.9	5.4	10.4	7.5
(m)	16.6	9.9	25.9	9.2

Also the correct sequence of contexts is shown through time. It should be noted that performance analysis in this section are given using the correct sequence of contexts.

The proposed algorithm outperforms the conventional KF and shows considerable improvements in terms of positioning errors especially in the indoor environment. In kinematic mode and outdoors the performance differences are lower. This is because in this case both methods use the same dynamic model but still there are improvements according to the adaptation of covariance matrices in the proposed algorithm.

There are larger improvements with the right choice of the model in the static indoors case since the proposed method uses both the adaptation of covariance matrix of the observations and the right dynamic model. The figure-eight motion is better matched to the static model with a larger process noise as opposed to the kinematic model. During turns, the proposed algorithm shows position improvements but these are not as large as for the rest of the test. This can be explained by the fact that the dynamic model used in the algorithm (constant velocity model) is not the best model fit for the turns.

By adding more models to the bank of Kalman filters to cover more differences between models, the algorithm is expected to perform better in more variant types of motions. The statistics of the results are given in Table 3.1.

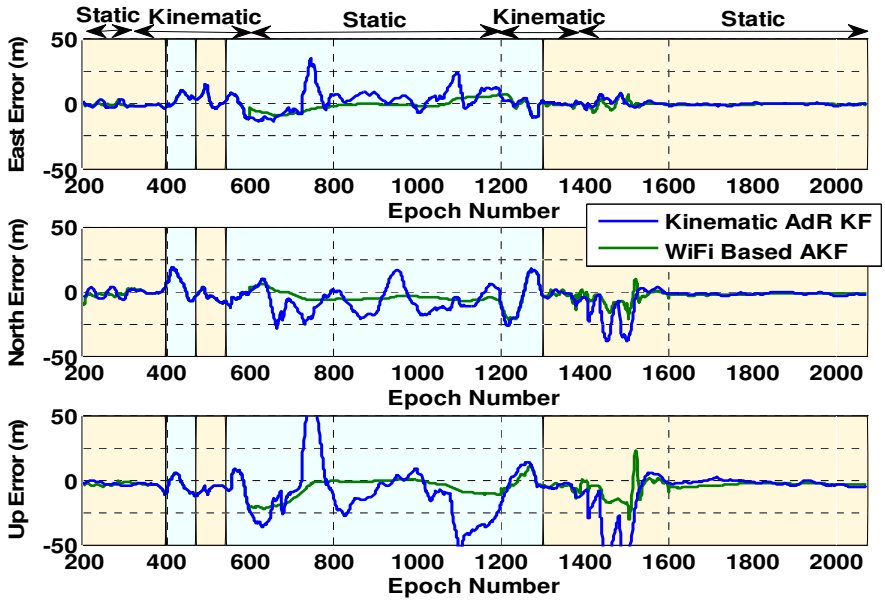

Figure 3.8: Performance comparison of proposed algorithm vs. adaptive R Kalman filtering with kinematic model (Yellow area indicates outdoors, blue area indicates indoors)

Table 3.2: Statistics of performance comparison of the proposed algorithm vs. adaptive R Kalman filtering with kinematic model

WMMAE Vs. AdR KF	Stat/Outdoor	Kin/Outdoor	Stat/Indoor	Kin/Indoor
RMS E	1.6	4.0	4.1	5.1
(m)	1.7	4.0	9.7	5.3
RMS N	4.4	5.5	5.8	11.7
(m)	9.8	5.8	12.6	12.5
RMS U	6.9	5.4	10.4	7.6
(m)	16.7	6.7	25.3	8.9

In Figure 3.8, the proposed algorithm performance is compared to that of the innovation-based estimator kinematic Kalman filter with observation covariance matrix adaptation. Since in the proposed algorithm both the dynamic model and the adaptation parameter are sensitive to the context, the WiFi-based

MMAE algorithm outperforms the conventional adaptive Kalman filtering. The results show that the WiFi-based MMAE algorithm improves the position errors by correctly switching between multiple models (as in static indoors). In kinematic outdoors the model is right for IAE KF but the adapting parameter (R) does not improve the performance. Also note that in kinematic indoors the performance of the two algorithms is very similar since both methods use the same dynamic model and also the same adaptation parameter (observation covariance matrix). The statistics of the results are given in Table 3.2.

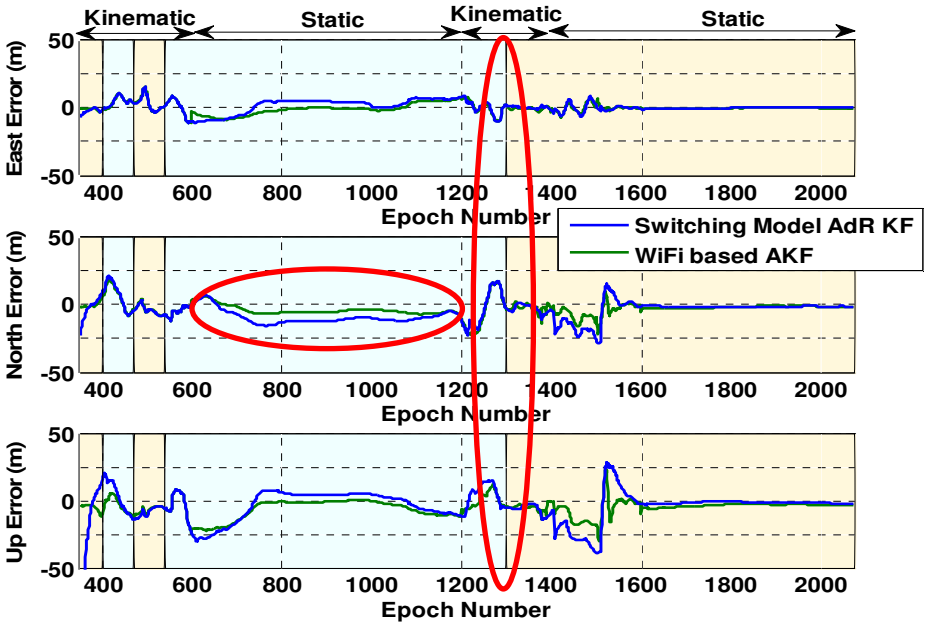

Figure 3.9: Performance comparison of proposed algorithm vs. switching model adaptive *R* Kalman filtering (Yellow area indicates outdoors, blue area indicates indoors)

Table 3.3: Statistics of performance comparison of the proposed algorithm vs. switching model adaptive R Kalman filtering

WMMAE Vs. AdR IMM	Stat/Outdoor	Kin/Outdoor	Stat/Indoor	Kin/Indoor
RMS E (m)	1.6 1.8	4.0 4.8	4.0 5.6	5.3 5.5
RMS N (m)	4.4 8.0	4.3 5.5	5.8 10.6	10.7 10.4
RMS U (m)	6.9 12.6	5.4 7.3	10.4 11.5	7.5 9.4

As mentioned before, the results presented in this section are based on the correct sequence of contexts. To show how switching the adaptation parameters based on external information improves positioning performance of the adaptive Kalman filtering, the performance of the proposed algorithm is compared in Figure 3.9 to that of the multiple model adaptive-*R* Kalman filter where the dynamic model is switched (weighted) as in the proposed algorithm but the difference is that individual Kalman filters perform adaptive *R* IAE Kalman filtering. In this case multiple-model Kalman filtering is used and each individual Kalman filter adapts its *R* matrix. Comparison with adaptive-*R* multiple-model KF shows that performance is very similar for the kinematic motion in indoor environment. This is because both the algorithms use the same model and the same covariance matrix adaptation. However, the modification to the proposed algorithm, which allows the non-matching IAE Kalman filters to adapt their *Q*-matrices, shows considerable improvements in indoor environments where both algorithms use correct dynamic model and the same adaptation parameter. In outdoor environments the adaptation parameter has changed in the proposed model, which results in improvements in terms of positioning errors. This

justifies the constraint-based adaptation of statistical characteristics (Q or R) proposed in the WiFi-based MMAE algorithm.

These results also show implicitly that the proposed method outperforms Interacting Multiple Model (IMM) adaptive Kalman filtering in which the individual KFs are weighted based on Markov chain states. The statistics of the results are given in Table 3.3.

3.4Context identification based on WiFi data

Now that is has been shown that knowing the context is useful, the next question is how accurately can the context be determined based on WiFi RSSI measurements. Simple tests have been implemented to identify contexts based on extracted features from WiFi data. It is of great importance that the tests are designed to effectively distinguish between different modes (indoors/outdoors, static/kinematic) while at the same time they be kept fairly simple to implement.

3.4.1 Identification of Static/Kinematic contexts based on WiFi data

It can be observed that the features (for instance mean and standard deviation of total SNR received) remain approximately constant during the times when the user is static. Therefore in the case of identifying static/kinematic contexts one simple test can be implemented by comparing the feature changes within sliding windows. The window length should be chosen as the smallest value through which the changes are observable. The length of sliding window represents the time within which one can distinguish between switching contexts (static/kinematic). A straightforward WiFi static/kinematic identifier has been implemented based on the standard deviation of average SNRs within sliding windows of length N epochs as

$$\mathbf{std} = \sqrt{\frac{\sum_{i=1}^{N}\left(\mathbf{x}_i - \bar{\mathbf{x}}\right)^2}{\mathbf{N}}} \tag{3.30}$$

where x is the vector of observations within a window of length N. For static mode it can be assumed that

$$\ell = \sqrt{\sum_{i=1}^{N}\left(\mathbf{x}_i - \bar{\mathbf{x}}\right)^2} = \mathbf{Const}. \tag{3.31}$$

so that

$$\mathbf{std} = \ell\sqrt{\frac{1}{\mathbf{N}}} \tag{3.32}$$

Setting the threshold depends on the expected observation standard deviation variations ℓ in the static mode and also the length of the sliding window. For a constant value of ℓ, the higher the window length, the lower the threshold since in this case smaller standard deviation values are expected. By computing the threshold assuming 1.5 dB variations in the standard deviation of the average SNRs within sliding windows of length 10 seconds for indoor environments, the decision threshold will be set to 0.5 dB as it can be seen in Figure 3.10. The window length of 10 s is chosen to allow for at least 95% probability of correct detection. To avoid complexity, the threshold is herein set based on a number of previously collected data sets in the similar environments. The allowed variation is set based on the average value of standard deviations observed for these datasets. The sequence of contexts achieved is plotted in Figure 3.11. Note that at the end of the data collection the Netstumbler and SPAN-LCI system were turned off while the u-blox was still collecting GPS data. So the data lengths are not exactly the same for all data types. The end epochs are considered Static/Outdoor mode for all data types. Using the appropriate threshold gives a decision sequence that is in high agreement with the sequence of correct

contexts. A double sliding window is used to smooth the rapid changes in the identified context sequence.

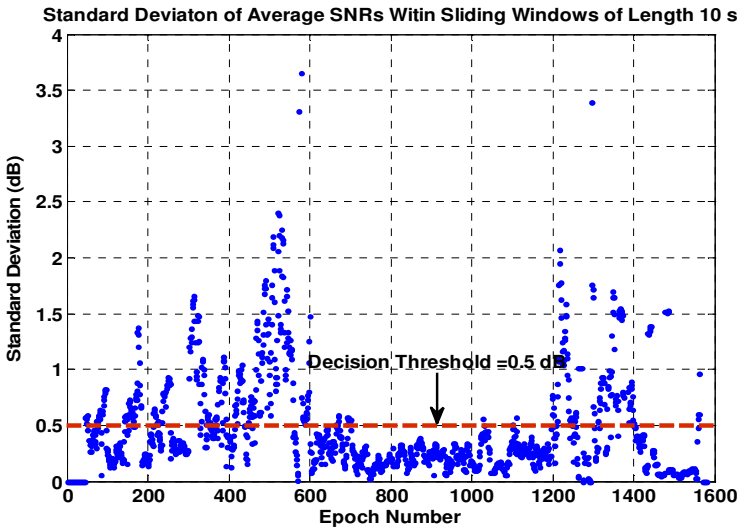

Figure 3.10: WiFi static/kinematic identification based on the standard deviation of average SNRs in dB

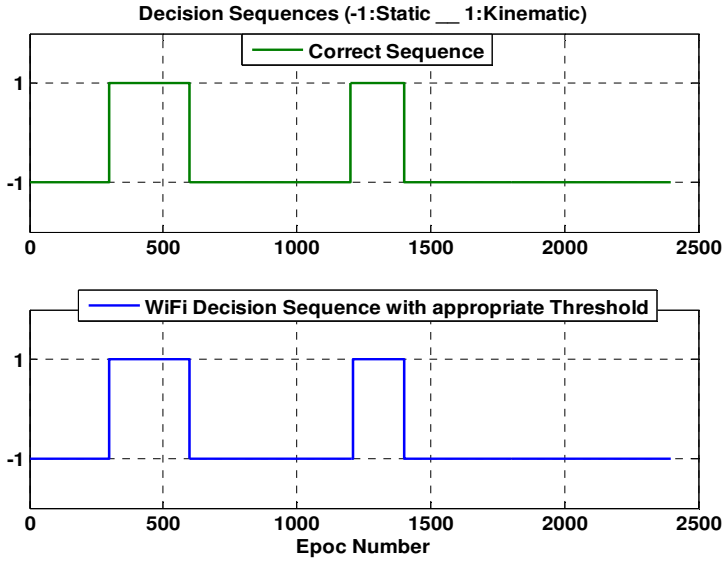

Figure 3.11: Static/kinematic decision sequence based on WiFi data

The threshold and the parameters required can be identified in different ways. One way is to use the known models for the WiFi features in order to come up with the approximate values. However, as explained before, the models developed so far are not very accurate, especially for indoor environments, and change from a specific situation to another. Another way is to use observations from a number of limited training datasets collected in a similar environment. Since low complexity threshold setting methods have been used here, for other new environments a short period of collected data can be used for preliminary setting of the threshold and the parameters, which can then be updated through time for a better accuracy.

Another option could be to set the threshold based on the real time field observations, which may lead to an adaptive threshold setting using the online information based on WiFi features. However, since here the aim is to demonstrate the possibility of using WiFi signals to identify contexts and also to avoid complexity, the threshold is set based on the few available datasets collected during previous research to come up with an approximate value for the test environment. The allowed variation is set based on the average value of standard deviations observed for these few datasets.

Decision procedure can be a soft versus a hard decision process, so that the decision sequence takes the values in the interval [0 1] instead of the binary values of 0 and 1. Herein, the hard decisions are smoothed based on a developed weighting algorithm. This can be considered as an equivalent way to come up with the weights between [0 1] instead of associating the absolute values of 0 or 1 to the contexts. The weighting algorithm will be described in details in Section 3.5.

3.4.2 Identification of Indoors/Outdoors contexts based on WiFi data

Three context identifiers are tested to distinguish between indoor and outdoor environments. The number of available access points (AP) can be considered as a very simple criterion for indoor/outdoor identification since it is expected that the number of indoor APs available exceeds the number available outdoors. However when the outdoor environment is close to indoors the number of available APs is not a good identifier since the outdoor coverage can be nearly as high as that inside. A simple way to overcome this problem is to modify the criteria to the number of available APs with a SNR above some threshold which can be identified offline as the average of the maximum number of APs available indoors and outdoors, defined based on the limited number of datasets. Figure 3.12 shows the threshold as a context identifier using the number of APs with SNR above.

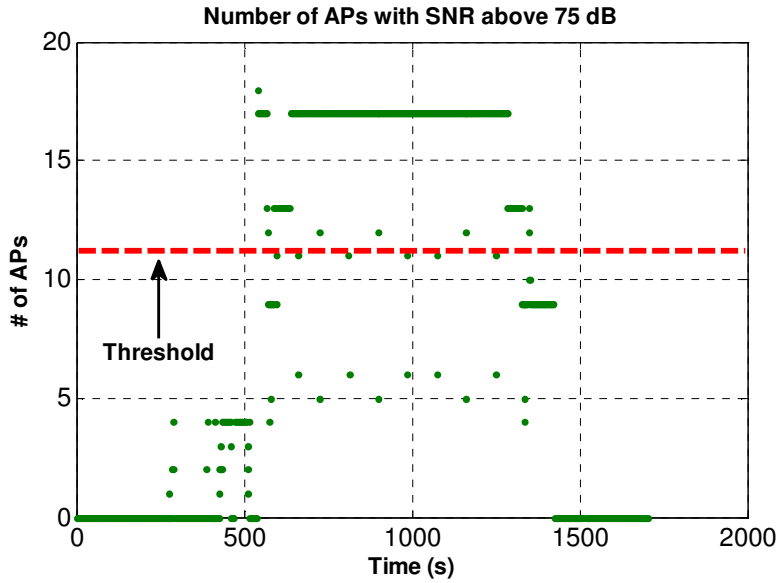

Figure 3.12: Identifying indoors/outdoors situations based on the number of available APs with SNR above 75 dB

The two other criteria used are based on the moving average of the highest SNRs received within a window length of N and the standard deviation of the total SNR received. These were chosen since the average and standard deviation of the received SNR are expected to be of higher values in indoor environments.

In the first method an equal weight moving average with a specific window length is applied to the vector of the 10 highest SNRs observed. So by appropriately setting the thresholds it is expected that one can distinguish between indoors/outdoors contexts using these criteria. Examples are shown in Figures 3.13 and 3.14.

One possible way to determine the threshold offline in a simple and reasonable way in this case is to set the decision threshold based on one set of training data or using a priori knowledge and modeling to obtain the expected values required:

Decision threshold = (Average Static SNR Indoors + Average Static SNR Outdoors)/2

Then the decision threshold can be applied to other datasets to identify context. Using this method the decision sequences obtained from WiFi data are plotted in Figure 3.15.

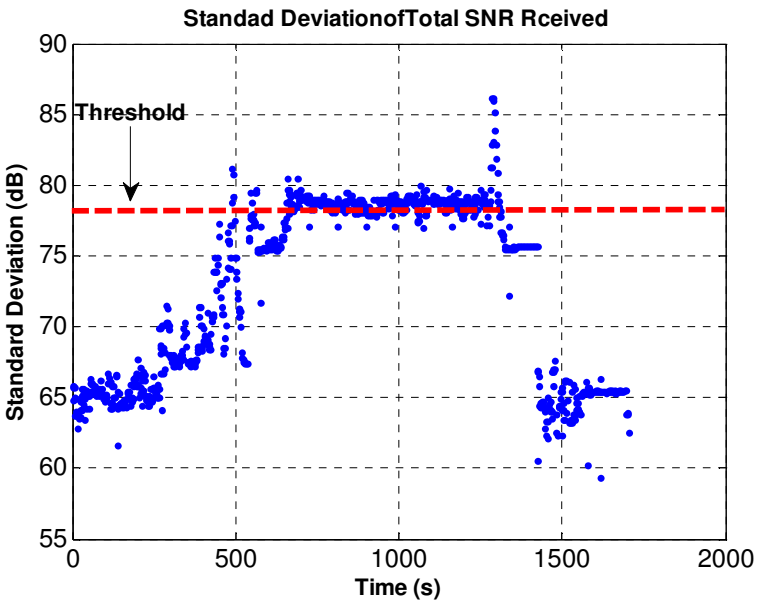

Figure 3.13: Identifying indoors/outdoors based on the standard deviation of the total SNR received

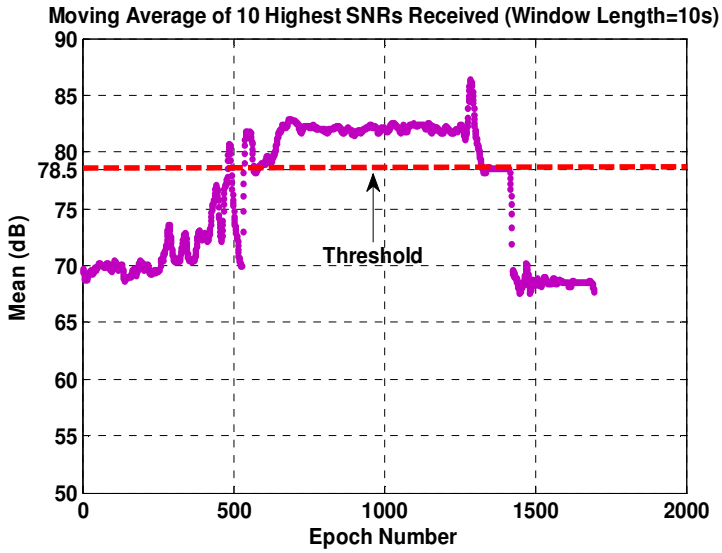

Figure 3.14: Identifying indoors/outdoors based on the moving average of 10 highest SNRs received

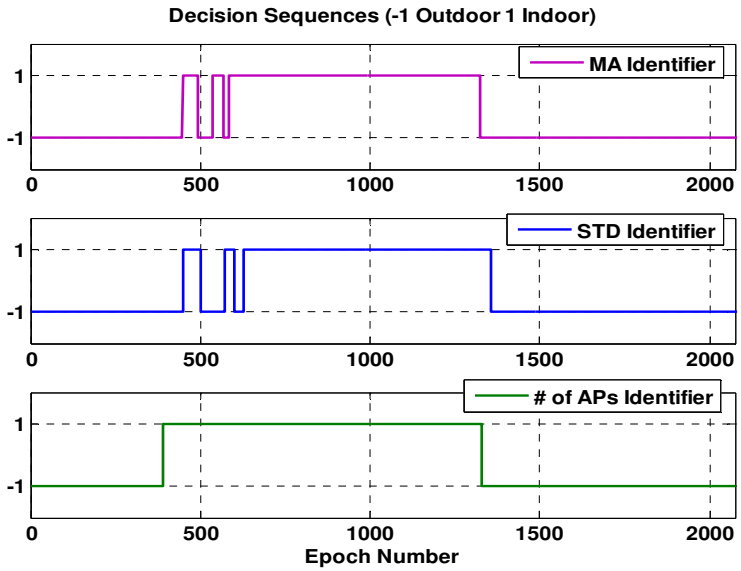

Figure 3.15: WiFi indoor/outdoor decision sequences

The two first decision sequences appear to be correlated since the two identifiers both use received SNR. There are some disagreements in the decision sequences obtained from the different context identifiers.

Also note that as expected, the indoor/outdoor decision sequences have difficulty distinguishing between indoors and outdoors when the user is very close to a building as shown in Figure 3.16.

Figure 3.16: Turn passed while coming out and going back to MacEwan Centre

3.5 DST Decision Fusion Block

The position domain results presented earlier were assuming the correct sequence of contexts, hence a very important factor which affects the performance of the algorithm is the probability of the correct identification and how well one can determine and distinguish different modes. The combination of the context identifiers can result in more reliable decisions under different situations. More reliable decisions result in the improvement of system performance.

To combine the different decision sequences in an effective and reasonable manner, the DST-based decision fusion is proposed. The Dempster-Shafer theory is a generalization of the Bayesian theory in which instead of requiring probabilities for each decision, belief functions are used to combine the decision sequences.

A function $bel: 2^{\Omega} \to [0,1]$ is a belief function if and only if (Murphy 2000, Richards & Jia 2007)

$$
\begin{aligned}
&(B_1)\ \ bel(\varnothing) = 0 \\
&(B_2)\ \ bel(\Omega) = 1 \\
&(B_3)\ \ for\ all\ \mho_1, ..., \mho_n \subseteq \Omega, \\
&\qquad bel(\mho_1 \cup ... \cup \mho_n) \geq \sum_{I \subseteq \{1,...,n\}} (-1)^{|I|+1} bel(\bigcap_{i \in I} \mho_i)
\end{aligned}
\tag{3.33}
$$

The idea is to obtain degrees of belief for one decision from subjective probabilities for a related question and then use Dempster's rule for combining these degrees of belief. This is a generalization of Bayesian theory to deal with uncertainties.

A function $m: 2^{\Omega} \to [0,1]$ is a mass function if and only if (Murphy 2000, Richards & Jia 2007)

$$(M_1)\ m(\varnothing) = 0$$
$$(M_2)\sum_{\mho\subseteq\Omega} m(\mho) = 1 \tag{3.34}$$

and can be written as

$$bel(\mho) = \sum_{O\subseteq\mho} m(\mathrm{O}) \tag{3.35}$$

Dempster's combination rule states that if m_1 and m_2 are mass functions their combination is denoted as $m_1 \oplus m_2(\mho)$ and

$$m_1 \oplus m_2 \oplus \ldots \oplus m_N(\mho) = c \sum_{Q_{ri};\bigcap_{i=1}^{N} Q_{ri}=\mho} \prod_{i=1}^{N} m_i(Q_{ri}) \tag{3.36}$$

where c is a normalizing constant.

The normalization constant is necessary to account for "leaks". Sometimes $O \cap C = \varnothing$, but $m_1(\mathrm{O})m_2(C) > 0$, due to the fact that $(M1)$ should be satisfied so that

$$c = (1 - \sum_{Q_{ri};\bigcap_{i=1}^{N} Q_{ri}=\varnothing} \prod_{i=1}^{N} m_i(Q_{ri}))^{-1} \tag{3.37}$$

It can be shown that this theory fails under high conflicts and does not take into account the correlations between the decisions. Hence a modified DST is used herein by introducing reliability factors and correlation coefficients to the algorithm. To deal with the correlative decisions, correlation coefficients ρ are introduced to the basic formula as

$$m_1 \oplus m_2 \oplus \ldots \oplus m_N(\mho) = c \sum_{Q_{ri};\bigcap_{i=1}^{N} Q_{ri}=\mho} \prod_{i=1}^{N} (1 - \rho_{1,\ldots,i}) m_i(Q_{ri}) \tag{3.38}$$

For simplicity the correlation coefficients are assumed to be known in advance, which is not an unrealistic assumption since the information of criteria used to design different identifiers are supposed to be available, which is the case here.

For combining two identifiers $m_1 \oplus m_2 \oplus ... \oplus m_N(\mho)$ simplifies to

$$m_1 \oplus m_2(\mho) = \frac{1-(1-\lambda m_1(\mho))(1-\lambda m_2(\mho))}{\beta} \tag{3.39}$$

where

$$\lambda = mass\ factor = \frac{1-\rho_{1,2}}{1-\rho_{1,2}/2} \tag{3.40}$$

and β can be considered as a sample space contraction as

$$\beta = sample\ space\ contraction = \frac{(1-\rho_{1,2}/2)^2}{1-\rho_{1,2}} \tag{3.41}$$

In addition, under conflict conditions, the DST theory fails. To deal with this problem it is proposed to introduce reliability factors to the combination algorithm and associate reliability factors r_i to different context- identifiers. The reliability coefficients can be treated as a priori known information or can be determined adaptively in an online manner (as an example the MDP-based control block can be used to determine the reliability coefficient of the context identifiers based on the amount of correction implied in the decision sequences) as

$$m_1 \oplus m_2 \oplus ... \oplus m_N(\mho) = c \sum_{Q_{ri};\bigcap_{i=1}^{N} Q_{ri}=\mho} \prod_{i=1}^{N} (1-\rho_{1,...,i}) r_i m_i(Q_{ri}) \tag{3.42}$$

To analyze the performance of the proposed decision fusion block to combine different decision sequences under correlation and conflicts, the three decision sessions obtained by three indoor/outdoor WiFi identifiers previously are combined using the regular DST theory and the modified DST theory to take into account the correlation between the decision sequences.

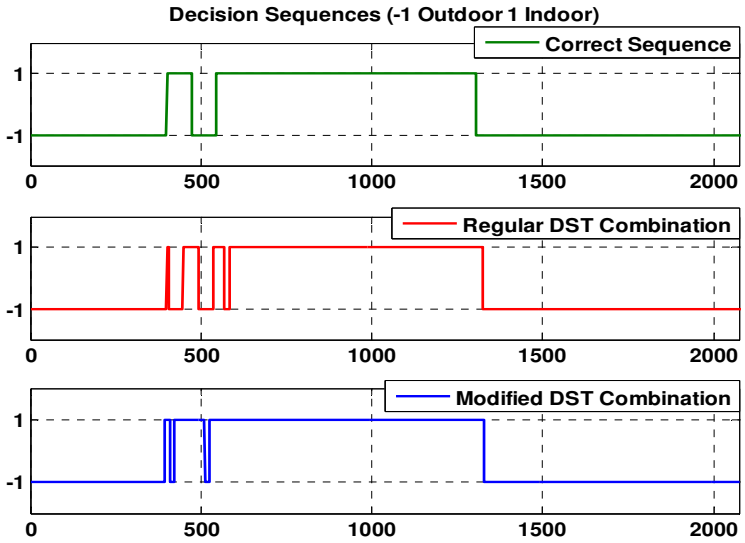

Figure 3.17: DST-combined decision sequences using regular and modified algorithms

The result is shown in Figure 3.17. By introducing correlation coefficients to deal with correlated decisions, the weight given to the correlated decisions is modified so that in incorrectly identified contexts the effect of higher number of identifiers selecting the incorrect mode is reduced. In other words, the agreements between three sequences will be highlighted, while in disagreements the weights will be more fairly and reasonably distributed in comparison to the regular DST.

The correlation coefficient of the two correlated decision sequences is 0.8 in this case. Using the achieved sequences from two decision blocks (regular and modified DST) as shown in Figure 3.17, the performances of the WiFi-based MMAE algorithm in the positioning domain using two methods for combining the decision sequences are compared in Figure 3.18. The use of the modified DST algorithm improves the performance of the proposed algorithm for epoch number where decision sequences are different (around epoch numbers 400 to 600) in terms of position error.

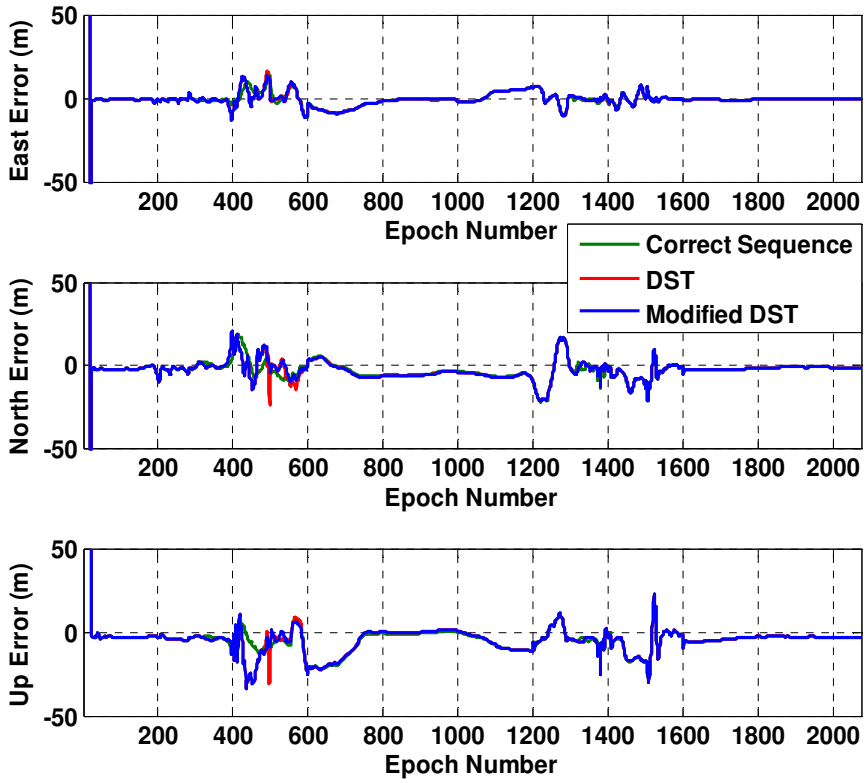

Figure 3.18: Performance comparison of the proposed algorithm using the regular and modified DST methods

Further discussion on the performance of the DST-based decision fusion block to handle the high conflict situations can be found through an example in the next part.

3.5.1DST-based decision fusion block performance under conflicts: an example

One of the applications of the proposed DST-based decision fusion block is combining the different decision sequences from context identifiers, which do not use the same source of external information. Examples include the use of IMU systems or GNSS signal power to identify the context. Although, it should be mentioned again that the goal of this research is to show how effectively WiFi signals can distinguish between contexts and not to use other sources of information to identify contexts. However, obviously a combination of different context identifiers can be used to improve the performance. Since the external information sources are supposed to be different in this case, the conflicts between the sequences may arise as a problem. As a simple example to elaborate how the proposed algorithm can be used in such situations, the decision sequence, obtained from velocity magnitude, is used as an alternative context identifier to determine static/kinematic modes (Figure 3.19). The threshold is chosen to be 0.2 m/s to distinguish between static and kinematic modes. Since this research is not about using IMU data to come up with the decision sequence, the case introduced here is just considered an example for further applications of the proposed decision fusion block and to analyze the performance of the modified DST block under conflicting decision sequences.

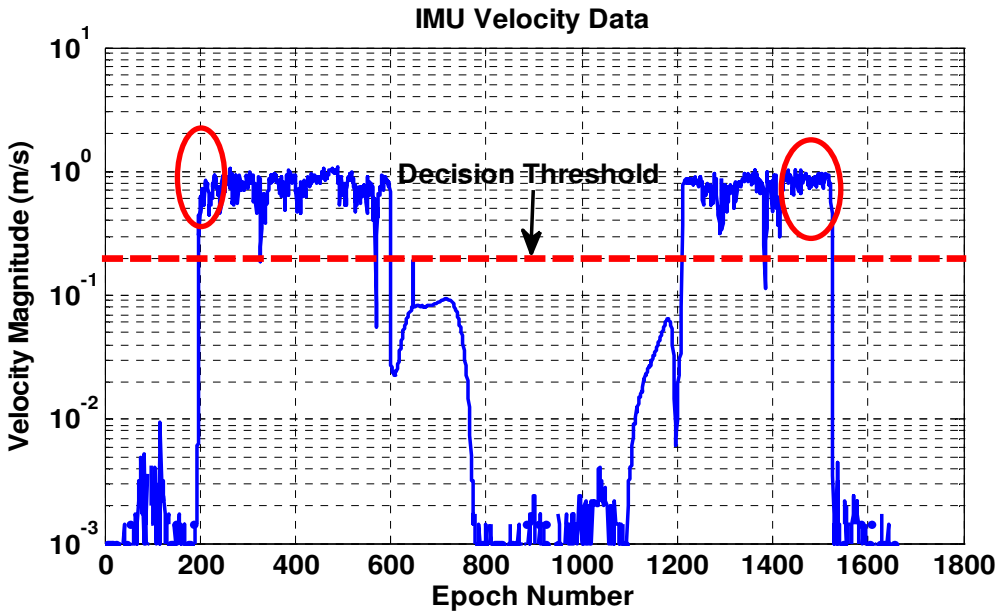

Figure 3.19: Velocity magnitude based on IMU data, red circles showing the conflicts with the correct sequence of context (kinematic/static)

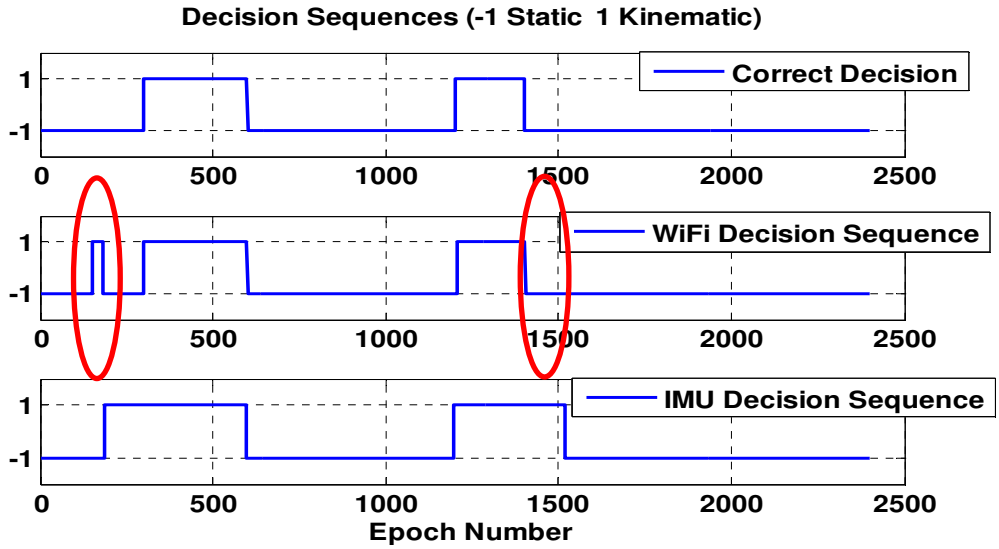

Figure 3.20: Static/kinematic decision sequences for WiFi and IMU context identifiers with the conflict areas are shown by red circles

In Figure 3.20, the resulting decision sequences and the conflict areas are shown. As it is also indicated in Figure 3.19, obviously the figure-eight motion is identified as kinematic mode in the decision sequence based on the IMU velocity magnitude while in the WiFi-based decision sequence, it is mostly

identified as static mode. Figure-eights are used for the calibration part. However, these parts of data are still considered in the processing in order to demonstrate how the developed algorithm deals with different types of motion and how the model uncertainties affect the performance. For figure-eight motion, using a static model with large process noise gives better performance in comparison to modeling with the kinematic model used herein. Hence, according to the fact that the figure-eight motion is a better fit in Kalman filtering with the static model, WiFi data can be considered to be more reliable in this sense. Assuming that this knowledge is used to define the reliability factors as a priori known information, the resulting decision sequences from combining two sequences of context identifiers are shown in Figure 3.21, using both regular and modified DST algorithms. In this special case, for combining the decisions, the reliability factors are introduced to the algorithm so that WiFi decision sequence is considered more reliable for identifying kinematic while a higher reliability factor is given to the IMU decision sequence for static context identification.

The performance of the proposed algorithm is analyzed in the positioning domain using the combined sequence from regular DST (with no reliability factors) and modified DST in Figure 3.22. As it can be seen the modified DST gives closer sequence to the correct sequence and results in the performance improvement of the proposed algorithm in terms of positioning error.

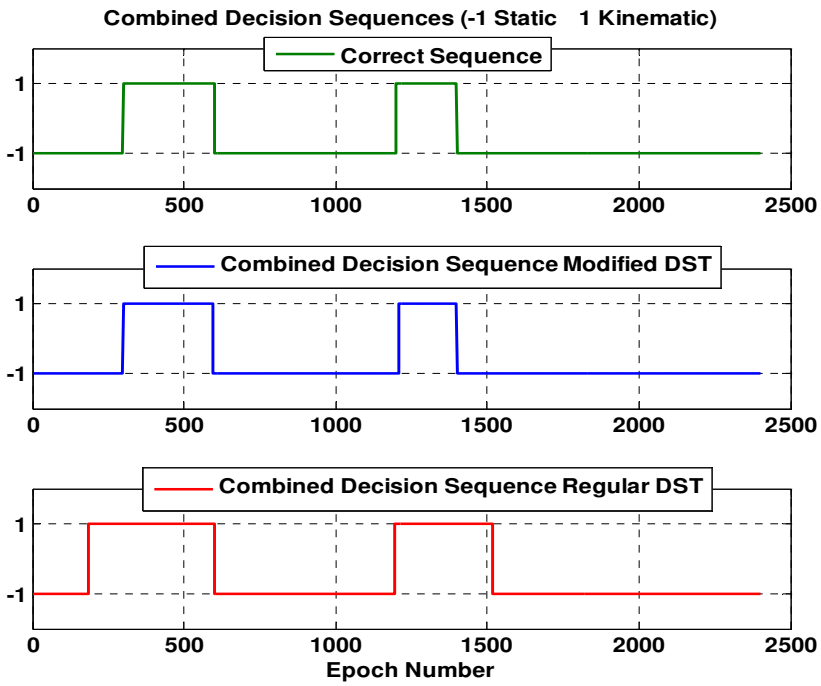

Figure 3.21: Combined decision sequences with regular and modified DST algorithms

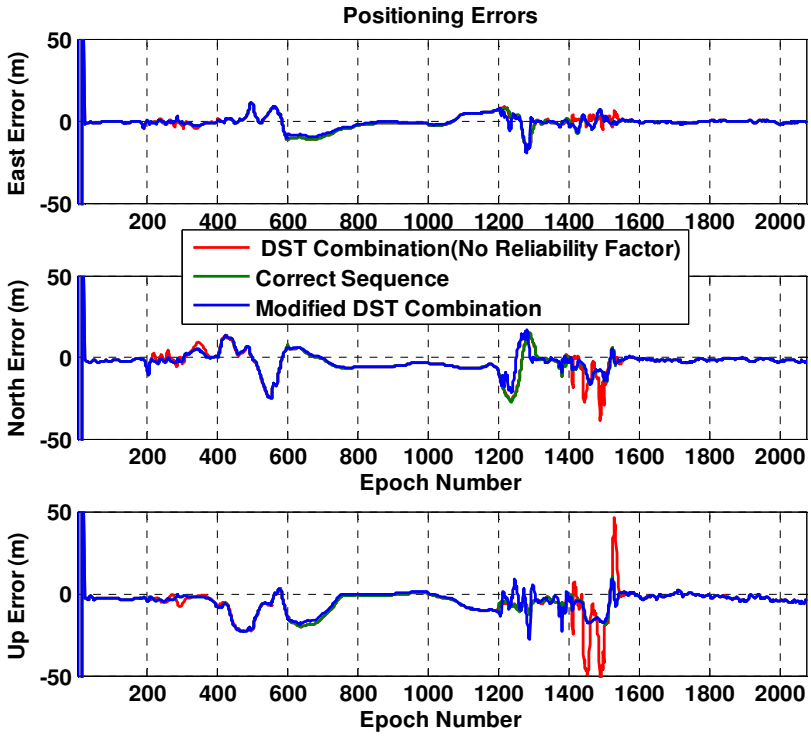

Figure 3.22: Performance analysis of the propose algorithm using the regular and modified DST algorithms

3.6 Weighting Block

In order to achieve a more robust performance a weighting block has been developed. On the one hand, the weights should not change abruptly since in this way the algorithm will be very sensitive to the errors in decision, on the other hand there shouldn't be long delays to update the weights when the state (static/kinematic) is actually changed since that will degrade performance of the developed algorithm. By assigning appropriate weights, a threshold should be kept between delays of the system to respond to a new detected state and system tolerance for abrupt changes based on WiFi decision errors.

Generally speaking, if WiFi identifies the context to be the same over longer period of time, it is more probable that the context has been identified correctly. Regarding the above, the weighting scheme is

developed to determine the weights with respect to the probability of detection (correct decision) of WiFi decision block in a way that they evolve with time according to the consecutive number of epochs for which the same state is decided by WiFi decision block. The weighting block is implemented by a simple KF for a known probability of correct decision on each context. For more elaboration, the performance of the WiFi-based MMAE algorithm has been tested by associating constant weights to individual Kalman filter outputs based on the probability of correct decision (which is considered to be known a priori in this case for simplicity of discussion). As an illustrative example, Figure 3.23 shows the positioning errors of the proposed algorithm with constant weighting scheme with high probabilities of correct decisions and for a static data set. This shows that the direct use of the probability of correct decision to weigh filter outputs is not effective even for high probabilities of detection.

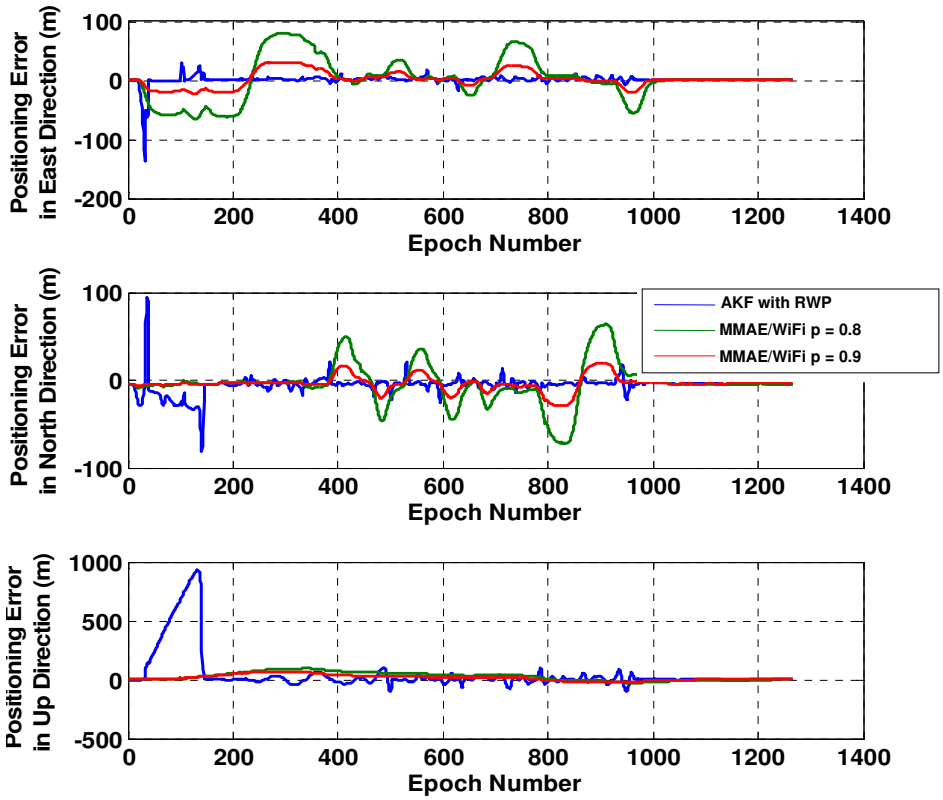

Figure 3.23: Positioning errors of the proposed algorithm with constant weighting scheme using probabilities of correct decision of 0.8 and 0.9

If the weights are fixed based on the probability of correct decision of the WiFi, since the output is the weighted sum of individual filter outputs, still a relatively high weight will be given to the estimates using the wrong model as well as more accurate models. This results in higher positioning errors as it can be seen in Figure 3.23.

The weighting block has been developed based on a simple Kalman filtering algorithm. The state of the Kalman filter determines the dynamic model of the system as

$$w = State\ of\ \ WiFi\ KF = KF\ \ with\ RWP\ \ weight = \begin{cases} 0 KF\ \ with\ RWV \\ 1 KF\ \ with\ RWP \end{cases} \tag{3.43}$$

If the final state estimate is 1, the dynamic model is RWP, otherwise for 0, the RWV model is applied.

The observation vector comes from the WiFi decision sequence where 1 represents RWP and -1 represents RWV dynamic model:

$$z = observation\ given\ by\ WiFi = \begin{cases} 1KF\ \ with\ RWP \\ -1KF\ \ with\ RWV \end{cases} \tag{3.44}$$

The weights are then defined based on the probability of correct decision, P_{corr}, as

$$P = Observation\ Covariance\ Matrix\ and\ \ Weight = \frac{1}{(\frac{1}{2} - P_{corr})^2} \tag{3.45}$$

The weights are defined in a way that when P_{corr} = 0.5, the variance of the observation is set to infinity (a large value) which means that no changes will be implied according to the new observations in this case. This is because P_{corr} = 0.5 represents a totally random decision sequence.

The design matrix is also defined based on the probability of correct decision as

$$H = design\ matrix = P_{corr} \tag{3.46}$$

The dynamic model used in this Kalman filter is a random walk position in this case as

$$w_{k+1} = w_k + Noise \tag{3.47}$$

and the transition matrix can be written as

$$F = 0, \Phi = 1 \tag{3.48}$$

The observation model is also given as

$$z_k = H_k x_k + v_k \tag{3.49}$$

Then a weight mapping is used to limit the output state of the Kalman filter within the interval [0 1]. To be more specific we want the final estimate to be between 0 and 1 while the output of the Kalman filter is in the range of [-∞ ∞]. The state is the weight given to the KF with the RWP model (near static model):

$$Weight = Weight\ Mapping = 1 - e^{-w_k^2} \tag{3.50}$$

The performance of the developed weighting block and how the weights evolve with time are shown in Figure 3.24.

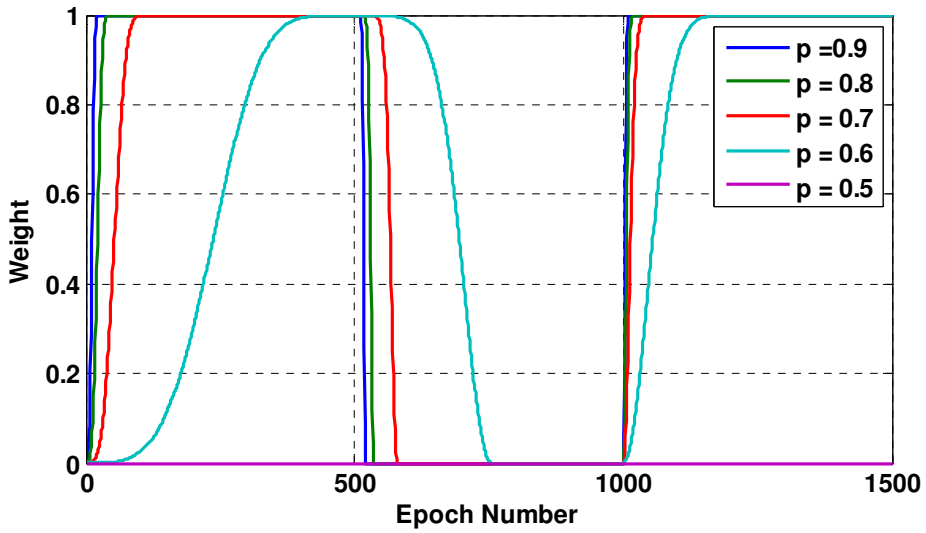

Figure 3.24: Associating weights (to RWP model) using different probabilities of correct decision using the developed weighting block

This plot shows the KF/RWP weights for different probabilities of detection. When the probability of detection increases, the delay before switching to new mode increases as well. This is reasonable since in this case we have more confidence in the external data (WiFi decision).

Having a probability of 0.5 means that the model is chosen on a complete random basis, i.e. no external information is available. To deal with this situation the weighting scheme is developed such that the KF with the random walk acceleration dynamic model is used for better tracking if the model is incorrectly chosen (in comparison to the random walk velocity dynamic model). If p=0.5, i.e. no external information is available, all the weights goes to KF/RWV output since there is a better chance that it tracks the RWP model in case of a wrong model. In this case one has:

$$\text{weight}_{KF/RWV} = 1 - \text{weight}_{KF/RWP} \tag{3.51}$$

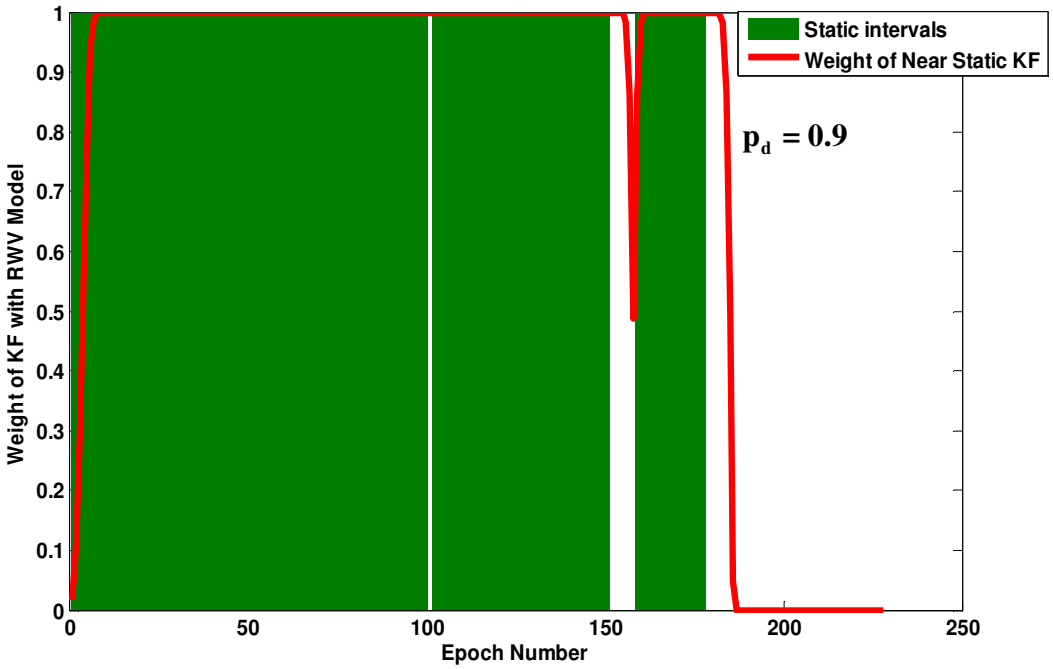

Figure 3.25: Performance of the developed weighting block to respond to abrupt changes in context sequence for P_d=0.9

Figure 3.25 shows how the weighting scheme reacts to abrupt changes of context where green areas represent the intervals when user is static and white areas when the user is kinematic. If the transition between contexts (based on WiFi decision) is fast, the algorithm avoids immediate switching to a

different model as there is high risk that the decision was made incorrectly. On the other hand when a specific mode is detected consecutively for a relatively long period of time the weight to the right model approaches 1. Hence, abrupt changes are ignored as shown in the plot. Weights are set to final values after passing 10 epochs and the delay is adjustable via KF parameters.

3.7 MDP Control Block

The control block is an optional block that can be added when higher robustness is required. The control block is based on the type 2 finite-state Markov Decision Process (MDP) that has been implemented with regard to the reward history in which a reward is realized based on the one-step transition between identified contexts in two consecutive epochs.

The reward function can be determined based on the output of the individual Kalman Filters to modify the final decision sequence and the model probabilities.

The use of the control block will increase the robustness of the system and reduce the sensitivity of the algorithm to false identifications in case of high uncertainties and with low reliability in the decision sequence (an example could be in places where no or a very poor WiFi coverage is available). Also the control block can be used to determine the reliability coefficient of the context identifiers based on the amount of correction implied by the decision sequences.

In brief the decision sequence was only based on WiFi so far and now by adding the control block, the information of how well each individual model fits the actual situation will now be used to come up with the final decision sequence. The basic idea of the Markov Decision Process (MDP) can be introduced as follows. An MDP considers a state space X and an action space A. At time epoch t, the state is denoted

as x_t and the action is a_t. The average reward function can be defined as a function of the action sequence at specific states as (Cao & Guo 2007)

$$\bar{r}(x_t, a_t) = \int r(x_t, a_t, x, u) P(dx \mid x_t, a_t) \mu_w(du \mid x_t, a_t) \tag{3.52}$$

where $\mathbf{a} = \{a_0, a_1, \ldots\}$ is the action sequence and $P(dx \mid x', a)$ is the state transition law when an action a is taken at state x'. $r(x_t, a_t, x, u)$ is a reward (cost) function. $\mu_w(du \mid x_t, a_t)$ is assumed to be the distribution law for the reward disturbance process. For any action sequence and initial distribution p_0, the average performance can be determined as (Cao & Guo 2007)

$$J(p_0, \mathbf{a}) := \lim_{N \to \infty} \sup \frac{\sum_{t=0}^{N} E[\bar{r}(x_t, a_t)]}{N+1} \tag{3.53}$$

Then a discounted performance can be defined as

$$V_\beta(p_0, \mathbf{a}) := \sum_{t=0}^{\infty} \beta^t E[\bar{r}(x_t, a_t)], \qquad 0 < \beta < 1 \tag{3.54}$$

where β is the discount factor. Here the reward function is defined for one-step transition between states as

$$Type\,2: q_i = E[g(X_n, X_{n+1}) \mid X_n = i] = E[g(i, X_{n+1}) \mid X_n = i] = \sum_{j \in E} g(i, j)\, p(i, j) \tag{3.55}$$

where $g(i, j)$ is the one step transition gain and $p(i, j)$ is the one-step transition probability. An optimum decision strategy (policy) is estimated so that the expected reward (performance measure) is maximized.

The transitions are controlled by both transition probabilities and reward history and a policy iteration method is used to find the optimum policy via two procedures of value-determination and policy-improvement which can be explained mathematically as follows:

$$\begin{aligned} &Value-\det er\min ation\ \ procedure: \\ &\mathbf{v}=\mathbf{B_0 q}\approx[\mathbf{I}+\mathbf{P}+...+\mathbf{P}^{s}+(s+1)\mathbf{P_0}]\mathbf{q} \quad where\ \mathbf{P}_0=\lim_n \mathbf{P}^n \end{aligned} \tag{3.56}$$

where q is the vector of next period expected gains and P is the transition matrix and $\mathbf{P}_0=\mathbf{P}_\infty$. Then for policy improvement procedure, one can write (Courcoubetis & Yannakakis)

$$\begin{aligned} &Policy-improvement\ \ procedure: \\ &g+v_i=q_i+\sum_j p(i,j)v_j \\ &we\ seek\ to\ improve\ policy\ d\ \ by\ \ selecting\ \ policy\ d^*=a_{ik}^*,\ to\ satisfy: \\ &q_i^*+\sum_j p_{ij}^* v_j=\max\{q_i(a_{ik})+\sum_j p_{ij}(a_{ik})v_j\ \ ;a_{ik}\in A_i\} \qquad 1\le i\le M \end{aligned} \tag{3.57}$$

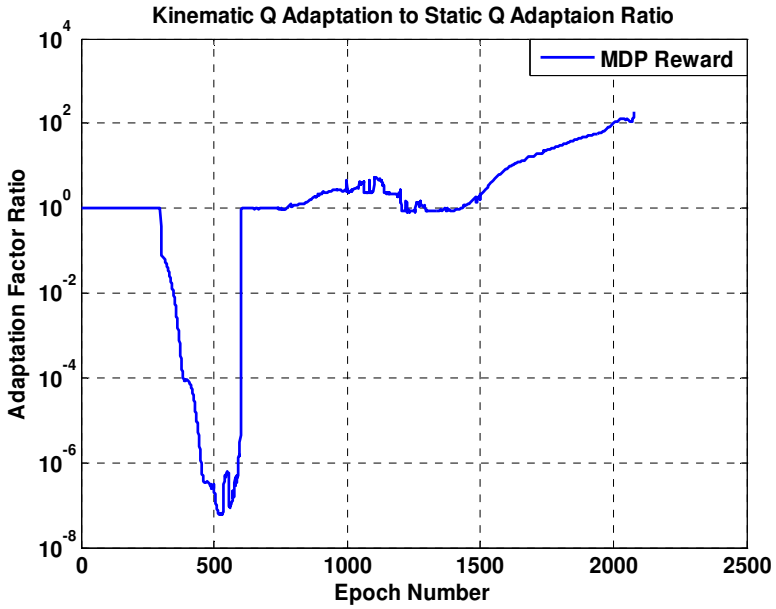

Figure 3.26: Reward function

The reward function is defined herein based on the ratio of the amount of adaptation (trace of the process noise matrix) of two different models (kinematic *Q* adaptation to static *Q* adaptation ratio) as in Figure 3.26. In other words the information that is used from the individual Kalman filters is how well the dynamic models fit to the actual mode of the system. A lower amount of adaptation in one dynamic

model compared to the other dynamic model could be considered as a criterion to conclude that the model is better fitting to the actual mode.

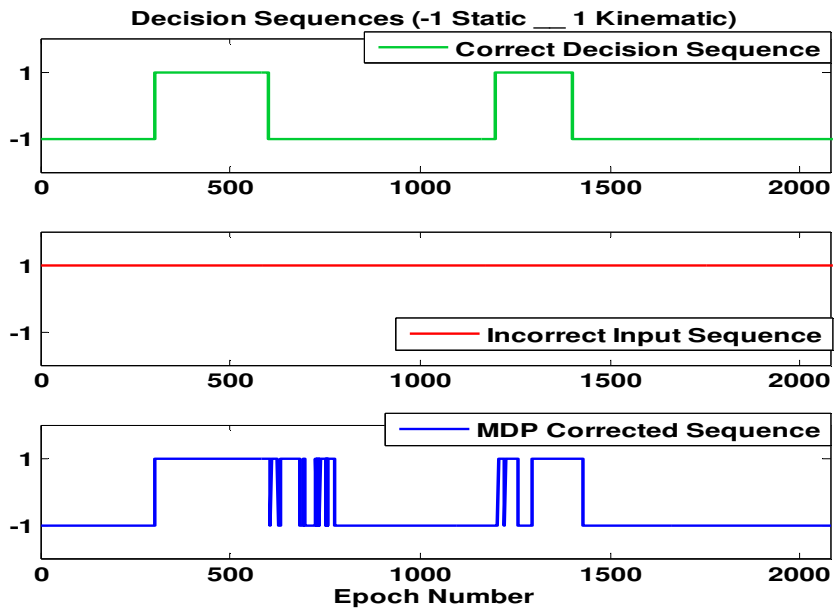

Figure 3.27: MDP corrected decision sequence for a totally corrupted sequence; a 29% match sequence is corrected to an 86% match sequence, which means having about 60% improvements

The performance of the MDP control block can be demonstrated in terms of the amount of correction it implies for the incorrect sequence. Two cases are considered: one is how the MDP block corrects a totally incorrect sequence where all the states are identified as kinematic. This can be the case where the WiFi context identified totally fails (e.g. there is no WiFi coverage) and the decision sequence is totally corrupted. The other case is the performance of the MDP control block with the collected real data; for this case the threshold of the WiFi identifier is chosen in a way where it shows a larger difference from the correct sequence. Considerable improvements are achieved in both cases as shown in Figure 3.27 and 3.29. The improved context identification also aids positioning performance as shown in Figure 3.28 and 3.30.

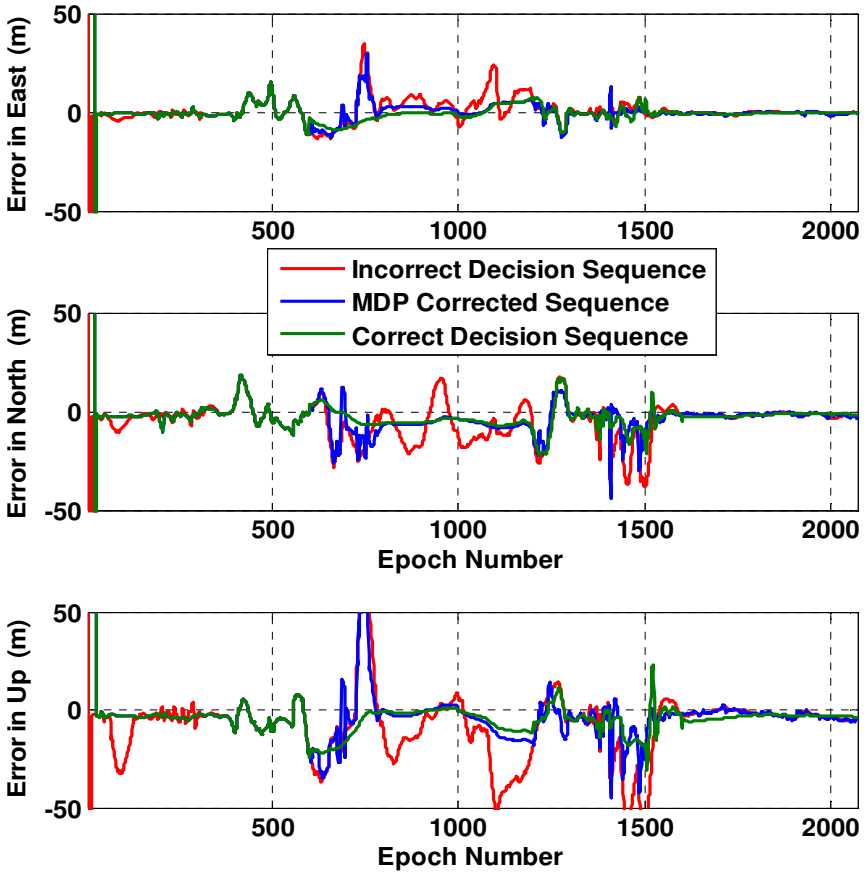

Figure 3.28: Performance analysis of proposed algorithm using the MDP control block with a totally corrupted sequence

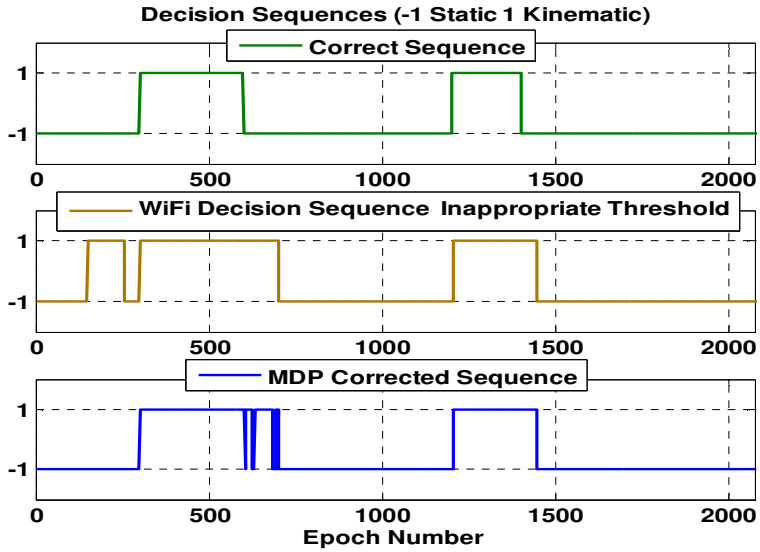

Figure 3.29: MDP corrected decision sequence for a WiFi sequence based on inappropriate threshold; an 87% match sequence is corrected to a 94% match sequence which means having a 49.8% improvement

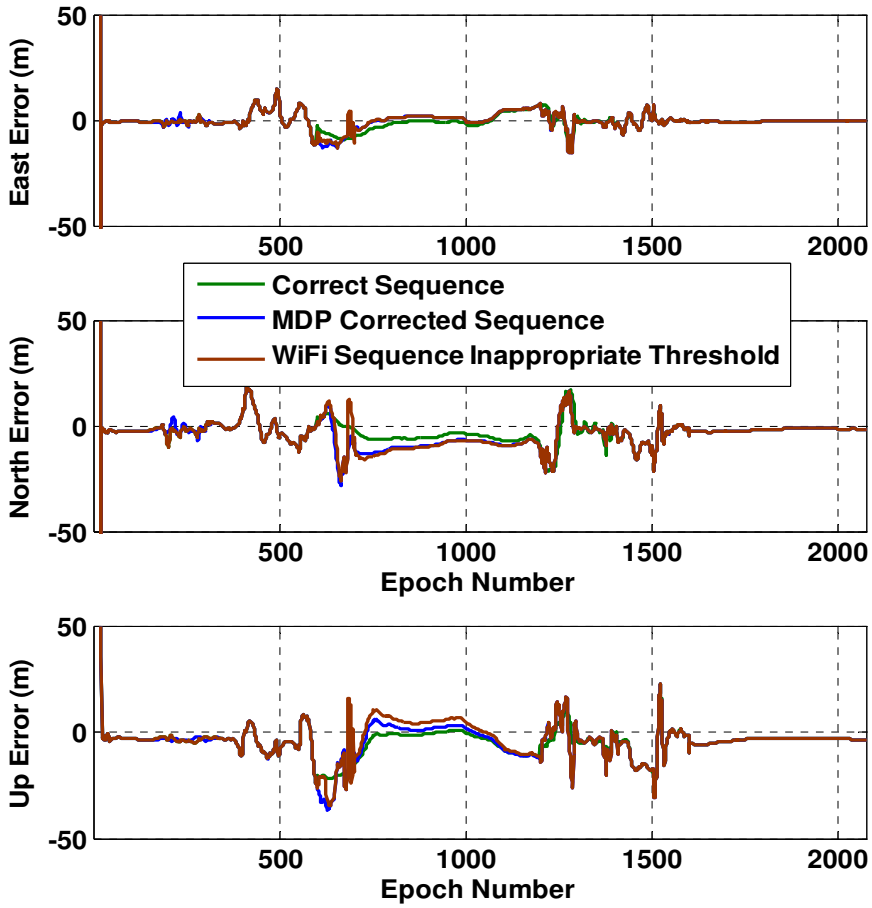

Figure 3.30: Performance analysis of the proposed algorithm using the MDP control block with a WiFi sequence based on an inappropriate threshold

3.8 Proposed Algorithm with Constrained Single Model Kalman Filter

It is also possible to replace the bank of Kalman filters in the proposed algorithm with a single kinematic Kalman filter and a velocity constraint that is activated by the static/kinematic decision sequence. The decision sequence and identified states are used to apply a zero velocity constraint to the single model Kalman filter. The zero velocity constraint consists of additional velocity observations in each direction with a variance of 0.001 $(m/s)^2$.

In the kinematic model filter the state vector and the observation vector are

$$X = \left[X_E \; X_N \; X_U \; V_E \; V_N \; V_U \; dt \; \dot{dt} \right]^T \tag{3.58}$$

$$Z = \left[Z_1 \; Z_2 \; Z_3 \cdots Z_N \right]^T \tag{3.59}$$

In the static model by implying the zero velocity constraint in ENU coordinates, the observation vector can be written as

$$Z = \left[Z_1 \; Z_2 \; Z_3 \cdots Z_N \; 0 \; 0 \; 0 \right]^T \tag{3.60}$$

The measurement noise covariance matrix and the design matrix are modified as

$$\mathbf{R}^{Static}_{(N+3)\times(N+3)} = \begin{bmatrix} \mathbf{R}^{Kinematic}_{N\times N} & \mathbf{0}_{N\times N} \\ \mathbf{0}_{N\times N} & \mathbf{R}^{Augmented\ Obs.}_{3\times 3} \end{bmatrix} \tag{3.61}$$

$$\mathbf{H}^{Static}_{(N+3)\times 8} = \begin{bmatrix} \mathbf{H}^{Kinematic}_{N\times 8} \\ 0\;0\;0\;1\;0\;0\;0\;0 \\ 0\;0\;0\;0\;1\;0\;0\;0 \\ 0\;0\;0\;0\;0\;1\;0\;0 \end{bmatrix} \tag{3.62}$$

The performance of this approach is compared with the MMAE algorithm in Figure 3.31. The two methods perform similarly. However the multiple-model outperforms the constraint method, particularly in the vertical direction. This can be explained by the fact that turning on the constraint may result in locking a position error into the system, which could be moderated by improving the weight associated with the constraints. This means that the performance of the single model method is expected to approach and get closer to the multiple model method by improving weighting of the constraints in the algorithm.

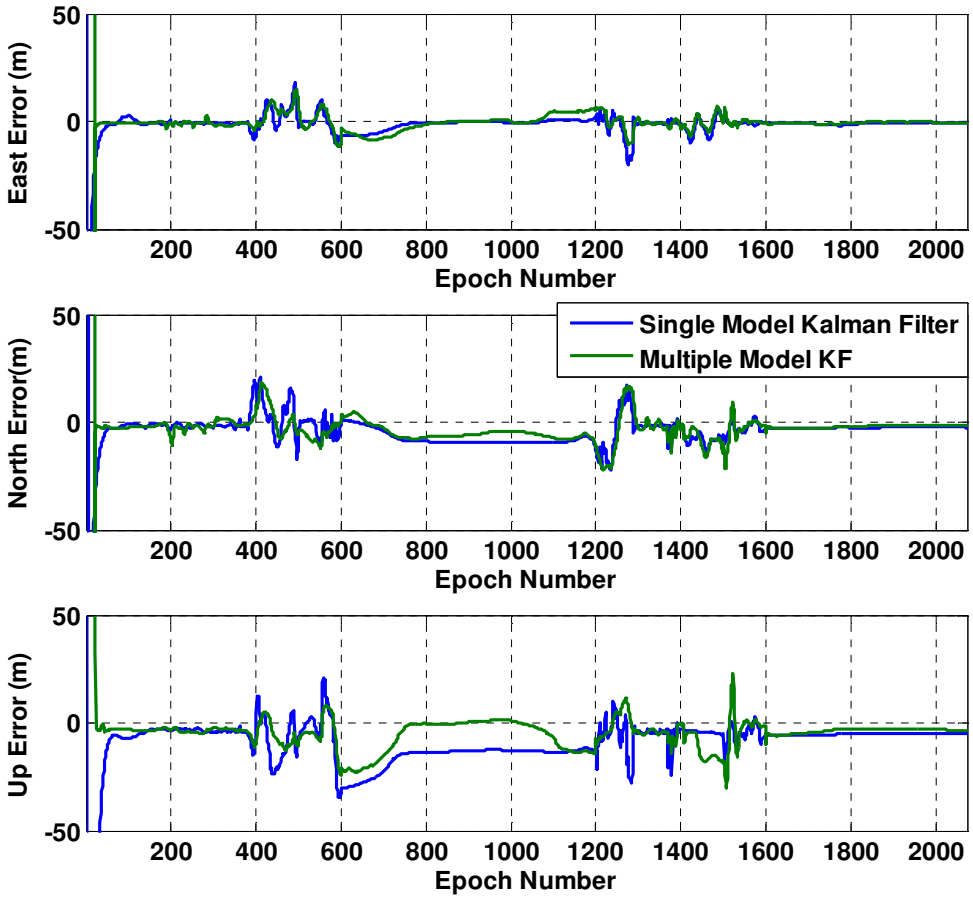

Figure 3.31: Performance comparison of the proposed algorithm when a single model KF replaces the bank of KFs

To conclude, this chapter focused on the integration of WiFi (as an external source of information) with GPS in the navigation domain through adaptive Kalman filtering and in a context-aware framework. The performance of the proposed method was analyzed and tested using real test data and several algorithms were developed to improve the performance and robustness of the system for different conditions. The proposed method is based on a two layer multiple model adaptive Kalman filtering and uses detected WiFi features to identify contexts. A decision fusion block has been developed based on the modified Dempster-Shafer theory for an effective combination of different context identifiers to improve the

probability of correct context identification**.** The modified method DST method permits effective combination of different context identifier to improve reliability even under high correlation and high conflicts. A control block based on a Markov Decision Process was shown to improve the robustness of the algorithm under the condition of unreliable decision sequences.

With WiFi becoming more and more ubiquitous, WLAN networks can also be good candidates for different types of WiFi and GPS integration in other domains. This, along with complementary availability of GPS and WiFi signals, provides motivation to integrate WiFi signals at the receiver with GPS as a promising approach to enable and speed up satellite acquisition in harsh indoor environments. The next chapter discusses signal level integration of WiFi and GPS and introduces the concept of WiFi-based assisted GPS acquisition using OFDM timing algorithms.

CHAPTER 4: SYMBOL TIMING ACQUISITION FOR COLLABORATIVE OFDM WLAN-BASED A-GPS

Wide deployment of the 802.11g/n protocols for implementing next generation WLAN has led to research on the integration of these networks and GPS as a promising approach to enhance GPS for indoor positioning. As discussed earlier, WLAN using the 802.11 standards can be employed in several different ways as a complementary positioning technology for GPS navigation and the two can be used in an integrated framework to provide a continuous and robust positioning service. This chapter introduces and presents receiver-level integration of 802.11g OFDM signals and GPS for a WiFi-based Assisted-GPS acquisition in a multipath NLOS environment.

In an A-GPS system, depending on the accuracy, timing information can be used either as coarse or fine time assistance. As mentioned in Chapter 2, fine-time assistance requires accuracies better than 1 ms and can be used to obtain the code ambiguity and possibly also to reduce the code-delay search space. This is only possible if the fine time assistance is accurate to significantly better than 1 ms, but if this can be achieved, then the fine-time assistance data will result in considerable reduction of the search space. A reduced search space will both improve the Time to First Fix (TTFF) and reduce the computational load on the receiver.

Although research describing A-GPS systems using assistance information from several wireless networks is widely published, to the best of the author's knowledge, no scheme has yet been investigated to use 802.11 WLAN signals (WiFi) to provide complete assistance information. Previous work in A-GPS has typically focused on obtaining assistance data via cell phone networks; A-GPS

systems using cellular networks are widely available commercially. Duffet & Hansen (2005) proposed to provide precise time information as assistance data in asynchronous communication networks such as a Global System for Mobile communication (GSM) or Wideband Code Division Multiple Access (WCDMA) networks. In asynchronous networks, a fixed GPS station is used to provide the precise timing information while relative timing of the received signals is used to approximate the user position. This provides a network synchronization map that enables precise timing from the fixed GPS reference in GPS denied areas.

Assistance information has also been demonstrated using other radio technologies. For example, Carlson & Koorapaty (2006) employ the Enhanced General Packet Radio Service (EGPRS) standard to send time and position assistance information over GSM and Time Division Multiple Access (TDMA) cell phone systems via a packet control channel. The time assistance is provided using a digital control channel (DCCH) over GSM networks.

With WiFi becoming ubiquitous, there are many WiFi-enabled devices that have access to GPS but are not necessarily enabled for GSM/CDMA2000/WiMAX services. This trend is particularly prevalent in the tablet computer market where WiFi only models are far outselling cell network enabled devices. Hence, using WiFi as a secondary network is a promising approach to provide assistance data for GPS acquisition in challenging environments. So far, the use of WiFi networks in A-GPS has been mostly confined either to providing position information in A-GPS acquisition algorithms (Weyn & Schrooyen 2008, Amidi 2010, Bhattacharya 2006, Sundaramurthy et al 2011) or to communicate already available assistance data in the access layer (Deric et al 2011).

Fine-time assistance using WiFi signals has recently been considered by Deric (2011). However, this research assumes that fine-time information provided by a third party is available to a WiFi-enabled device. Thus, the method mostly investigates approaches to communicate assistance data within a cooperative WiFi network in the access layer using the IEEE 802.11v protocol to synchronize WiFi receivers.

It is proposed here instead to monitor 802.11g OFDM signals in the physical layer in a collaborative A-GPS scheme where reference time information can be communicated from WiFi users (whether mobile users or fixed infrastructure) currently tracking GPS to WiFi users attempting to acquire GPS signals. The method can be implemented into existing tablets as long as the synchronized sampling is available for acquiring WiFi and GPS (either on a same chip or on different chips with shared clocks). Depending on the application, the method can be developed in an ad hoc manner while communication of information happens between collaborative nodes or in a centralized manner where the information can be controlled and sent via an AP.

In this chapter, the basic concept of the WiFi-based A-GPS structure is introduced. The proposed method is developed using a low complexity OFDM-based fine timing acquisition algorithm to estimate high-accuracy timing for the 802.11g signal structure with microsecond accuracy. These time estimates are then used as aiding data for A-GPS acquisition. Preliminary tests are conducted and results show that WiFi-based time estimates can be used as GPS fine-time assistance data to limit the code-delay search space to up to ±2 chips in a controlled laboratory LOS environment. Then, this chapter addresses the question of effectiveness of low-complexity OFDM time estimation methods in a collaborative A-GPS framework under NLOS multipath environments with low signal to noise ratios. Performance of time

domain correlation-based methods is evaluated and several methods are combined in order to develop a more effective algorithm under such conditions. It is shown that the system is still capable of providing fine time to limit the code delay search space. However, in order to achieve a more robust system and a timing accuracy enough to estimate the correct chip in challenging NLOS multipath environments, new time estimation techniques with higher complexity orders are needed. This will be addressed in Chapter 5.

4.1 System Model for Collaborative OFDM WLAN-Based A-GPS

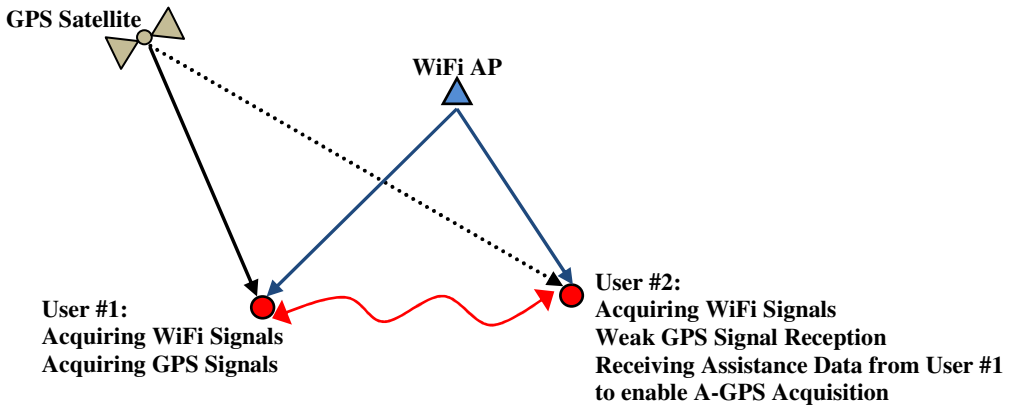

Figure 4.1: Schematic view of the proposed WiFi-based A-GPS method for two collaborative users; users perform synchronous GPS and WiFi signals sampling, User #1 acquires GPS along with WiFi and can serve as a monitor node, User #2 acquires WiFi and receives assistance information from User #1 to perform A-GPS acquisition in challenging environments

In order for asynchronous WiFi access points to provide fine-time and frequency assistance data, WiFi packets must be detected by multiple users within the range of the same access point. The corresponding WiFi times are estimated in the receivers and the WiFi time offset between these receivers can be computed. If at least one of these users also has an estimate of GPS time, it can serve as a monitor node. A monitor node consisting of a GPS and a WiFi receiver sharing a common clock can determine the

relative clock offset between GPS time and the access point's clock. This information can then be communicated to other user receivers (Figure 4.1). A user that receives the same WiFi signals can then estimate its GPS time/frequency offset as follows:

$$T_{GPS}^{'} = T_{GPS} + \partial t_{WiFi/GPS} + \partial t_{WiFi} \tag{4.1}$$

where T_{GPS} and $T_{GPS}^{'}$ are the GPS times at the monitor and user receiver, respectively, and $\partial t_{WiFi/GPS}$ is the time offset between WiFi and GPS estimated at the monitor. ∂t_{WiFi} is the WiFi time offset between receivers. Note that $T_{GPS}^{'}$ does not account for any difference in distance between the receivers and the WiFi access point. However, since the typical range of an access point for indoor environment is on the order of 50 m, this will result in a maximum error of 100 m (about 0.3 μs) which is still less than the target fine time accuracy of 1 μs.

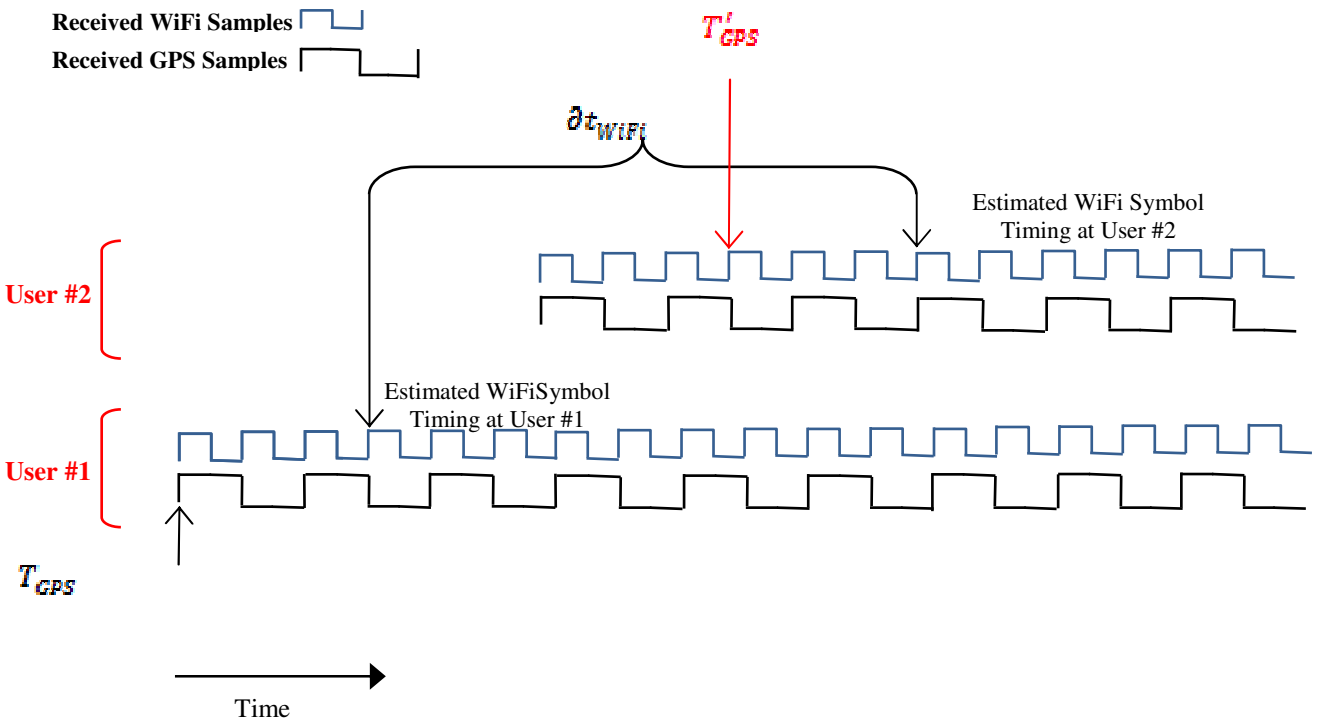

Figure 4.2: Synchronous sampling of WiFi and GPS at each of the users allows time offset estimation between received WiFi& GPS signals at two receivers; User #1 acquires GPS to obtain time reference T_{GPS} and estimates WiFi fine symbol timing to calculate WiFi/GPS offset, User #2 acquires WiFi to compute offset between corresponding symbol timings at two collaborative receivers and uses time information from User #1 to estimate GPS fine time assistance for A-GPS acquisition

The basic concept of the proposed method (as described in Equation (4.1)) is shown in Figure 4.2, which illustrates GPS and WiFi samples collected by two collaborative receivers. In order to develop a WiFi-based A-GPS with fine-time/frequency aiding, it is necessary to develop a system that allows a user to simultaneously acquire GPS and WiFi samples. Thus an implicit requirement for implementing this method is to have WiFi/GPS time synchronized samples. The corresponding start times of symbols from different access points must be distinguished. This is important in cases where receivers are within range of several access points or are relatively far apart in multipath or NLOS environments. As a

simple approach, 802.11g beacon frames can be decoded and SSID and time stamp information can be used to resolve the ambiguities. Another factor that can contribute to the time and Doppler uncertainties in the search space is the clock drift. This issue can be solved by updating the time estimates using the broadcast signals which are sent every 100 ms, and also tracking the symbol timing using the CPs in each transmitted symbol. This is further explained in more detail in Section 4.2 and in Chapter 5.

Using the WiFi-based fine-time estimate of the GPS time $T_{GPS}^{'}$ at the user receiver, along with position information obtained from a database of access point locations, the search space for GPS acquisition can be narrowed to the correct code delay chip for each frequency bin within the search space. If the access point coordinates are unknown, the GPS coordinates of the monitor receiver can be used instead with the same result. Having accurate time along with position also allows for further reduction of the frequency search space by calculating a more accurate expected Doppler for the available satellites. This will result in reducing the search space and in accelerating the acquisition in weak signal environments.

Depending on the application, communication of the reference time and assistance data can be implemented either within an ad-hoc network of WiFi users or by using the AP serving as a central station to transfer the assistance data upon request.

4.2 Time Offset Estimation Between WiFi Users

The offset between two collaborative receivers is calculated by differencing the symbol timing estimates obtained by two WiFi receivers. The first step is to compute corresponding timings for different receivers (in term of samples). Different OFDM time estimation techniques have been suggested in literature.

There exist several time estimation techniques for OFDM receivers. In the conventional correlation-based technique the arrival time is estimated as the time index that maximizes the correlation function between received signal and a known sequence (Knapp & Carter 1976, Hertz 1986). The main advantages of this technique is the low complexity order which makes it easy to implement and allows for real time applications and also independence from any a priori information. However, in the presence of multipath this method has suboptimal performance and cannot resolve closely spaced multipath signals (Zekavat & Buehrer 2012).

Deconvolution techniques are frequency-domain methods based on inverse filtering (Hahm et al 1997). The received signal is represented as the convolution of the transmitted signal and the channel impulse response and the arrival time can be estimated by dividing the Fourier transform of the received signal by the Fourier transform of the transmitted signal. These methods allow for better resolution of closely-spaced multipath signals but are not still considered as a high-precision technique for many applications (Zekavat & Buehrer 2012). Other drawbacks of this method can be high sensitivity to SNR and their increased complexity order. Furthermore, a coarse estimation of time is needed as a priori information for FFT windowing.

In Saarnisaari (1996) and Iannello (1986), Maximum Likelihood techniques are developed to estimate the multipath time delays and coefficients. These methods resolve the reception paths in a serial manner and can be considered as a multipath mitigation method; they need no a priori information and have less sensitivity to noise levels in comparison to two previously mentioned techniques. However, the solution is still suboptimal in multipath environments and has a much higher complexity order.

Subspace-based techniques use the orthogonality between subspaces to estimate channel parameters and decompose the observation vector to a noise subspace and a signal subspace (Jakobsson et al 1998, Stocia& Moses 2005). As these methods involve eigenvector decomposition, they are considered to have high complexity and are not suitable for practical implementations. Two well known subspace-based techniques for time delay estimation are MUSIC (Wang et al 2001, Li et Pahlavan 2004) and ESPRIT (Van der Veen 1997, Saarnisaari 1997), which provide an increased resolution in multipath environments. These methods perform well in high noise levels but need a priori knowledge of the number of paths (Zekavat & Buehrer 2012).

As another solution, Blind Source Separation techniques can be used for channel parameter and time estimation. These methods are based on separating a set of signals from a set of mixed signals with no or minimal a priori information (Cardoso 1998). The advantages of these methods are the low estimation error standard deviation and lower sensitivity to noise. However, like subspace methods, the Blind Source Separation methods suffer from high complexity that makes them impractical.

For preliminary analysis purpose, the performance of the proposed method is tested herein using low-complexity correlation techniques for WiFi time offset estimation. Using these methods, the possibility of implementing a WiFi-based A-GPS system is demonstrated under controlled LOS laboratory environment. Then, the performance of the method is analyzed and tested while operating in a more real environment under low SNR and multipath conditions. A timing algorithm is developed and it is shown that how combining different correlation-based techniques can result in an improved performance under such situations. By confining the proposed WiFi-based A-GPS method to use low-complexity time estimation techniques, this chapter provides an idea of the trade-off between computational complexity

and performance degradation. This then leads to the development of robust and more accurate algorithms for challenging NLOS environments, which is the subject of the next chapter.

4.2.1. OFDM Correlation-based Time Estimation Methods

Correlation properties of the transmitted OFDM blocks are used to estimate symbol timing and detect the start sample of the received symbols at each receiver. Autocorrelation properties are introduced in the structure of CP-based OFDM signaling using guard intervals, while cross-correlation can result from the use of known training sequences in the 802.11g OFDM preamble (namely STS and LTS). There are also pilot symbols with good autocorrelation properties embedded in the OFDM signals. However, since WLAN OFDM systems operate in burst packet transmission mode with a limited number of pilots (i.e. 4 pilots), the use of pilots is not an appropriate option for time estimation purposes (Wang et al 2003, Ai et al 2006). As a result, for fast time and frequency recovery, time domain correlation-based methods with lower computational complexity are preferred to frequency domain methods. In other words, practical timing methods can be developed based on the autocorrelation properties of the received signal introduced by ten identical 16-sample segments in the STS field, two identical 64-sample segments along with the 32-sample guard interval in the LTS field and also the 16-sample cyclic prefix in the head of each transmitted OFDM symbol as described in Chapter 2 (Wang et al 2005, Cho et al 2010, Nasir et al 2010, Schmidle & Cox 1997, Van de Beek et al 1997).

In general, to implement a low-complexity symbol timing estimation method, time-domain autocorrelation techniques using STS, LTS or CP can be expressed as

$$\hat{\delta} = \arg\max_{\delta}\{\frac{\left|A[\delta]\right|^2}{B^2[\delta]}\} \tag{4.2}$$

where $A[\delta]$ and $B[\delta]$ are the correlation sequence and the received energy at the δ^{th} sample delay, respectively. The Short Training Sequence can be used for coarse symbol timing and packet start sample calculation purposes using a normalized correlation metric as above. The algorithm can be implemented by MA (Moving Average) filtering of the correlation output with filter length equal to integer multiples of the length of one of the STS identical parts (16 samples) (Schmidle & Cox 1997). Normalized auto-correlations with delay of $K \times L\_STS = K \times \frac{Length\_STS}{10} = K \times 16$ create a plateau of the length *10-K*, *K=1,…, 9*. Autocorrelation functions with different delays can then be linearly combined for a more accurate timing estimation (Pan et al 2007).

With *y*[n] being the received signal as expressed in Chapter 2 and by using the long training sequence, the autocorrelation metric can be formed using identical halves of the LTS with

$$A[\delta] = \sum_{k=0}^{\frac{(LTS\_Length-32)}{2}-1} y^*[\delta+k]\, y[\delta+k+\frac{(LTS\_Length-32)}{2}] \tag{4.3}$$

$$B[\delta] = \sum_{k=0}^{\frac{(LTS\_Length-32)}{2}-1} \left| y[\delta+k+\frac{(LTS\_Length-32)}{2}] \right|^2 \tag{4.4}$$

The CP-based autocorrelation technique can be formed by

$$A[\delta] = \sum_{k=0}^{L-1} \mathrm{y}[\delta+k]\, \mathrm{y}^*[\delta+k+N] \tag{4.5}$$

This estimation method uses double sliding windows of lengths *L* and *N*, where *L* is the CP length (equal to 16 samples) and *N* is the OFDM data block length (not including CP). The complexity of this method is of order *L*.

It can be shown that the CP based correlation technique is the Maximum Likelihood (ML) estimation of the start sample timing by forming the log likelihood function for the arrival time and the frequency offset as (Van de Beek et al 1997)

$$\begin{aligned}\Lambda(\delta,\varepsilon) &= \log f(y \mid \delta,\varepsilon) \\ &= \log(\prod_{k\in I} f(y[k], y[k+N]) \prod_{k\notin I\cup I'} f(y[k])) \\ &= \log(\prod_{k\in I} \frac{f(y[k], y[k+N])}{f(y[k])f(y[k+N])} \prod_{k} f(y[k]))\end{aligned} \tag{4.6}$$

where ε is the frequency offset, *f(.)* is the probability density function, and *I* denotes the subset of CP samples, while I' denotes the subset of samples copied into CP. The correlation properties of *y* are used to obtain the above log likelihood function:

$$E\{y[n]y^*[n+k]\} = \begin{cases} \sigma_s^2 + \sigma_n^2 & k = 0 \\ \sigma_s^2 e^{-j2\pi\varepsilon} & k = N \\ 0 & O.W. \end{cases} \tag{4.7}$$

Assuming a jointly Gaussian distribution for the received data the log likelihood function can be written as

$$\Lambda(\delta,\varepsilon) = \mid \Upsilon[\delta] \mid \cos(2\pi\varepsilon + \angle \mid \Upsilon[\delta] \mid) - \rho\Phi[\delta] \tag{4.8}$$

where

$$\Upsilon[n] = \sum_{k=n}^{n+L-1} y[k]y^*[k+N] \tag{4.9}$$

and

$$\Phi[n] = \frac{1}{2}\sum_{k=n}^{n+L-1} \mid y[k] \mid^2 + \mid y[k+N] \mid^2 \tag{4.10}$$

$$\rho = \left| \frac{E\{ y[k] y^{*}[k+N] \}}{\sqrt{E\{ | y[k] |^2 \} E\{ | y[k+N] |^2 \}}} \right| \tag{4.11}$$

ρ can be considered as the magnitude of the correlation coefficient. By maximizing the log likelihood function in two steps for arrival time and frequency offset as

$$\max_{(\delta,\varepsilon)} \Lambda(\delta,\varepsilon) = \max_{\delta} \max_{\varepsilon} \Lambda(\delta,\varepsilon) = \max_{\delta} \Lambda(\delta, \hat{\varepsilon}_{ML}), \tag{4.12}$$

the ML estimation of arrival time is

$$\hat{\delta}_{ML} = \arg\max_{\delta} \{ | \Upsilon[\delta] | - \rho \Phi[\delta] \} \tag{4.13}$$

For an a priori known frequency offset of zero, the ML estimation of the timing becomes

$$\hat{\delta}_{ML} = \arg\max_{\delta} \{ \mathrm{Re}\{ \Upsilon[\delta] \} - \rho \Phi[\delta] \} \tag{4.14}$$

Figure 4.3 shows the ML time estimates as the maximizing indices of $\Lambda(\delta, \hat{\varepsilon}_{ML})$. The FFT size is 64 and CP length is 16 samples.

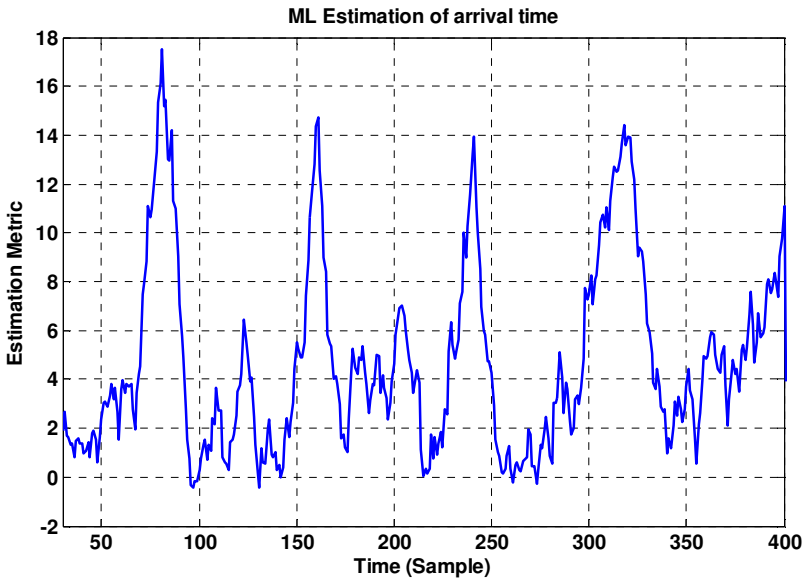

Figure 4.3: OFDM ML arrival time estimates as the maximizing indices of $\Lambda(\delta, \hat{\varepsilon}_{ML})$ (Van de Beek et al 1997)

As another similar CP-based technique with the same complexity order, the minimum distance estimation metric can be formed by minimizing the squared difference between the sliding windows and can be described as

$$A[\delta] = \sum_{k=0}^{L-1} \left| y[\delta + k] - y^{*}[\delta + k + N] \right|^{2} \tag{4.15}$$

In addition to autocorrelation methods, cross-correlation of the received signal with a priori known sequence (i.e. the known LTS or STS) can be applied to recalculate the start sample within the detected packet to achieve a more accurate timing estimate.

Figure 4.4 shows decision metrics (normalized correlation) used for four low-complexity time-domain correlation techniques for an 802.11g OFDM signal in an AWGN channel with a delay of 300 samples. It demonstrates how STS-based autocorrelation and cross correlation methods can be used to obtain a

primary estimate of the start sample. In the STS autocorrelation method, the MA filter length is set to 9×16 samples. The STS cross-correlation method uses the normalized correlation of the received samples with the a priori known STS sequence (10×16 samples) as the decision metric. Figure 4.4-b shows how two LTS-based correlation methods can be used to obtain a fine estimate of the start sample of the LTS using the primary coarse estimate of the start sample of STS. Using the primary estimate of the start sample where the STS occurs (300 in this case) these correlation-based methods are applied to search the start sample of the LTS within the expected range of its occurrence. Herein, LTS-methods search from sample 400 (300+100) to detect the start sample. The LTS cross correlation method uses the normalized correlation between received samples and the known LTS (without the GI). The CP-based method uses the correlation properties introduced by the 32 sample GI in the LTS to detect the start sample of the LTS (including the GI) whenever the normalized correlation value crosses a certain threshold.

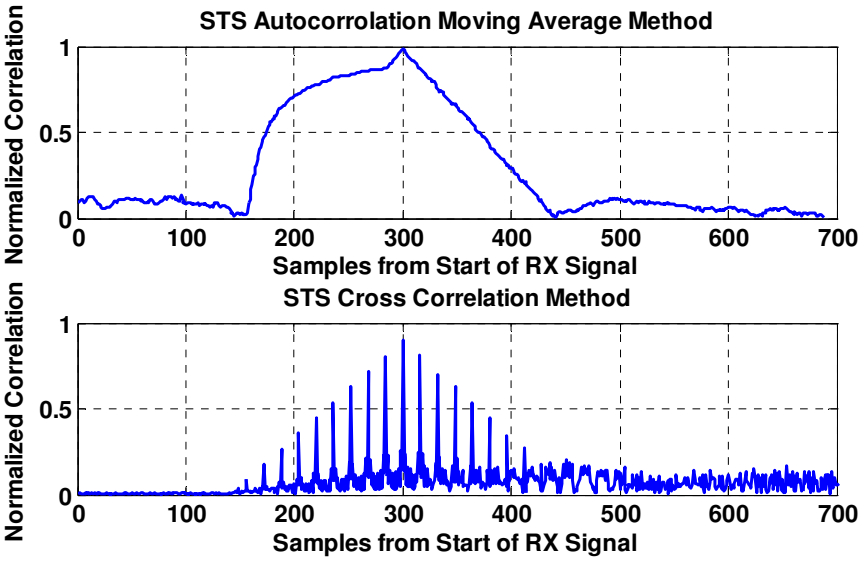

(a)

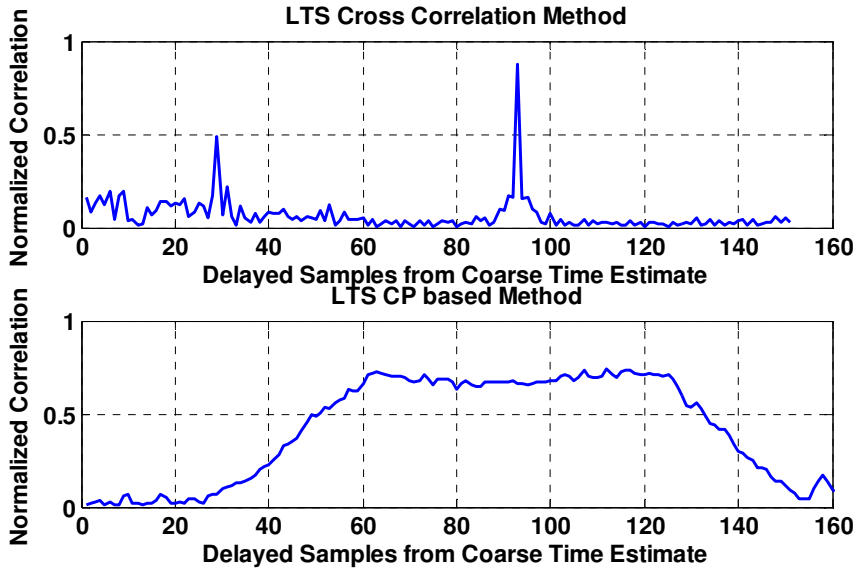

(b)

Figure 4.4: Output of four different time-domain correlation-based methods; (a) represents two coarse timing methods using STS; (b) an estimate of timing is achieved using two correlation based LTS methods and the coarse estimate from (a)

Furthermore, performance of the two CP-based methods (i.e. the minimum distance method and the correlation method) is shown in Figure 4.5 for different delay values and assuming additive white Gaussian noise (Cho et al 2010). The performances are compared in terms of the error in detecting the correct delay time. The maximum detection error for SNR=10 dB and CP length equal to 16 samples over 1000 iterations is found to be 6 samples (300 ns), which falls well within the required accuracy limit for A-GPS acquisition applications.

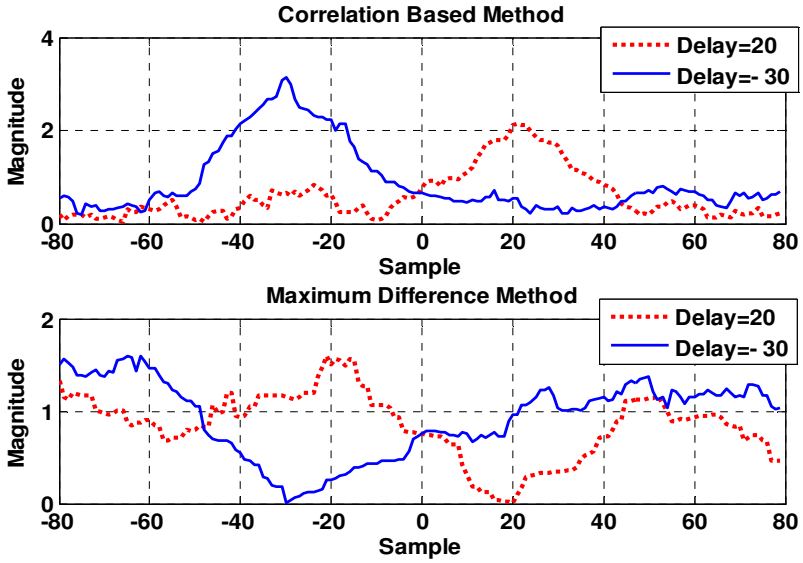

Figure 4.5: Performance analysis of time domain CP-based symbol timing estimation methods (Cho et al 2010)

After computing corresponding start samples of the received WiFi signal at the two collaborative receivers, the offset is computed by differencing these estimated timings.

4.2.2. Cramer-Rao Lower Bound for Time Offset Estimation

Cramer-Rao Lower Bound (CRLB) calculations can be used to obtain achievable bounds on the accuracy of time offset estimation between WiFi users. The CRLB theorem states that for the data $\boldsymbol{y}$ and the vector parameter θ, under the regularity condition where (Kay 1993)

$$E\{\frac{\partial \ln f(y;\theta)}{\partial \theta}\} = 0 \tag{4.16}$$

the covariance matrix of an unbiased estimator is lower bounded as (Kay 1993)

$$C_{\hat{\theta}} - F^{-1}(\theta) \geq 0 \tag{4.17}$$

where $\boldsymbol{F}$ is referred to as the Fisher information matrix for $\boldsymbol{y}$ and is given as

$$[F(\theta)]_{i,j} = -E\{\frac{\partial^2 \ln f(y;\theta)}{\partial \theta_i \partial \theta_j}\} \tag{4.18}$$

Hence,

$$\text{var}(\hat{\theta}_i) = [C_{\hat{\theta}}]_{i,i} \geq [F^{-1}(\theta)]_{i,i} \tag{4.19}$$

Herein, the unknown parameters are time delay and the $M \times N$ unique samples of Y as nuisance parameters where M is the total number of OFDM blocks received.

The Fisher information matrix has a block structure as

$$F = \begin{bmatrix} A_{1\times 1} & B^T_{MN\times 1} \\ B_{MN\times 1} & C_{MN\times MN} \end{bmatrix} \tag{4.20}$$

and the first element of F corresponds to the time parameter.

Assuming that the observations at each receiver are raw samples, the log-likelihood of the received signal of OFDM symbol blocks, i.e. $Y = \{y_i[n]\}$, $i = 1,...,M$, is given as (Martin et al 2011)

$$\ln f(Y \mid U, \delta) = \text{const.} - \frac{1}{2\sigma_v^2} \sum_{m=0}^{M(N+L)} (y[m] - E\{y[m]\})^2 \tag{4.21}$$

By defining

$$z[m] = \sum_n u[n] s'[m-n] \tag{4.22}$$

where $s(t) = s_0(\frac{t}{T})$ is the pulse shape and $s' = ds(t)/dt$, sub-matrices *A, B* and *C* can be evaluated for $\delta = 0$ as

$$-E\{\frac{\partial^2 \ln f(Y \mid U, \delta)}{\partial \delta^2}\} = \frac{1}{\sigma_v^2} \sum_m (\frac{\partial \mathrm{E}\{\mathrm{y[m]}\}}{\partial \delta})^2 = \frac{1}{\sigma_v^2} \sum_m (z[\mathrm{m}])^2 \tag{4.23}$$

$$\begin{aligned} -E\{\frac{\partial^2 \ln f(Y \mid U, \delta)}{\partial \delta \partial u[k_0]}\} &= \frac{1}{\sigma_v^2} \sum_m (\frac{\partial E\{y[m]\}}{\partial \delta})(\frac{\partial E\{y[m]\}}{\partial u[k_0]}) \\ &= -\frac{1}{\sigma_v^2} \sum_m z[m](\frac{\partial E\{y[m]\}}{\partial u[k_0]}) \end{aligned} \tag{4.24}$$

$$-E\{\frac{\partial^2 \ln f(Y \mid U, \delta)}{\partial x[m_0] \partial u[k_0]}\} = \frac{1}{\sigma_v^2} \sum_m (\frac{\partial E\{y[m]\}}{\partial u[m_0]})(\frac{\partial E\{y[m]\}}{\partial u[k_0]}) \tag{4.25}$$

Thus one has

$$A = \frac{1}{\sigma_v^2} \sum_m (z[\mathrm{m}])^2 \tag{4.26}$$

$$B[k_0] = \frac{1}{\sigma_v^2} \begin{cases} -z[k_0] & \text{for } k_0 \text{ as a data sample} \\ -z[k_0 - N] - z[k_0] & \text{for } k_0 \text{ as a CP sample} \end{cases} \tag{4.27}$$

$$C = \frac{1}{\sigma_v^2}\begin{bmatrix} I_{N-L} & 0 \\ 0 & 2I_L \end{bmatrix} \otimes I_M \tag{4.28}$$

Hence

$$VAR[\Delta\hat{\delta}_{CP}] \geq [A - B^T C^{-1} B]^{-1} \tag{4.29}$$

and the following Cramer-Rao Lower Bound (CRLB) can be achieved for this method (Martin et al 2011):

$$VAR[\Delta\hat{\delta}_{CP}] \geq 2\sigma_v^2 \left(\sum_{m \in CP} \left(\frac{\partial E\{y[m]\}}{\partial \delta} - \frac{\partial E\{y[m-N]\}}{\partial \delta} \right)^2 \right)^{-1} \tag{4.30}$$

$$VAR[\Delta\hat{\delta}_{CP}] \geq \frac{T^2}{M\gamma} \left(\sum_{m \in CP} \sum_{k \notin CP} \left(s_o'[k-m] \right)^2 \right)^{-1} \tag{4.31}$$

where σ_v^2 is the noise variance, γ is the SNR, *i* denotes the index of the last *L* samples within each symbol, M is the total number of OFDM symbols received.

The above CRLB can be considered as a fundamental theoretical lower limit on the variance of the offset estimation based on the presented observation model using raw received samples. For a sampling rate of 20 MHz and an SNR of 20 dB, the achievable accuracy is 0.1 μs, which more than satisfies the accuracy limits for fine-time A-GPS applications.

As mentioned earlier, the complexity of the correlation-based method is of order of *L* (length of the preamble). Hence, the effect on the required processing time is negligible. This is the main motivation to

use correlation based methods for preliminary implementation and performance analysis of the proposed A-GPS structure.

4.3 Preliminary Implementation and Performance Analysis in a Controlled LOS Environment

The WiFi-based A-GPS method was first implemented in a controlled line of sight laboratory environment with high signal to noise ratios. For developing the proposed method, multichannel National Instrument (NI) PXI-5661 front-ends were used to simultaneously sample WiFi signals along with GPS signals. The NI system is able to sample the spectrum up to 2.7 GHz and provides 20 MHz of bandwidth. This allows for primary testing of the system by observing one WiFi data channel using the 802.11g protocol and one GPS data channel (L1 with centre frequency of 1.574 GHz) for each of the users.

A single 802.11g wireless router is used as the WiFi access point transmitting a standard 6 Mbits/s QPSK modulated OFDM signal on 802.11g Channel 1, with beacon intervals of approximately 0.1 s. I/Q samples were collected with the two receivers for the same channel with a centre frequency of 2.412 GHz. The router transmit power is set to high level.

4.3.1. Preliminary Testing of Correlation-based Timing Algorithms

For a preliminary performance analysis, the estimation of the time offset between WiFi receivers was performed using the cyclostationary properties introduced in 802.11g signals by Cyclic Prefix (CP). As described in the previous section, two low-complexity practical CP-based time-domain symbol timing estimation methods were tested, i.e. the correlation-based method and the minimum distance method.

WiFi users (two NI front ends) are in the range of the AP and receive LOS OFDM signals with relatively high SNR.

Figure 4.6 shows the magnitude of received complex samples and detected frames (beacon packets) in the first receiver. The Delay and Correlate Algorithm (Schmidl & Cox 1997) is used here for packet detection in the presence of a preamble. To detect the packets, the correlation of the received signal and its delayed version is normalized by the energy of the signal and then compared to a certain threshold as given below, where L is the length of the preamble:

$$\frac{\sum_{\delta=0}^{L-1} y[n+\delta]\,y^{*}[n+\delta+L]}{\sum_{\delta=0}^{L-1} \left| y[n+\delta+L] \right|^{2}} > threshold \tag{4.32}$$

The threshold value depends on the SNR. Here, with a controlled test environment and assuming a high SNR LOS signal, the threshold was chosen according to AP transmit power parameters in order to detect the strongest broadcasted beacon and reject existing interference in the same frequency band as the received signal. As it can be seen in Figure 4.6 the beacon frames are repeated approximately every 0.1 s as expected. The lower power bursts are interference from existing WiFi infrastructure in the test environment.

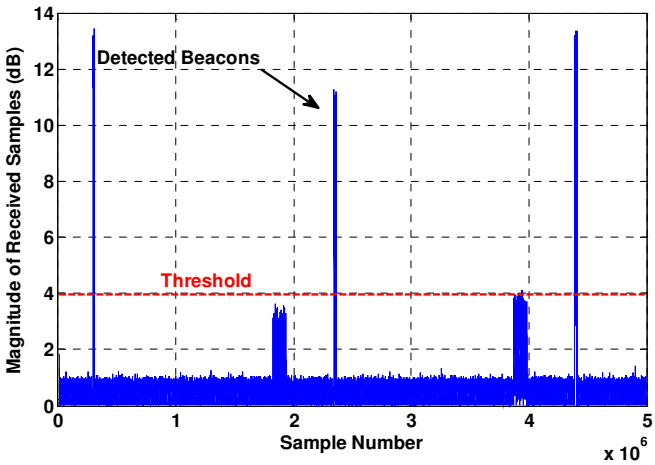

Figure 4.6: Detected beacon frames at the first receiver. Timing of the strongest beacons is acquired.

The correlation-based symbol timing acquisition algorithm is then applied to two received OFDM signals at the two WiFi receivers. Figure 4.7 shows the estimated symbol start time for the two receivers.

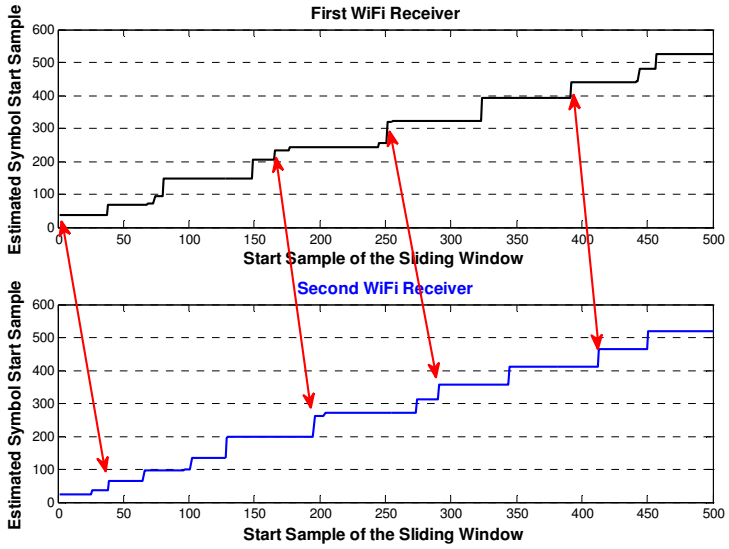

Figure 4.7: Estimated Symbol Start Time for the two Receivers

To determine the time offset between two RXs, the corresponding symbols should be detected. In the controlled test environment with receivers acquiring relatively high SNR signals, no ambiguity is

introduced into the signals. Thus, a correlation-based estimation technique was sufficient to distinguish common symbols in two receivers.

Figure 4.8 shows correlation coefficients between received OFDM signals in one receiver and the delayed versions of the signal received by the second receiver for different delays in terms of samples. As it can be seen, local maxima can be used to identify the offset between two sequences. Using 52 OFDM subcarriers and a 16 bit CP, the average distance between the detected local maxima is expected to be 68 samples, which is consistent with the obtained result.

It should be noted that, in real data environments it would be necessary to resolve the ambiguity in order to precisely distinguish and estimate the time offset. In that case detected timestamps from beacon frames could be used to detect corresponding frames.

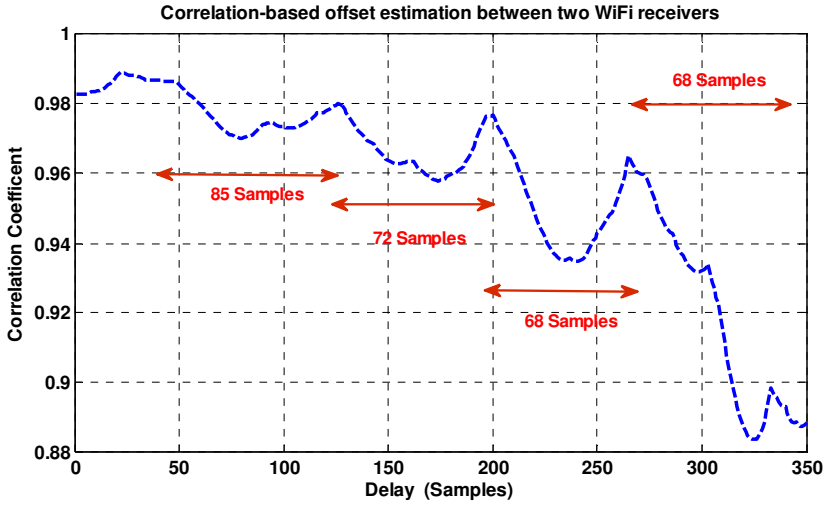

Figure 4.8: Correlation-based time offset estimation between two WiFi receivers for the controlled test environment

Having estimated the offset between the received signals at two receivers, as depicted in Figure 4.9, it can be shown that the achieved accuracy lies within the accuracy requirement for A-GPS acquisition. In

this case, the mean offset between two receivers for the estimated start time of the detected symbol is 31 samples, which corresponds to approximately 1.5 μs.The standard deviation of the offsets in estimated symbol start times is found to be 9.53 samples or equivalently near 0.5 μs. Thus, the primary results assure that the error budget resulting from time offset estimation between two receivers remains within the acceptable required accuracy range.

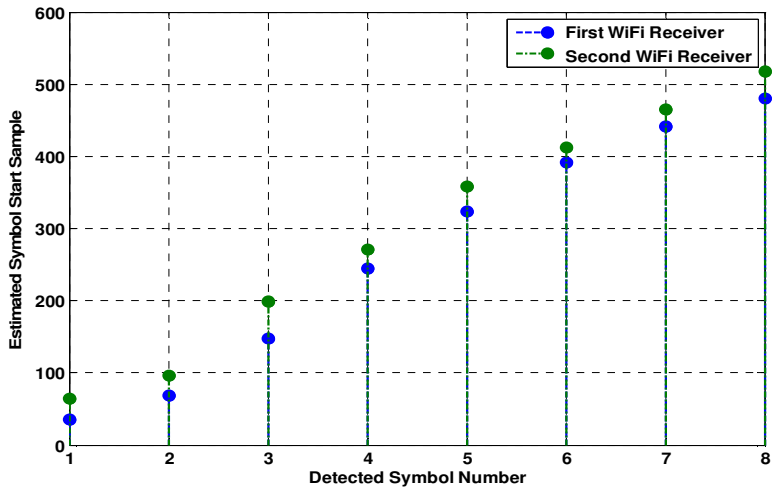

Figure 4.9: Time offset between estimated symbol start samples for two receivers

4.3.2. Preliminary Testing of the Proposed WiFi-based A-GPS method

To implement the proposed WiFi-based A-GPS method experimentally, collaboration between two WiFi users which simultaneously receive and sample WiFi/GPS signals is assumed. In this scenario one of the WiFi users is able to acquire and track GPS time while the second user is experiencing weak indoor GPS signals.Two users are in the range of the same WiFi AP (802.11g WLAN router).

Using the CP correlation-based method, the achieved timing results for an average GPS C/N_o of 22.6 dBHz are shown in Table 4.1.

Table 4.1: Timing Analysis for Average C/N_o of 22.6 dBHz

WiFi/GPS Estimated Offset at Rx #1 (s)	Mean Offset between WiFiRxs (μs)	Estimated GPS time at Rx #2 (s)
0.0132	2.1	146545.826653

A-GPS processing was performed using the PLAN Group GSNRx™ software receiver (Petovello et al 2008). Using the acquired micro-second timing offset from received WiFi signals, the performance of the proposed method was compared to different A-GPS schemes and also to a high sensitivity GPS receiver for two different average received SNR values as shown in Table 4.2. The approximate coordinates of the WiFi receiver can be estimated using the known coordinates (Using a look-up table).

Table 4.2 compares performance of the proposed A-GPS acquisition to other A-GPS schemes using different assistance information for one minute of data in a weak signal test environment. The results are shown for two different average C/N_o values of 22.6 dBHz and 18.7 dBHz.

Table 4.2: Performance Comparison for different GPS Acquisition Schemes

GPS Acquisition scheme	Number of satellites acquired		Time to acquire first satellite (s)		Time to acquire last satellite(s)	
	Average C/N_o (dBHz)		Average C/N_o (dBHz)		Average C/N_o (dBHz)	
	22.6	18.7	22.6	18.7	22.6	18.7
Conventional with no aiding	2	0	2.05	NA	12.68	NA
High sensitivity Rx	5	5	0.81	13.71	6.21	19.31
A-GPS with position aiding	2	0	2.05	NA	7.02	NA
A-GPS with position and coarse-time aiding	6	4	0.22	0.90	2.69	9.25
Proposed WiFi-based A-GPS	6	4	0.14	0.45	1.40	3.17

When no aiding information is available, the receiver is not capable of acquiring any satellite in this weak signal environment. This also applies to the case where the only available assistance data is the approximate position, which is obtained using the a priori known coordinates of the WiFi AP. In the case when several APs are available, the decoded AP SSIDs along with a look up table can be used to determine the approximate position of the users. In this particular environment, the high sensitivity receiver (HSGPS) is still capable of acquiring five satellites in total.

Having coarse time assistance information allows initiation of the acquisition process. The number of acquired satellites depends on the ability of the receiver to detect correlation peaks for different SNR values. Satellites with consistent losses of lock, which resulted in re-acquisition attempts, are rejected as false peaks.

An approximate position limits the number of bins to be searched by providing the expected Doppler frequency for each satellite. By having an approximate position, the expected Doppler can be computed to limit the frequency search space. This explains how the acquisition time is reduced when position information is available. As an example, for an average C/N_o of 22.6 dBHz, the expected Doppler frequency of SV 7 is computed to be -1352.96 Hz where the estimated Doppler is -2615.72 Hz. This narrows the search space to ±1262.9 Hz around a center frequency of -1352.96 Hz. The expected Doppler is the computed Doppler frequency using the a priori available information while estimated Doppler represents the Doppler estimate achieved after acquiring the satellite.

Having a coarse estimate of time allows for further reduction of the frequency search space by providing better estimates of Doppler frequencies, as shown in Table 4.2. Actually, for frequency assistance, each 1 s of timing error will result in up to a 0.8 Hz error in the expected Doppler (Van Diggelen 2009).

For the case with a lower C/N_o (18.7 dBHz), as soon as the coarse time information is available for aiding along with the approximate position, acquisition becomes possible. However, the accuracy is not enough to limit the code delay search. For SV 7 with position assistance only, the expected Doppler is -2789.27 Hz while the estimated Doppler frequency is -2852.02 Hz. This means that the frequency search space is further reduced to 62.75 Hz around the center frequency of -2789.27 Hz.

By using the proposed algorithm and providing fine time to the second WiFi receiver, one can limit the number of chips to be searched to ±2 within each specific frequency bin. Considering the case for an average C/N_o of 18.7 dBHz, the acquisition time for the first satellite is reduced and improved by about 0.44 s with respect to A-GPS with coarse time information. Since time is known to ±1μs, the fine time

assistance contribution to expected code delay search space is ±1.023 chips or less than ±2 chips. As expected, the acquisition times have been reduced for all cases when the fine time information is available and it can be concluded that the proposed method outperforms both the commercial HS-GPS receiver with cold start and the coarse time A-GPS approach.

4.4 Performance Analysis of the Proposed Method in NLOS Multipath Environment

Although the time-domain correlation techniques described in Section 4.2 satisfy the accuracy requirements for providing fine-time assistance information for A-GPS, the performance of these methods degrades under severe multipath environments and shadowing effects. Figure 4.10 shows a schematic view of a multipath non-line-of-sight scenario for collaborative receivers in the range of multiple access points. The number of code-delay bins to be searched using A-GPS acquisition depends on the accuracy of the available fine-time data. In an ideal situation with LOS signal reception and relatively high SNR values where the algorithm is capable of providing GPS time estimate at the second receiver within an accuracy of 1 μs, the search space is reduced to ±1.023 chips or less than ±2 chips. In weak signal multipath environments the accuracy of the estimated timing is degraded but as long as it satisfies the fine-time accuracy requirements (some value less than 1 ms), it still can be used to reduce the code-delay search space. Hence, it is necessary to evaluate the performance of the time estimation methods in terms of providing an A-GPS system with fine time assistance data under different channel and signal conditions.

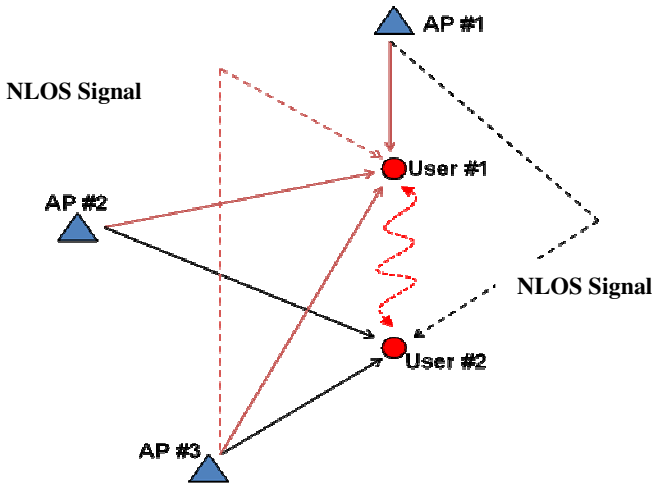

Figure 4.10: Schematic view of the proposed collaborative method in a NLOS multipath environment; User #1 is acquiring GPS and User #2 performs A-GPS to acquire satellite signals

4.4.1. Theoretical Analysis and Algorithm Development for WiFi Time Offset Estimation Under Multipath

In general, by assuming a multipath channel model with P paths and i^{th} channel gain and delay of the form

$$h(n) = \sum_{p=1}^{P} \alpha_p \, \delta(n - \tau_p) \tag{4.33}$$

the complex baseband received signal can be expressed as

$$y(n) = [\sum_{p=1}^{P} \alpha_p \, u(n - \tau_p)] \exp(j 2\pi \varepsilon n) + \upsilon(n) \tag{4.34}$$

As mentioned in Chapter 2, several models have been proposed in the literature for indoor multipath channels, among which two popular yet simple models are the Rayleigh fading and Saleh-Valenzuela (S-V) models.

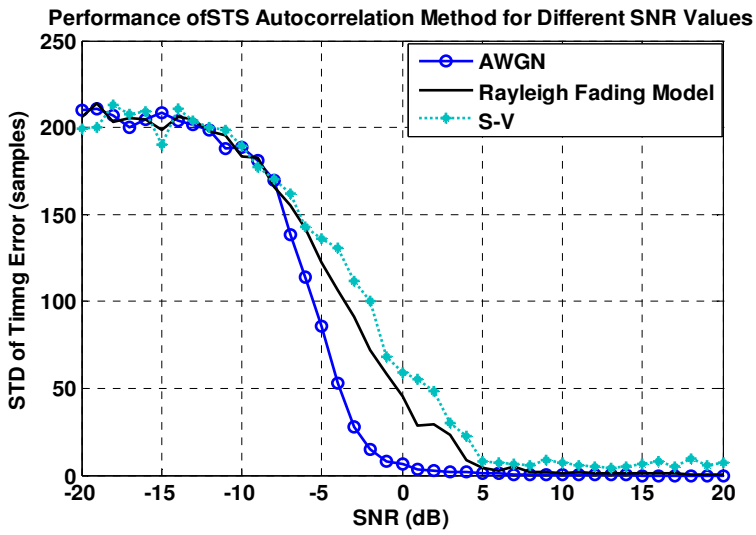

Figure 4.11: Performance degradation of STS-based autocorrelation method for multipath environments with RMS delay spread of 50 ns

Figure 4.11 shows the performance of the correlation-based frame detection and symbol timing method for an AWGN channel and the two multipath channel models, i.e. a Rayleigh fading channel with exponential decaying power factors and an S-V channel. In both cases, an RMS delay value of 50 ns is assumed and simulation is performed for 1000 realizations of different channels. As expected, under multipath conditions the timing estimation accuracy of the first sample degrades. As SNR decreases, the method shows higher error standard deviation values for symbol timing. Under multipath conditions, for an SNR of 0 dB, the standard deviation of the estimated error is found to be 53 samples while the same SNR value for an AWGN channel results in a 6 sample estimated error standard deviation. For this method, in weak signal multipath environments with SNR= -20 dB, the estimated standard deviation exceeds 200 samples (10 μs).

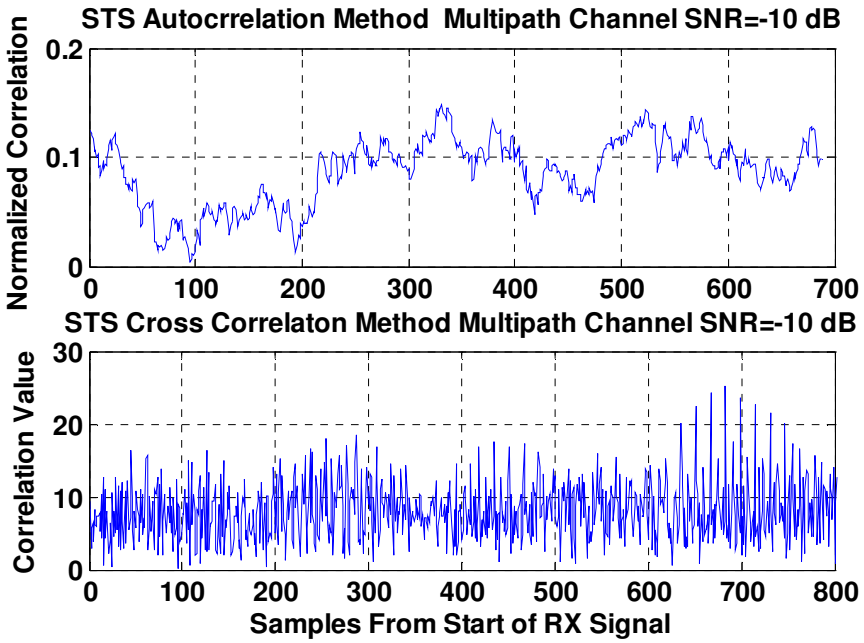

Figure 4.12: Performance of STS-based methods under multipath Rayleigh fading channel condition with increased number of paths and increased SNR; true delay is 300 samples

Since the offset between WiFi users is computed by subtracting the estimated time values at the two receiver ends and assuming the same standard deviation at the second receiver, the standard deviation of the error is $\sqrt{\sigma^2_1 + \sigma^2_2} = \sigma\sqrt{2} = 283$ samples (about 14μs). Hence, using this method only, the GPS code delay search space can be limited up to ±15 chips. The accuracy is still better than 1 ms and the achieved timing information can be considered as fine-time assistance data for A-GPS acquisition.

Figures 4.12 and 4.13 show the performance degradation of two of the four methods (i.e. the STS autocorrelation method and the STS cross correlation method) under low SNR conditions (SNR= - 20 dB) and also for an increased number of channel paths with SNR= -10 dB. According to their structure, different symbol timing algorithms experience different levels of performance degradation under poor channel conditions. For example, the STS-based autocorrelation method is more susceptible to lower SNR values in comparison to the STS-based cross-correlation method. For the former, the largest peak

occurs with about 200 samples of error while for the latter method, the maximum correlation value is found with less than 10 samples of error. The STS-based cross-correlation method shows a higher level of sensitivity to the number of channel paths as shown in Figure 4.12 and 4.13. The same ten peak pattern with a 16 sample separation between consecutive peaks (according to the ten time repeat pattern of the STS sequence) exists for each received multipath signal. As a result the maximum can occur in a different delay instead of the direct path signal delay.

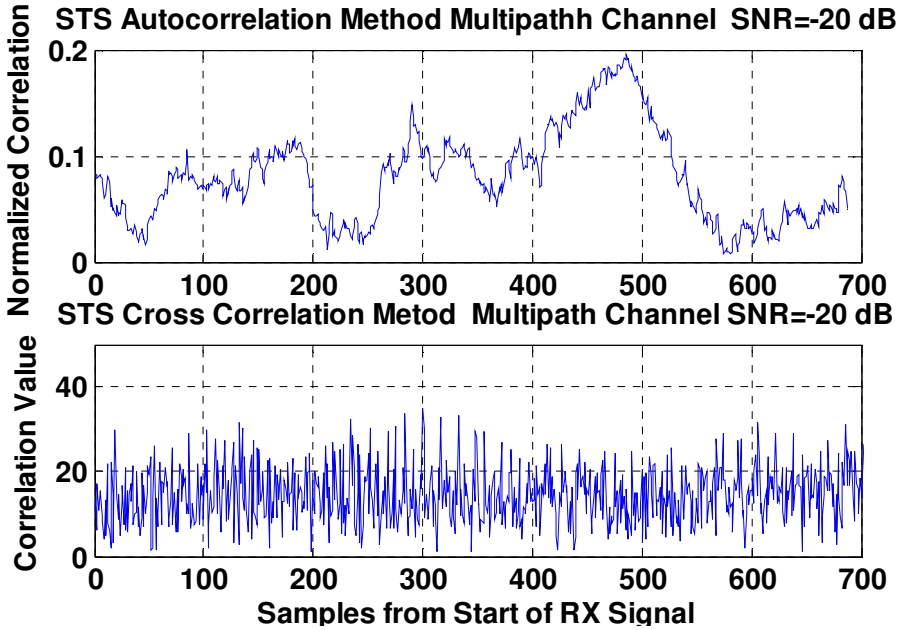

Figure 4.13: Performance of STS-based methods under multipath Rayleigh fading channel conditions with a decreased number of paths and decreased SNR; the true delay is 300 samples

This suggests an approach for combining multiple methods based on the correlation properties of OFDM signals for a more robust symbol timing estimation in challenging environments. First, a rough estimate of the start of the packet is obtained using the STS-based autocorrelation method with a MA filter of length $9 \times L$. Then limiting the search window according to the computed start sample, a combination of

correlation-based methods is used to achieve a more accurate estimate of the timing. The procedure can be explained as the following five steps:

a) Packet detection and coarse timing is performed to detect the start of the frame. The STS-based autocorrelation method is used with an MA filter of length $9\times L$ samples, where $L=16$ samples for 802.11g OFDM signaling.

b) Using coarse start timing estimated from step *a,* STS-based cross-correlation method is performed to obtain an estimate of the start sample of the detected packet:

$$Estimated\ Sample_{Step\,b} = Start\ Sample\ of\ STS \tag{4.35}$$

c) Using the estimated start sample from step *b* and known LTS repetitive pattern (64 samples), LTS-based cross-correlation method achieves an estimate of the start sample of LTS identical halves (after GI):

$$Estimated\ Sample_{Step\,c} = Start\ Sample\ of\ LTS + GI\_Length \tag{4.36}$$

where GI_Length is 32 samples in this case.

d) The CP-based autocorrelation method is used to achieve an estimate of the start sample of LTS:

$$Estimated\ Sample_{Step\,d} = Start\ Sample\ of\ LTS \tag{4.37}$$

e) Based on the results from steps *b* to *d*, the estimated values of the start sample of the detected data frame are computed and combined via averaging to achieve a more accurate estimate of symbol timing (start sample of data symbol) for the received signal:

$$Start\ Data\ Sample_{Step\ b} = Estimated\ Sample_{Step\ b} + STS\_Length + LTS\_Length \tag{4.38}$$

$$Start\ Data\ Sample_{Step\ c} = Estimated\ Sample_{Step\ c} + LTS\_Length - GI\_Length \tag{4.39}$$

$$Start\ Data\ Sample_{Step\ d} = Estimated\ Sample_{Step\ d} + LTS\_Length \tag{4.40}$$

$$\begin{aligned} Estimated\ Sample_{Step\ e} &= Start\ Sample\ of\ Data\ Frame \\ &= Ave.(Start\ Data\ Sample_{Step\ i}), \qquad i = \{b, c, d\} \end{aligned} \tag{4.41}$$

where STS_Length is 160 samples and LTS_Length is 160 samples including GI_Length of 32 samples and two identical halves of 64 samples.

In general, the multipath environment can affect the performance of the proposed system in two ways. Firstly, it influences the accuracy of the estimated symbol timing and therefore the accuracy of the time offset estimation between collaborative users and secondly, it adds to the error budget of the final fine-time assistance estimation because of the additional delay of the received multipath signals from reflection paths. This error is related to the delay spread of the underlying channel. Hence, the error term should be included in the time estimation by considering the maximum channel delay spread for the worst-case scenario as:

$$T_{GPS}^{'} = T_{GPS} + \partial t_{WiFi/GPS} + \partial t_{WiFi} + \partial t_{Max\ Channel\ Delay} \tag{4.42}$$

4.4.2. Experimental Results

In order to experimentally evaluate the effectiveness and performance of the proposed timing algorithm in an A-GPS structure, tests were conducted in a multipath-rich indoor environment. WiFi routers were set as APs to transmit 802.11g OFDM broadcast signals with different transmit powers. The equipment

and main hardware set up is as explained in Section4.3 and again, each user sampled WiFi and GPS signals with a multichannel National Instruments PXI-5661 front-end. Figure 4.14 shows a view of the data collection set up.

Figure 4.14: Data Collection Set Up

The two collaborative WiFi/GPS users were in the range of three WiFi access points. The indoor environment was a four-story university building that has glass skylights allowing receiver #1 to acquire GPS signals and communicate the estimated WiFi/GPS time offset to receiver #2. Receiver #2 was located such that it experienced a weak GPS signal environment (with average C/N_o of 19.48 dB) requiring A-GPS for signal acquisition (Figure 4.15).

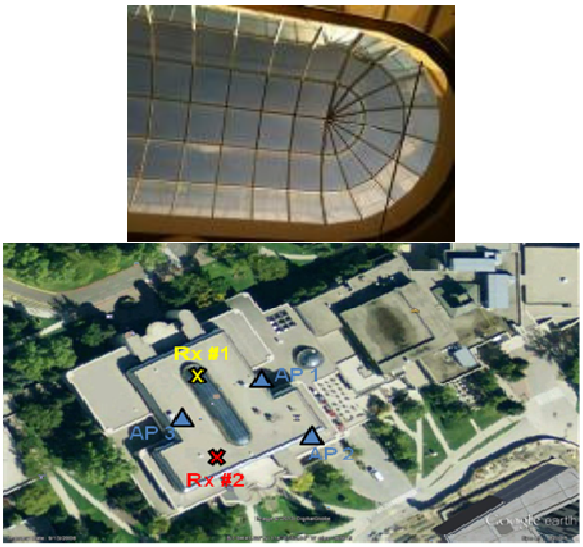

Figure 4.15: Data collection environment; top picture shows the glass ceiling, bottom picture shows the placement of the APs and receivers in the data collection scenario

The time-domain correlation-based methods implied in the estimation algorithm (as described in five steps) are applied to the WiFi samples collected by each user to estimate symbol timing and compute time offsets. Figure 4.16 shows the performance of the offset estimation algorithm for a detected packet (after performing step *a*). The estimated start sample is found to be sample 6062, 5920 and 5959 from steps *b*, *c* and *d* (STS-based cross-correlation, LTS-based cross-correlation and CP-based methods), respectively. Thus, the maximum distance from the mean value of 5981 samples (the final estimate from step *e*) is found to be 81 samples (4.1 µs). In this case, using the estimated offset between the two receivers, the code delay search space can be limited to ±9 code chips. As discussed earlier, the accuracy achieved under high multipath and low SNR exceeds 1 µs accuracy and hence is not sufficient to limit the code delay search space to one chip but is still within the acceptable accuracy for providing A-GPS fine-timing assistance data.

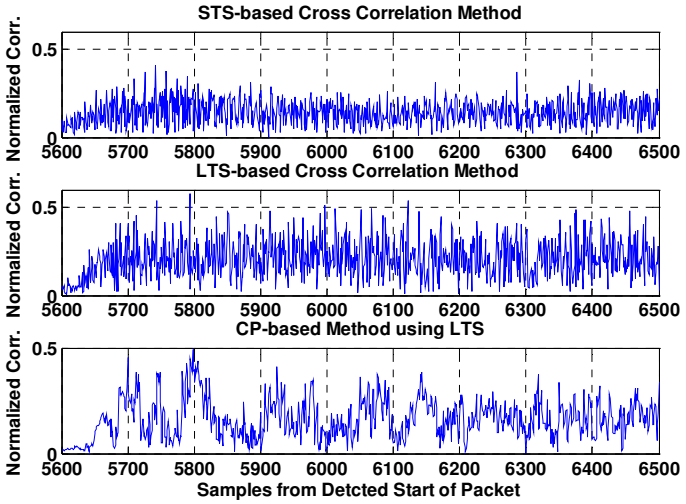

Figure 4.16: Example of start data sample estimation for a detected packet from AP #1.The start sample is found to be 6062, 5920 and 5959 using method b, c and d, respectively, with maximum of 81 samples (4.1 μs) from the mean value 5981 samples (final estimate from step e)

Table 4.3 shows computed mean offset values between two collaborative receivers for detected burst signals from AP#1. For comparison, an ML cross-correlation method is also applied to two received sequences at the two receivers to find the start sample of each symbol within detected packets. This method is different from the method proposed here (subtracting estimated timing at receiver #1 from estimated timing at receiver #2) since it assumes that both sets of raw received samples at the two receivers are available at a central node (eg. an AP) and the offset estimation can be performed by cross correlating these sequences (in a CP-based method).Centralized offset estimation allows for higher accuracy but it will impose intense bandwidth requirements to transfer the raw data and perform cross correlation between collaborative receivers, especially if the collaboration takes place for a network of users (Martin et al 2011). Thus the time offset between cooperative users is estimated herein in a distributed manner by differencing the final time estimates. The standard deviation of the difference between estimated offsets using these methods (i.e. centralized and distributed offset estimation) is

found to be 142 samples or 7.1 μs for access point #1. According to the fact that the cross-correlating method uses the raw samples from two receivers, it achieves a more accurate estimation of the time offset. The standard deviation of the difference between these two estimates can be considered as representative of the accuracy of the proposed method to compute the offset between WiFi receivers.

Table 4.3: Estimated offset values for detected burst signals from three access points

	A=Mean offset using cross-correlation between signals received at two RXs	B= Mean offset between two receivers estimated at RX #1 (timing 1- timing 2)	Standard deviation of difference Std (A-B)
Access Point #1	57 samples	163 samples	142 samples
Access Point #2	29 samples	81 samples	63 samples
Access Point #3	42 samples	138 samples	119 samples

Using the time-domain correlation-based algorithms, the mean offset between received WiFi sequences from access point #1 at the two receivers is computed to be 163 samples (equivalent to 8.15μs). The WiFi offset is then averaged over the estimated offsets using the signals received from all three APs. The accuracy of the estimated offset between receivers is also evaluated using WiFi packet recordings and decoded time stamps within received frames at receiver #1.The estimated WiFi/GPS offset at receiver #1 is 50.01 μs. After estimating the WiFi-based time offset between the users and the offset between GPS time and WiFi at receiver #1, it is possible to estimate the GPS time at receiver #2. The estimated offset values and final GPS time estimate at receiver #2 for the conducted test along with the estimated accuracies are shown in Table 4.4.

Table 4.4: Timing Analysis for Average C/N_o of 19.48 dB-Hz

WiFi/GPS Estimated Offset at Rx #1 (μs)	Mean Offset between WiFiRxs (μs)	Estimated offset accuracy with regard to centralized method (μs)	Estimated offset accuracy using WiFi packet decoding (μs)	Estimated GPS time at Rx #2 using the proposed method (s)
50.01	8.15	7.10	9.02	072581.221342

Using the time estimate at receiver #2, assisted GPS acquisition is then performed using GSNRx™ (Petovello et al 2008). The performance of the proposed method is compared to other A-GPS schemes and also to a commercial HSGPS receiver. The time to acquire the first satellite for each method is shown in Table 4.5. Satellites with a consistent loss of lock, which resulted in re-acquisition attempts, have been rejected as false peaks and performance is compared for acquired common satellites between different schemes. In other words, only successfully acquired satellites are included.

Table 4.5: Performance Comparison for different GPS Acquisition Schemes for an average GPS C/N_o of 19.48 dB-Hz

GPS Acquisition scheme	Number of satellites acquired	Time to acquire first satellite (s)	Time to acquire last satellite(s)
Conventional with no aiding	0	NA	NA
High sensitivity Rx	5	2.88	6.98
A-GPS with position aiding	0	NA	NA
A-GPS with position and coarse-time aiding	3	2.12	5.44
Proposed WiFi-based A-GPS	3	1.07	4.39

Having no aiding information (a conventional cold-start) results in failure to acquire any satellites in five minutes of collected data in this environment. This is also the case when the only available assistance data is the approximate position. Using the approximate position information, the expected Doppler can be computed to limit the frequency search space. However, in low SNR environments, this would not be sufficient to assist GPS acquisition. The commercial HSGPS receiver was capable of acquiring five satellites in 6.98 s in this case.

Having coarse-time assistance data along with the approximate position information allows the receiver to have a relatively more accurate prediction of the visible satellites. As Table 4.5 shows, an approximate position along with the coarse GPS time estimate with accuracy of 2 s (typical time accuracy provided by hand-held commercial WiFi receivers) allows for acquiring three satellites in 5.44 s with the first satellite having been acquired in 2.12 s. This is an improvement over having no assistance data, as expected. Coarse-time allows for better estimates of Doppler frequency and thus leads to decreased times to acquire satellites in view. However, the accuracy is still not high enough to limit the code delay search.

WiFi-based fine-time assistance (as estimated using the proposed method) allows for a reduction in the code delay search space. With an accuracy of about 9 μs, the code delay search space is limited to ±10 chips. This is still a considerable improvement compared to a 1023 chip search space and the acquisition time for the first satellite has been reduced to 1.07 s when the fine time information is available under weak signal multipath conditions. Reducing the search space has an additional advantage of reducing the computational load on the receiver and save power.

In conclusion, the ability to use WiFi signals to provide fine-time assistance for GPS acquisition in a collaborative scheme has been demonstrated herein using the 802.11g standard with OFDM signaling. This is accomplished by monitoring WiFi and GPS signals at the intermediate frequency sample level and estimating high accuracy relative timing between two receivers, using a practical low complexity method. Time domain correlation-based methods have been combined to achieve a more accurate estimate of the WiFi time offset between the receivers. Performance of the proposed WiFi-based A-GPS method has been analyzed for different environments including NLOS low SNR WiFi reception conditions, where several access points can be within the range of multiple collaborative users. It has been shown that the relative timing between the two users can be estimated with a theoretical accuracy of up to 0.1 μs in a high SNR LOS situation but degrades to about 14 μs in a realistic multipath NLOS environment with very low SNR values. Combining this between-receiver time estimate with a known GPS time computed by one of the receivers and the approximate position of both receivers allows the second receiver to receive fine-time assistance with accuracy of the order of 10 μs. This allows a reduction in both the code and Doppler search spaces that speeds up acquisition of satellites in weak signal environments. Different factors contributing to achievable time estimation accuracy in the proposed method have been described and test results demonstrate that 9 μs level fine-time assistance can be achieved. This is within the required accuracy limits for A-GPS fine time assistance data. The performance of A-GPS acquisition has then been evaluated using the WiFi-based time assistance for real test data collected in an indoor multipath environment. Results have demonstrated that the estimated fine time data reduces the elapsed time to acquire the satellites in view in such conditions.

The next chapter will focus on improving time estimation techniques in terms of the achievable accuracy in different high multipath/low SNR environments.

CHAPTER 5: IMPROVED WIFI-BASED A-GPS SCHEME FOR LOW SNR MULTIPATH ENVIRONMENTS

As demonstrated in Chapter 4, performance of correlation-based methods degrades in multipath environments and under low SNR conditions. This can introduce large errors in the time offset estimation between collaborative WiFi receivers and thus decrease the accuracy of time assistance data to perform A-GPS acquisition.

OFDM timing algorithms can be divided into two groups: pre-FFT algorithms and post-FFT algorithms. Post-FFT algorithms normally use the pilots to estimate a higher accuracy time and frequency offset having an initial estimate. Pre-FFT algorithms exploit the structure of the signal such as using CP, the short training sequence or the long training sequence.

In this Chapter a novel pre-FFT symbol timing estimation technique based on Gaussian Mixture (GM) modeling is proposed to achieve a robust and accurate performance under low SNR multipath environments. First the effects of the multipath channel on timing correlation output are demonstrated for different possible channel profiles and based on this, the proposed method is described. Performance of the method is then evaluated in low SNR NLOS situations both theoretically and using real test data. The tests show significant improvements over conventional methods. Using the proposed GM-based method, the estimated offset between WiFi users is computed and applied to the WiFi-based A-GPS scheme as presented in Chapter 4. The overall performance of the A-GPS structure is then assessed for different data collection scenarios.

5.1 CP-based Correlation Function Output in Presence of Multipath

As described in Chapter 2, the multipath channel impulse response between the transmitter and the receiver is generally modeled as

$$h(\tau) = \sum_{p=1}^{P} \alpha_p e^{-j2\pi f_c \tau_p} \delta[t - \tau_p] \tag{5.1}$$

where α_p is the attenuation factor for the p^{th} path. Depending on the magnitude of the direct path (LOS path), channel profiles can be divided into three major groups, namely the dominant direct path (DDP), non-dominant direct path (NDDP) and undetected direct path (UDP) (Pahlavan et al 1998). In a DDP channel, the dominant path is the direct path while in an NDDP channel, it is the direct path but not the strongest path. However the direct path is still detectable using a modified and probably more complex method. A channel is considered a UDP channel for a receiver when the direct path goes below the detection threshold of the receiver and is thus undetectable. This can happen due to the low sensitivity of the receiver and under low SNR conditions.

As explained in Chapter 4, due to the redundancy introduced by CP, correlation-based methods can be used as practical pre-FFT techniques to estimate the symbol timing in DDP situations (strong LOS reception). By rewriting the received signal as

$$y[n] = \sum_{p=0}^{P-1} \alpha[p] u[n - \delta - p] e^{j2\pi\varepsilon[n-p]/N} + \upsilon[n] \tag{5.2}$$

the output of the correlation function is

$$
\begin{aligned}
A[m] &= \sum_{k=m}^{m+L-1} y[k]y^*[k+N] \\
&= \sum_{p=0}^{P-1} \alpha^2[p] e^{-j2\pi\varepsilon[n-p]/N} \sum_{k=m}^{m+L-1} u[k-\delta-p]u^*[k-\delta-p+N] + \eta[m] \\
&= \sum_{p=0}^{P-1} A_p[m] + \eta[m]
\end{aligned}
\tag{5.3}
$$

where $A_p[m]$ is the output of the correlation function for the p^{th} path and $\eta[m]$ represents noise and interference. Hence due to the linearity of expectation functions, the combination of expectations for each path is the sum of correlator outputs for the paths. For a single path *p,* the expectation of the correlator output for an AWGN channel is the following triangular function (Williams et al 2005):

$$
E\{\sum_{k=m}^{m+L} y[k]y^*[k+N]\} = \begin{cases} \sigma_s^2 e^{-j2\pi\varepsilon} & \delta - L < k - M(\mathrm{N}+\mathrm{L}) < \delta + L \\ 0 & otherwise \end{cases}
\tag{5.4}
$$

For a multipath channel, as in Equation 5.1, the correlator output is the sum of shifted correlation functions. For a CP-based correlation function the width of each component equals $2\times CP\_Length$. Figure 5.1 shows the output of the correlator in AWGN channel for two paths.

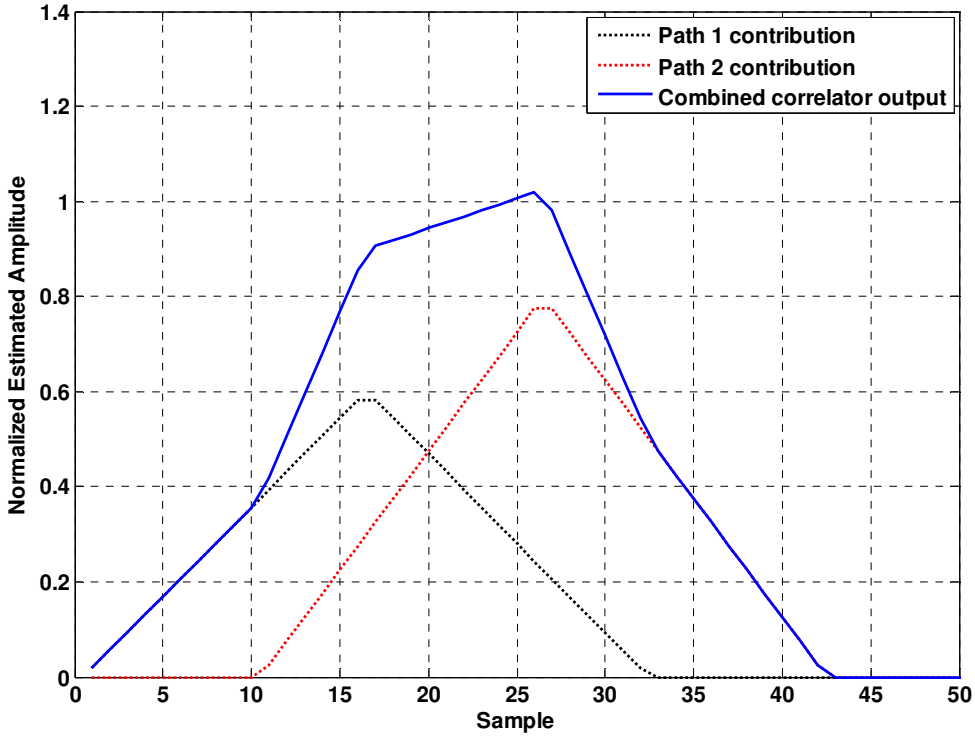

Figure 5.1: Combined Correlation function for a two-path channel

No assumptions about channel fading characteristics are made except that the channel is quasi-static and remains time invariant for the duration of one transmitted symbol. As demonstrated in Figure 5.1, the peak of the correlator output for a multipath channel does not necessarily occur at the arrival time of the direct path which can be the main source of timing error for correlation-based methods in multipath environments as mentioned earlier. Note that Figure 5.1 only aims to illustrate an example of how different multipath components contribute to the correlator output under ideal conditions based on Equation 5.4 and is not representative of real world data situations. Obviously, the general concept still applies in situations where multipath effect occurs in a destructive manner.

Different solutions have been addressed in the literature to improve the performance of correlation-based detection in multipath channels. Leading edge detection of the correlator output is proposed in Palin et al (1998) using a threshold value. However since the method is based on setting a crossing threshold to detect the first edge, for time variant correlation amplitudes the threshold needs to be changed accordingly. This can lead to performance degradation especially in time variant SNR conditions and for complex channel models (Williams et al 2005). Some other proposed methods try to exploit the ISI-free portion of the CP. In Huang et al (1999), due to the fact that the phase remains constant for the ISI-free area and is otherwise random, changes in phase estimates are detected as estimations for timing values. The main drawbacks of this method are its dependence on ISI-free portions and its sensitivity to frequency offset; the method also requires relatively long averaging periods. In order to achieve a lower variance, Palin and Rinne (1998) proposes to use a second correlation function. This method is based on the assumption that for most of the channels there are slight changes of the correlator output for two adjacent symbols. The variance is lower using this method, however the mean value is close to the one achieved by simple correlation-based methods. Williams et al (2008) proposed a derivative method as a low complexity pre-FFT timing method with improved performance in multipath environments. This method is based on properties of derivative of the summed correlation function. Assuming no noise, the slope of the derivative of $A[m]$ is monotonically increasing up to the peak of the first component. Hence, the ideal timing point is determined by detecting the time at which the derivative of the summed correlation function starts to decrease. A smoothed estimate of the derivative and backward LS fitting is used to improve the performance of the derivative method in practical situations. However, this method requires threshold setting and is also sensitive to the length of the filter used for the derivative operation. More importantly,

the method is very noise sensitive and may result in high false alarms for low SNR conditions. This draws attention to the need to develop a method that includes the benefits of the derivative method, such as its independence on the channel characteristics, but still performs well in presence of correlator noise.

5.2 Proposed Pre-FFT GM-based Timing Method

The additive nature of the correlator outputs, as demonstrated in the previous section, motivates the use of pattern recognition algorithms in order to detect the arrival times under low SNR conditions. The approximation theory presented in Li & Barron (2000) justifies the choice of Gaussian functions to model each path contribution to the correlator output under noise. This theory states that a large enough mixture of Gaussian functions can arbitrarily closely fit any density in an ML sense. Hence, Gaussian mixture modeling allows for a blind estimation of channel parameters.

Based on the summed correlation function characteristics, it is proposed here to estimate the timing points of the arriving paths using Gaussian Mixture (GM) modeling as

$$A[m] = \sum_{p=1}^{P} \omega_p \mathrm{N}[m; \mu_p, \Sigma_p] \tag{5.5}$$

where P is the number of mixtures (number of paths) and $\mathrm{N}[m; \mu_p, \Sigma_p]$ is a normal distribution with mean μ_p and covariance matrix of Σ_p. μ_p and Σ_p represent the delay and the width of the P^{th} path component respectively. ω_p is the mixture weight for the P^{th} path, which represents the relative magnitude of the channel impulse response for that path. Path delays can then be obtained by fitting the

parameter vector for the mixing Gaussian multipath channel characteristics. Figure 5.2 shows an example of GM representation of two path components for a sample noisy correlator output.

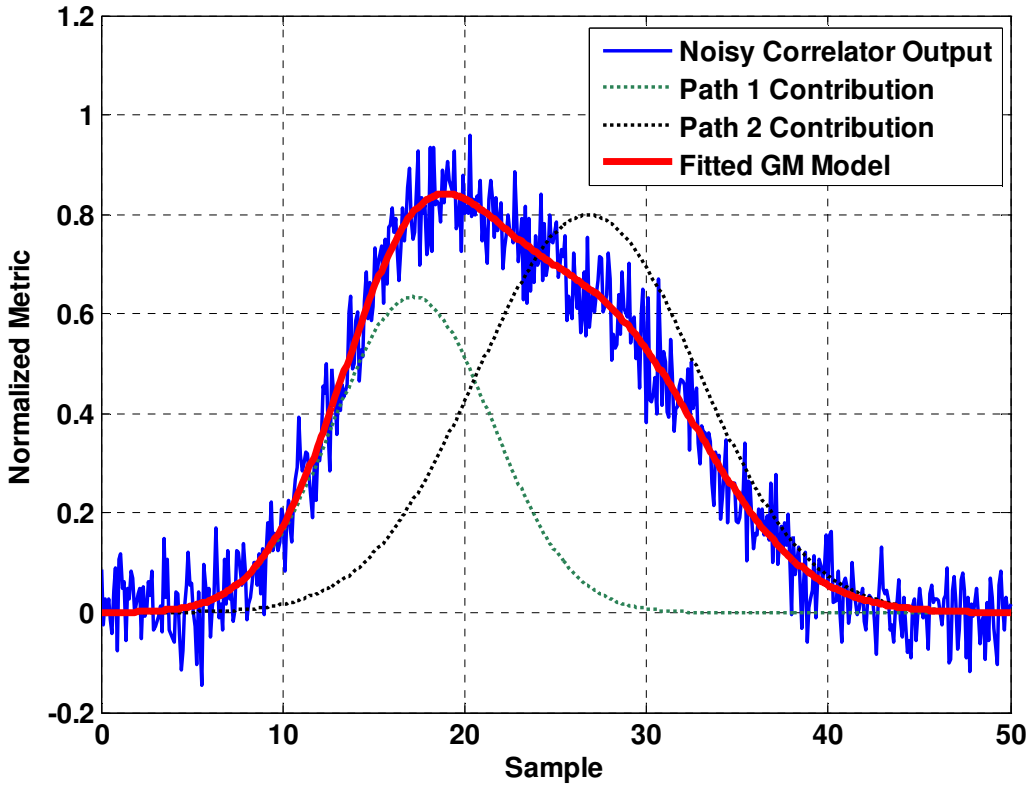

Figure 5.2: Example of GM fitting for a sample noisy correlator output in a two-path channel

Relaxing the assumptions on the correlator noise statistics and considering a GM model for the summed correlation output, the parameters of the Gaussian components $(\sum_p, \mu_p, \omega_p)$ can be estimated in a nonlinear iterative procedure. In the context of CP-based OFDM timing estimation with known CP length, the width of the Gaussian components can be assumed as a priori known information to constraint the optimization algorithm in order to achieve a better estimate of other parameters. Therefore, the proposed method is implemented for a constrained GM modeling with fixed width.

In order to fit the vector parameters, optimization techniques should be implemented. One common iterative optimization algorithm is the Expectation Maximization (EM) method, which iteratively performs an E step (Expectation step) and an M step (Maximization step) to converge to a local optimum in the parameter space. The EM method yields an ML estimate of the vector parameters (Moon 1996). Although the EM algorithm has good convergence ability even for poor initial values, the convergence rate can be very slow (Press et al 1992). Hence, in order to achieve a faster convergence, the optimization method proposed by Nelder & Mead (1965) is used. The method is called the Downhill Simplex Method (DSM) and is a derivative-free optimization technique based on function evaluations. The fact that the DSM method doesn't use the derivative functions makes it an appropriate method especially in constraint mode. With *N* being the dimension of the parameter area, the optimization starts from *K+1* points building an initial simplex and the main idea is to bracket the minimum and gradually isolate it. A simplex can be considered as the simplest volume in the parameter region. Based on the function values, the simplex is reflected or shrunk away from the extreme point. The general concept of the DSM can be explained following the development in Quinten (2012). The goal is to find a local minimum of a function *y* of *K* variables θ, as

$$y = g(\theta_1, ..., \theta_K) \tag{5.6}$$

Assuming the local minimum y_m occurs at corresponding variables θ^m simplex of *K+1* points with vectors θ^1..., θ^{K+1} is formed. Then the best point (y_{min}, θ_{min}), the worst point (y_{max}, θ_{max}) and the second worst point (y_v, θ_v) are determined. In the next step a mirror centre is created using all point except the worst point as

$$\theta^s = \frac{1}{K} \sum_{\theta^i \neq \theta^{\max}} \theta^i \tag{5.7}$$

Then a lower volume simplex is obtained by reflecting the worst point to the mirror center as

$$\theta^r = \theta^s - \kappa_1(\theta^{\max} - \theta^s) \tag{5.8}$$

Three methods are used to form a new simplex. The expansion method accelerates the reduction of the simplex volume, the contraction method keeps the simplex volume small and the compression is used around the actual best point. All these steps are performed repeatedly to achieve the best point. Figure 5.3 shows these steps for a three point simplex from *K=2* parameters.

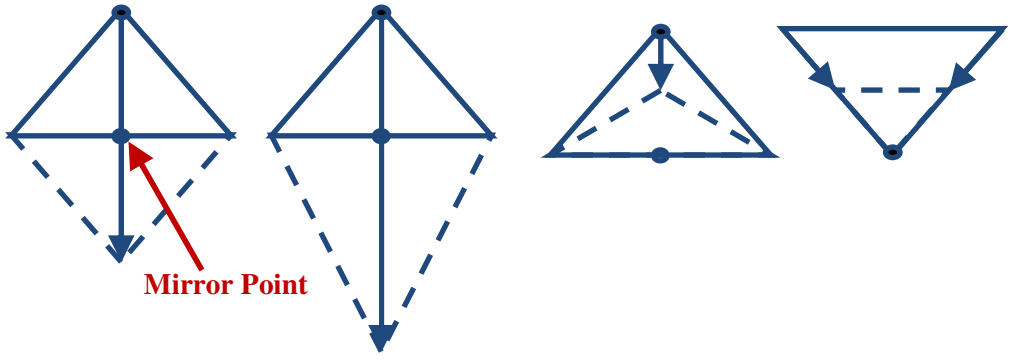

Figure 5.3: The steps in DSM method (after Quinten 2012): (a) Reflection (b) Expansion (c) Contraction and (d) Compression

The flowchart of the DSM algorithm is shown in Figure 5.4. After the first reflection, the expansion point is obtained as

$$\theta^e = \theta^s - \kappa_2(\theta^r - \theta^s) \tag{5.9}$$

This point is compared to (y^r, θ^r) to determine the next step as shown in Figure 5.4. κ_1 and κ_2 are Nelder-Mead Parameters.

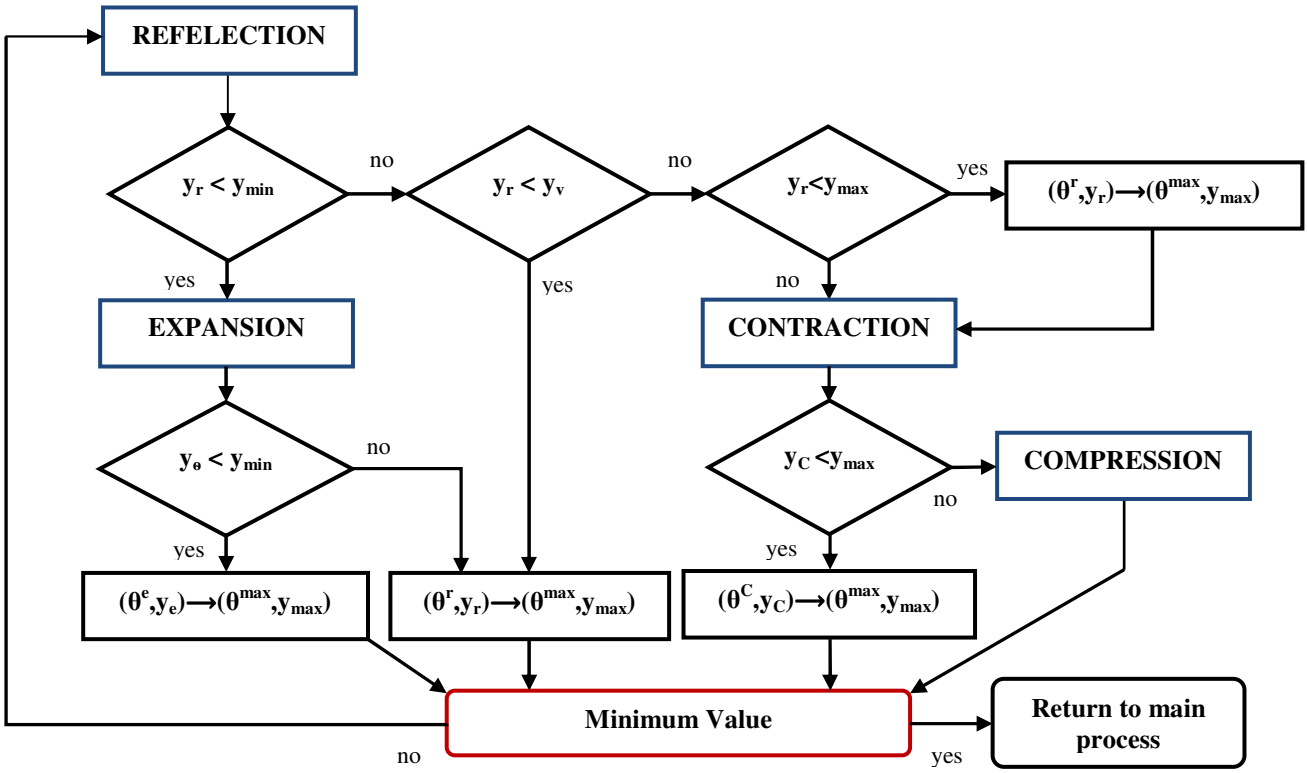

Figure 5.4: Flowchart of DSM method (after Quinten 2012)

After performing the DSM method the vector parameters for the Gaussian mixture model is estimated for a constrained width. The proposed GM-based method does not require a priori knowledge of the channel statistics or the number of paths, achieves high accuracy timing estimations under low SNR conditions and allows for first path detection in non-dominant DP channels. The GM method can also be implemented for real-time tracking of the time offset under time-variant channel characteristics using CPs in transmitted symbols.

5.3 Theoretical performance analysis of the GM-based timing method

To estimate arrival times for 802.11g signals in a multipath environment, the proposed method is implemented by constraining the width of the Gaussian components to the CP length. Constraining the

algorithm may result in a higher average fitting error, but results in a higher timing accuracy. Figure 5.5 shows an example of how the method performs on a sample correlator output using a constrained and an unconstrained algorithm. Five paths are assumed for the multipath channel. In the constrained GM method the width of the components is fixed to 32 samples while in the unconstrained GM method the width is also estimated as a parameter of the Gaussian components. The fitting error of the constrained GM is found to be 4.2 % while unconstrained GM achieves lower fitting error of 3.9 %. However, the mean timing estimation accuracy is 0.83 samples when the algorithm is constrained and 2.1 samples for unconstrained method.

As the ultimate goal of the algorithm is to detect the first arriving path in harsh environments and improve the time offset accuracy between WiFi users, the number of paths need not be known or estimated in advance. By considering an arbitrary yet practical number of paths depending on the environment, the method can detect the first arrival time (along with some other arrival times) with high accuracy. If the number of paths is known {e.g. by using MDL method (Vanderveen et al 1998)}, the method can be used to accurately determine all the timing points and also the weights for each multipath channel component.

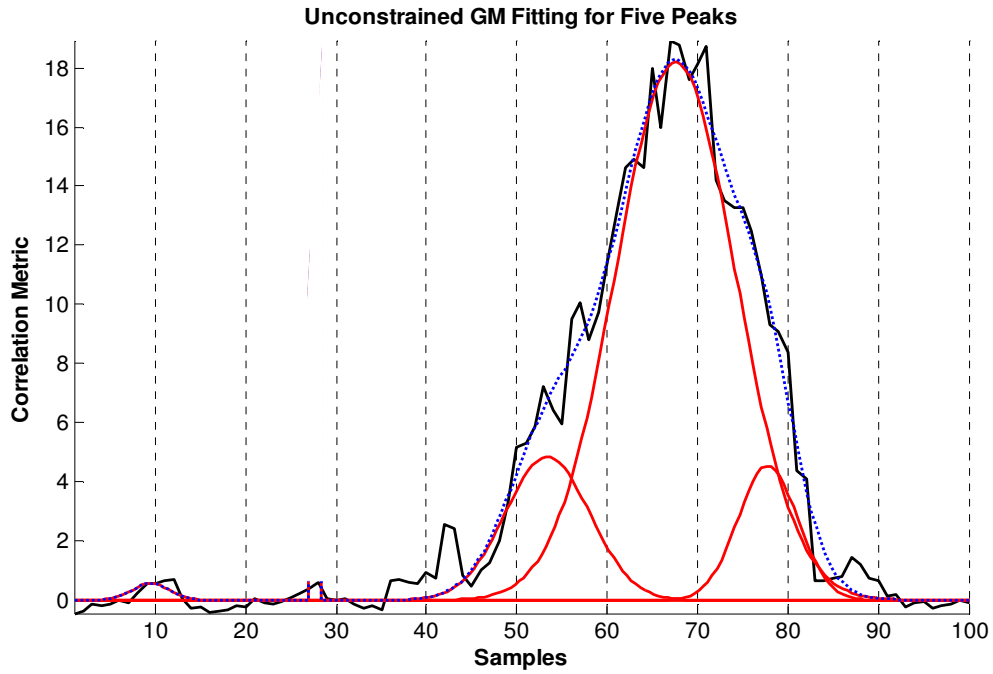

(a)

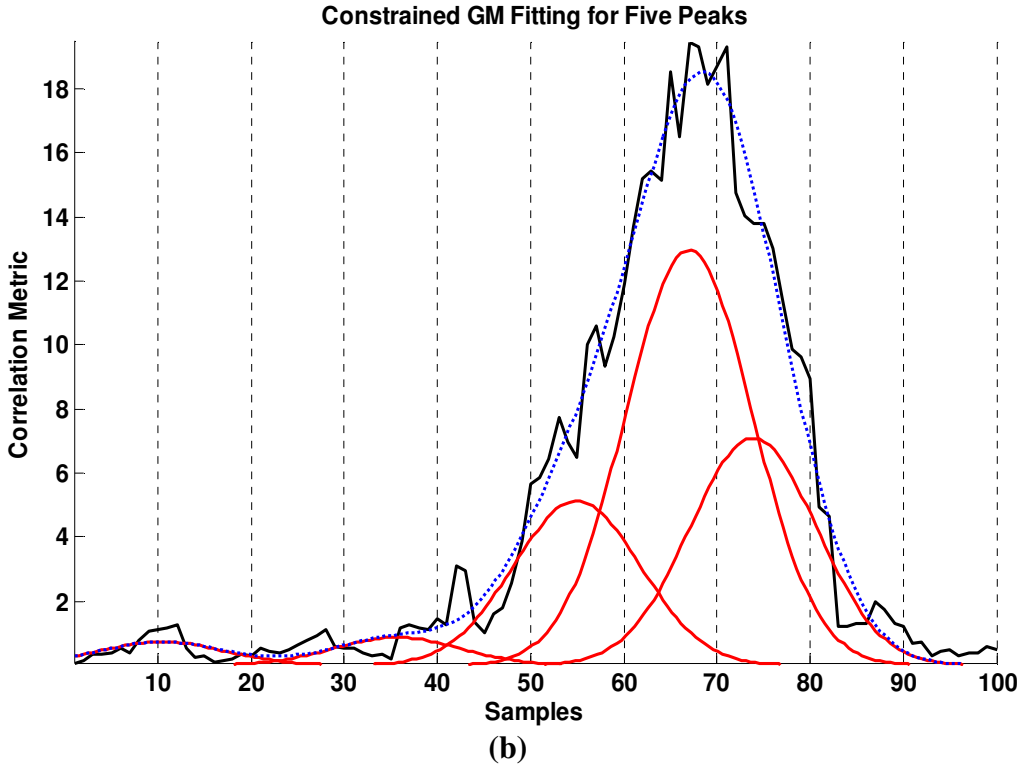

(b)

Figure 5.5: GM method performance; (a) unconstrained and (b) constrained GM method

To illustrate the improvement of arrival time estimation in low SNR and under non-dominant DP multipath environments, the proposed timing method is implemented for a sample two-path multipath channel with a low power first path signal. The number of components is assumed to be five. Figures 5.6 and 5.7 show the results for a single OFDM packet using the CP-based GM method and the conventional correlation based pre-FFT method. Figure 5.6 demonstrates the standard deviation of timing error for two methods. As it can be seen, the proposed method achieves considerable improvements in terms of standard deviation of the error and remains robust under low SNR conditions while with the correlation-based method the error increases rapidly when SNR decreases. To compare the bias of the estimation in the two methods, Figure 5.7 shows the mean timing error in terms of samples; the mean error of the GM-method is nearly zero for the entire SNR range while the correlation-based method bias approaches to the arrival time of second path and so does not detect the DP. The results of Figures 5.6 and 5.7 are a representation of high accuracy and robustness of the proposed method in low SNR multipath environments. By using correlation-based methods, for low SNR values the bias reduces and approaches to zero, which is justified by the dominant effect of noise in this situation. This along with the increased standard deviation of error, demonstrates performance degradation of correlation based methods and a reduced ability to estimate signal parameters with decreased SNR values as expected. When the SNR increases, the standard deviation decreases but the correlation based method erroneously estimates the arrival time of the dominant path as the timing point. This is demonstrated in Figure 5.7 where the bias increases with SNRs.

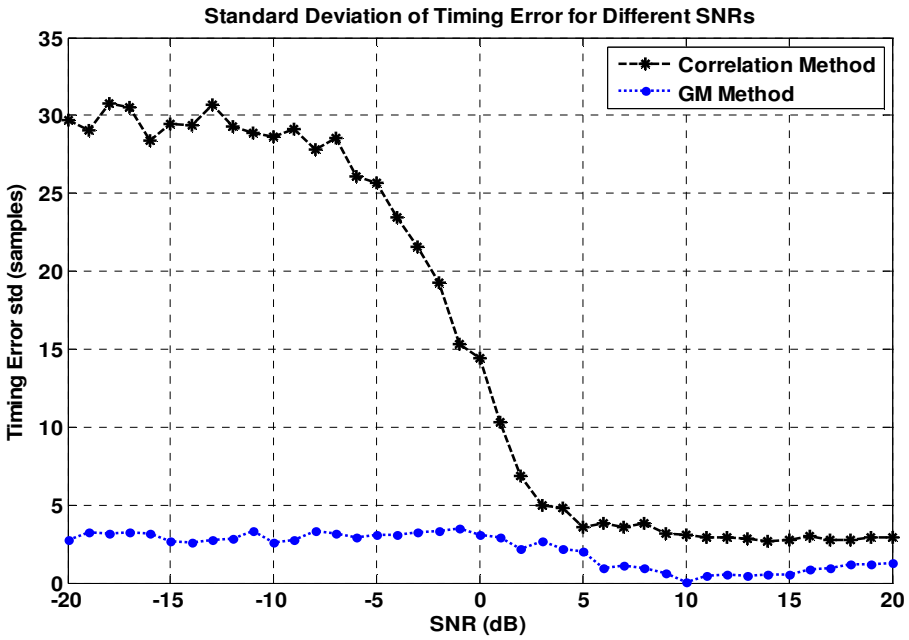

Figure 5.6: Performance comparison of GM and conventional correlation based method - standard deviation of timing error for different SNRs

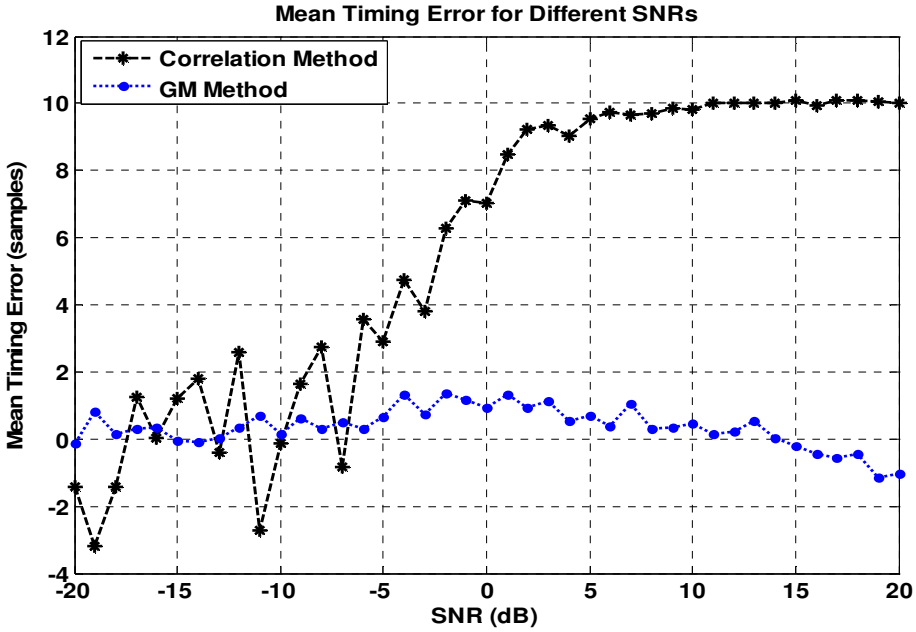

Figure 5.7: Performance comparison of GM and conventional correlation based method - mean timing errors for different SNRs

Figures 5.8 and 5.9 show the performance of the GM-based method as a function of the ratio of the first to second path amplitude for a fixed SNR of 5 dB. The GM method outperforms the correlation method in terms of both the timing accuracy and the robustness to detect the first arriving path in harsh environments.

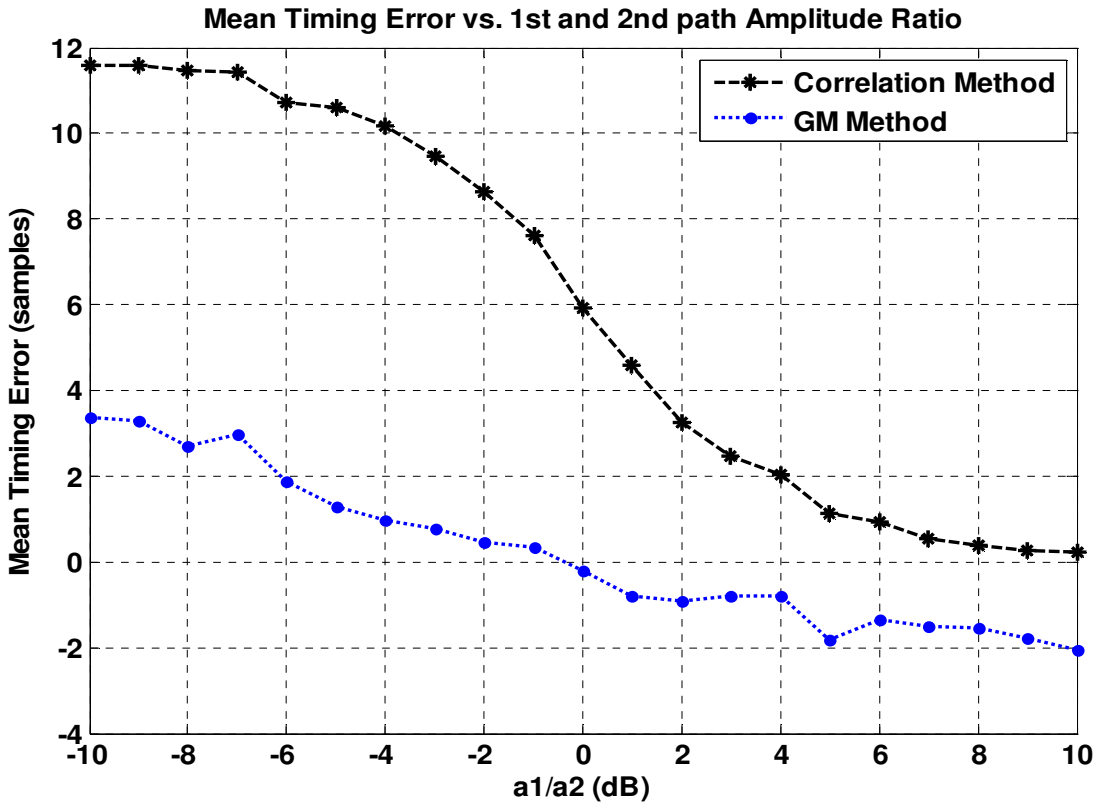

Figure 5.8: Performance comparison of GM and conventional correlation based method - mean timing errors for different first to second path amplitude ratios

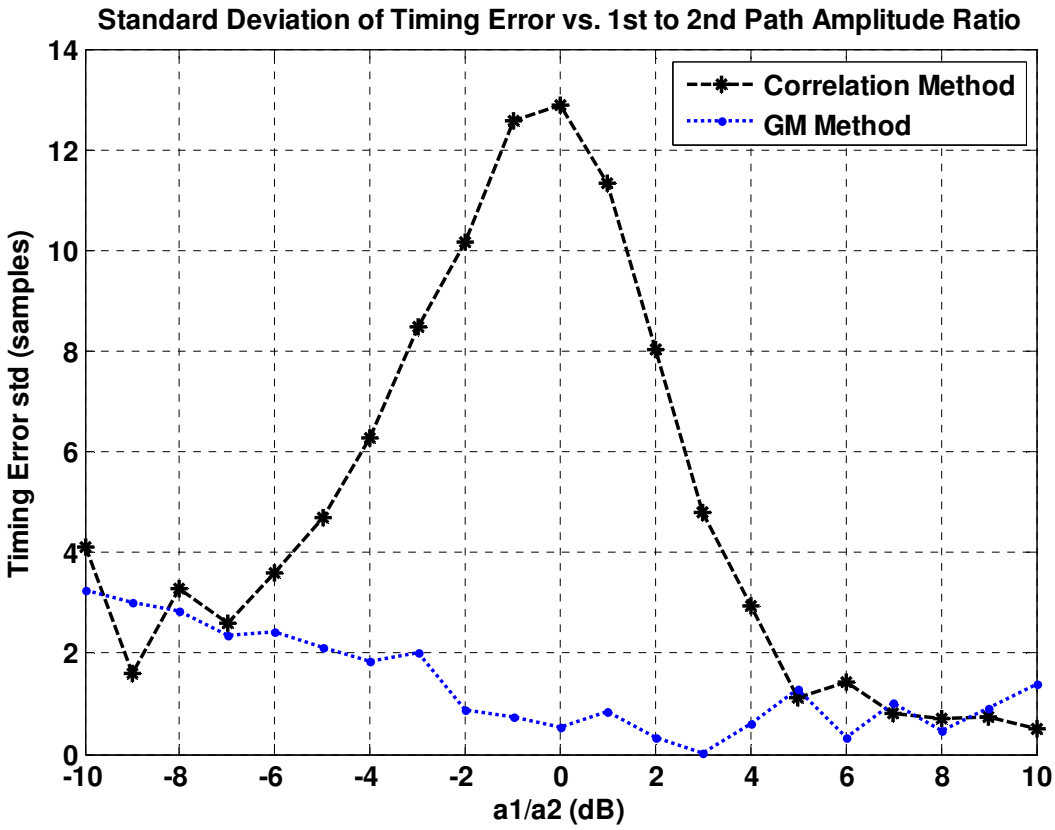

Figure 5.9: Performance comparison of GM and conventional correlation based method - standard deviations of timing error for different first to second path amplitude ratios

5.4 Experimental results

In order to test the GM-based timing algorithm and apply it to the A-GPS acquisition structure, tests were conducted in two different indoor multipath environments. Environment # 1 is the same multipath environment as in Section 4.4.2 {a four-story university building with glass skylights (MacHall building)}. Environment #2 is the upper level of a university building with a hallway containing a glass ceiling and wide glass windows (Oval building). In terms of GPS signal reception, Environment #2 provides better C/N_o and satellite visibility in comparison to Environment #1. Figure 5.10 shows views

of Environment #1 and Environment #2. In both environments two collaborative WiFi/GPS users are within the range of same WiFi APs. To test the proposed timing method in low SNR multipath environments, the transmit power of the OFDM 802.11g routers was set to low. One receiver was placed such that it could acquire and track GPS and the other receiver was placed such that it experienced weak GPS signal reception but was able to perform A-GPS acquisition. The equipment and hardware set up is the same as explained in Section 4.3 and Section 4.4.

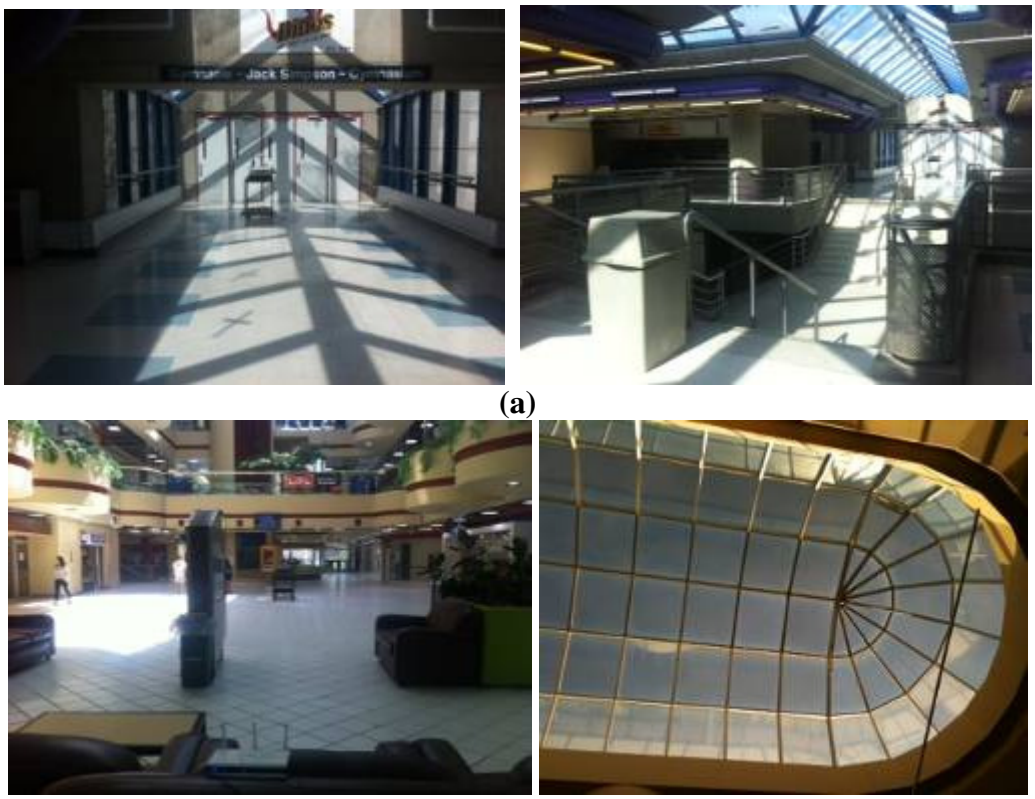

(a)

(b)

Figure 5.10: View of data collection environments: (a) Environment #2 (Oval) (b) Environment #1 (MacHall)

As explained in Chapter 4, the WiFi timing offset between users is determined by determining the time offset between Receiver # 1 and Receiver # 2. If the non-dominant direct path arrival time can be estimated, the overall performance of the proposed WiFi-based A-GPS method will improve. In other words, by detecting the first arriving path, the additional error term introduced in the proposed WiFi-based A-GPS method (i.e. $\partial t_{Max\ Channel\ Delay}$ due to the multipath channel) as in

$$T_{GPS}^{'} = T_{GPS} + \partial t_{WiFi/GPS} + \partial t_{WiFi} + \partial t_{Max\ Channel\ Delay} \tag{5.10}$$

can be avoided. Hence, the timing offset between WiFi users can be computed with a better accuracy and this in turn can reduce the A-GPS acquisition search space.

The OFDM timing algorithm to estimate the corresponding arrival times in a WiFi receiver is implemented in two main steps:

1. Using the developed correlation-based method as described in Section 4.4.1, an initial symbol timing estimate is achieved for the received signal.
2. Using the initial symbol timing, the constrained CP-based GM timing method is performed on the OFDM data block, for a high accuracy timing estimation and also tracking timing points along the transmitted OFDM block.

After detecting the timing points at the two receivers (in terms of samples), the offset is computed by subtracting estimated values. The WiFi offset is then applied to the A-GPS scheme to assist GPS acquisition for Receiver # 2 in harsh environments, as described in Chapter 4.

Figures 5.11 and 5.12 show the performance of the developed GM technique and the CP-based correlation method on the real test data for two different SNR conditions. Both methods are implemented using CPs and the initial symbol timing estimate. The distance between the detected peaks for a block of OFDM signal, according to the CP redundancy, should be 80 samples. In the higher SNR environment shown in Figure 5.11, the correlation-based method creates higher peaks but is still not capable of resolution between paths. The timing error for this method is found to be 17 samples with the threshold set to 0.7 for a normalized correlation output. The timing point is detected when the normalized correlation exceeds this threshold. In the low SNR environment shown in Figure 5.12, the correlation-based method is not able to detect the non-dominant peak occurring at 11 samples and, with a threshold of 0.7, results in a mean timing error of 118 samples. The GM method estimates the position of the peaks due to direct path occurring at samples 11.0, 91.4, 180.9 and 260.0, which gives a mean error of 0.6 sample. As can be seen in Figures 5.11 and 5.12, the GM technique can also be used as a method to determine the timing points of the other arriving paths in an indoor channel. As results show, the other advantage of the GM method over the correlation based method is that it does not create the plateau generated in the CP-based correlation method and thus avoids ambiguities in estimating the timing value.

As explained in Chapter 2, a multipath channel can be considered as clusters of rays arriving at different times. The exact number of paths does not need to be known as a priori information for the purpose of this research. As long as the number of paths is selected using typical values for a particular environment, the method is able to provide timing estimates of the first path with high accuracy. For the test environment used here (Figure 5.10), 16 to 18 multipath clusters are assumed (IEEE P802.11

WLANs 2004). For the data set presented here, changing the number of paths from 10 to 18 results in an average standard deviation of about 3 samples (0.15 μs) in estimating the arrival time of the first path. This shows the low sensitivity of the method to the selected number of paths.

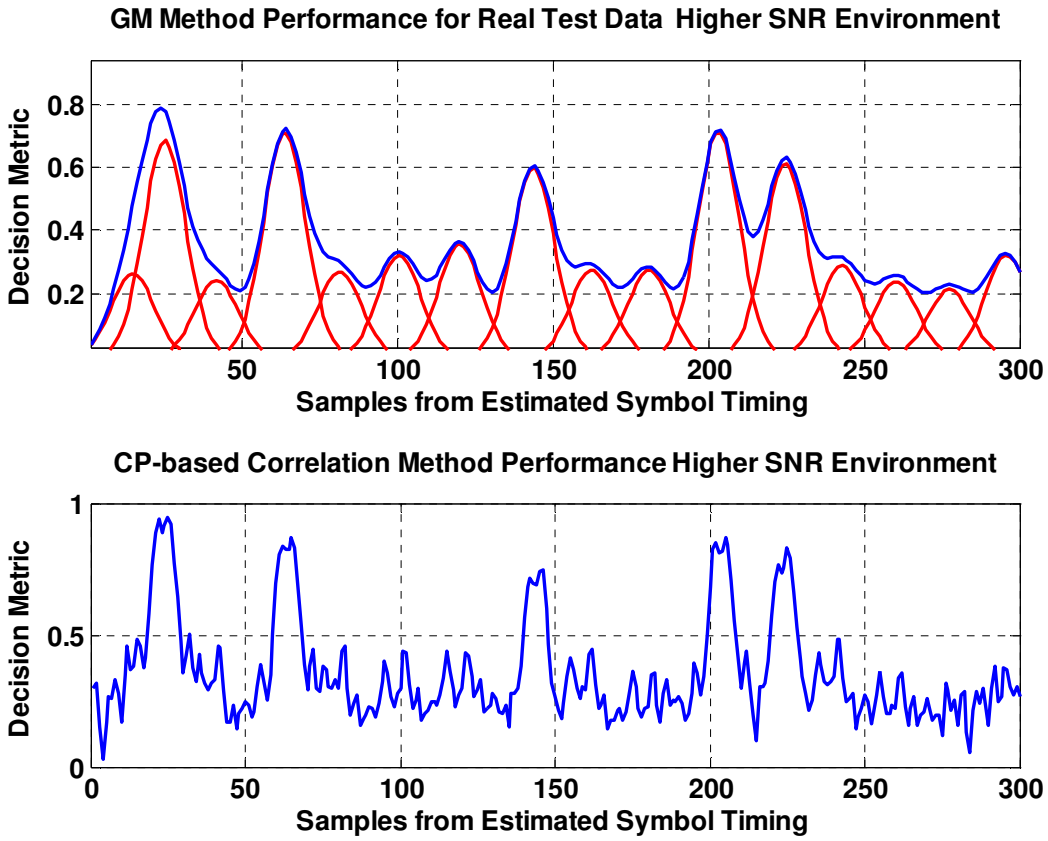

Figure 5.11: GM method performance on real data with relatively high SNR

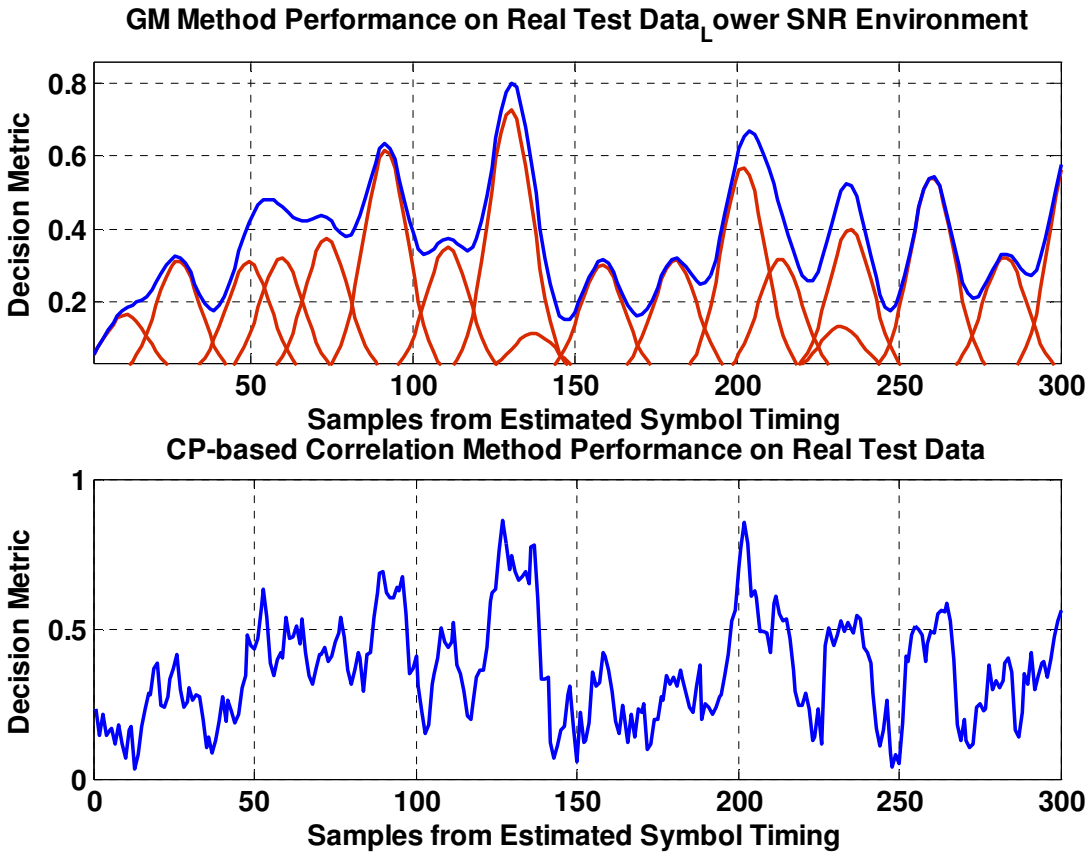

Figure 5.12: GM method performance on real data with relatively low SNR

Table 5.1 shows the standard deviations of the estimated timing at Receiver # 1 for the two test environments. The accuracy of the estimated offset between receivers is also evaluated using WiFi packet recordings and decoded time stamps within received frames. Significant improvements are achieved in term of timing accuracy using the constrained GM-based method. Timing accuracies of 21 samples and 16 samples represent 1.05 μs and 0.8 μs respectively and can narrow the GPS code-delay search space to a few chips.

Table 5.1: Standard deviations of estimated timing for two environments

Standard Deviation of Estimated Timing	Environment #1 MacHall	Environment #2 Oval
Correlation Method	126 samples	72 samples
GM-based Method	21 samples	16 samples

Using the developed timing algorithm, the mean offset between the two WiFi receivers is computed to be 41 samples for Environment #1 and 33 samples for Environment #2, respectively. The estimated mean offset is then used along with the WiFi/GPS offset estimate at Receiver #1 to achieve the fine timing estimate at Receiver #2. The computed offset values and assistance time estimates at Receiver #2 are shown in Table 5.2.

Table 5.2: Estimated offset values and GPS time for two environments

	Mean Offset Between WiFi Receivers	WiFi/GPS Estimated Offset at Receiver #1	Estimated GPS time at Receiver #2
Environment #1 (MacHall)	2.05 μs	68.07 μs	584438.030482
Environment #2 (Oval)	0.8 μs	49.04 μs	599711.269451

Then having the time estimates at Receiver #2, the A-GPS acquisition is performed using GSNRx^{TM} (Petovello et al 2008) as explained in Chapter 4. Different A-GPS schemes and also a commercial HSGPS are compared to the proposed structure with fine-time estimates in terms of number of satellites acquired and time to acquire the first satellite. Ten minutes of data is used and as described in Chapter 4, satellites with frequent losses of lock are not considered. The results are shown in Table 5.3.

Table 5.3: Performance Comparison for different GPS acquisition schemes (The average C/No for Oval is 27.71 dBHz and that for MacHall is 20.14 dBHz)

GPS Acquisition scheme	Number of satellites acquired		Time to acquire first satellite (s)		Time to acquire last satellite(s)	
	MacHall	Oval	MacHall	Oval	MacHall	Oval
Conventional with no aiding	0	4	NA	2.90	NA	11.03
High sensitivity Rx	5	7	3.42	1.84	16.42	9.84
A-GPS with position aiding	0	4	NA	2.88	NA	10.26
A-GPS with position and coarse-time aiding	3	5	2.37	1.09	7.60	7.03
Proposed WiFi-based A-GPS	3	5	1.13	0.65	6.38	7.14

In Environment #1, which has lower C/N_o values (average of 20.14 dBHz), the conventional cold start with no aiding as well as A-GPS with approximate position assistance fails to acquire any satellite. Having coarse time aiding allows for the acquisition of satellites in view and improvements are achieved both in terms of time to acquire the first satellite and time to acquire the last satellite as expected. The commercial HSGPS acquired five satellites in 16.42 s.

As explained in Chapter 4, having a coarse estimate of time allows for Doppler frequency estimation which leads to shorter satellite acquisition times. This results in reduced acquisition times in comparison to conventional cold start and A-GPS with approximate position. As an example, a timing accuracy of 2 s allows for acquiring five satellites in 7 s in Environment #2.

As can be seen in Table 5.3, the developed WiFi-based A-GPS scheme achieves performance improvements in both scenarios over other methods. The reason is the code delay search space reduction with fine time assistance. With an accuracy of about 1.5 μs for Environment #1, the search space can be reduced to ±2 chips, which is a considerable improvement over searching ±1023 chips. Hence, in Environment #1, the acquisition time is decreased to 1.13 s using the WiFi-based A-GPS scheme.

In conclusion, as a continuation of the research presented in Chapter 4, this chapter has developed a novel constrained GM-based timing method in order to improve the accuracy and robustness of the WiFi time offset estimation in NLOS multipath environments and under low SNR conditions. The performance of the developed GM method has been evaluated for non-dominant low power direct path and the results have demonstrated that the method can estimate the first arriving path with high accuracy and maintain robustness for very low SNR values. Other than the first arriving path, based on the number of components used for GM fitting, the method is also capable of estimation the timing points of the multipath channel and thus can be used as a channel estimation technique especially for post-FFT algorithms. The proposed GM-based timing is then applied to implement the WiFi-based A-GPS scheme as explained in Chapter 4. The performance of the overall system is then evaluated using real test data. Experimental results for two different multipath environments demonstrate the performance improvement of the implemented system in NLOS multipath environments. By detecting the non-dominant first arriving path and achieving about ±2 μs timing accuracy, the acquisition results approached the ones achieved for dominant LOS environments as shown in Chapter 4.

CHAPTER 6: CONCLUSIONS AND RECOMMENDATIONS

This chapter presents the main conclusions of this thesis where WLAN signals have been integrated to GPS in order to resolve GPS shortcomings and achieve improved performance in challenging environments. Furthermore, recommendations for possible future work to enhance the proposed algorithms and developed schemes are represented.

6.1 Conclusions

Based on the results and analysis demonstrated in this thesis, a summary of the conclusions and outcomes are presented in this section.

6.1.1 Context-aware WiFi/GPS integration in the navigation domain

In the navigation domain, a WiFi-based MMAE Kalman filter algorithm has been implemented and based on the performance assessments of the system developed herein, the conclusions are:

- Repeatability and consistency of the WiFi signal features have been investigated based on which WiFi context identifiers have been developed using simple yet effective identification algorithms. To identify contexts. WiFi features are used such as the number of available APs or the number of APs with RSS exceeding a certain threshold, the mean and the variance of the total RSS from available APs, etc. The developed identifiers have been shown to be able to effectively determine motion contexts such as static/kinematic and environmental contexts such as indoors/outdoors. By using the appropriate threshold and parameters, the achieved decision sequences match the correct sequence of contexts for more than 90% of the time.

- The contexts identified by WiFi signals are used as external information in the proposed two-layer MMAE Kalman filtering algorithm. Each individual Kalman filter is matched to a different dynamic model and the adaptive parameters are adjusted according to the context. The method has been assessed for different test environments and results demonstrate considerable performance improvements in terms of positioning error. The proposed algorithm outperforms conventional Kalman filtering and IAE Kalman filtering by adapting the dynamic model and the process noise in the test environment.

- A modified DST-based algorithm is developed to combine decision sequences from different identifiers. It has been shown that the method enhances the performance of the WiFi-based adaptive KF in terms of positioning accuracy and robustness. The DST method is developed such that it is capable of handling conflicts between the identifiers to improve the probability of correct identification.

- A weighting block has been developed to avoid both delay of response to identified contexts and abrupt changes. This decreases the sensitivity of the algorithm to errors in decision sequences and also counters performance degradations due to delay in response.

- A finite state MDP control block has been developed for improved robustness. The control block reduced the sensitivity of the algorithm to false identifications in case of high uncertainties and with low reliability in the decision sequence. Another advantage of the developed MDP block is that it can be used to determine the reliability coefficient of the context identifiers based on the amount of correction implied by the decision sequences.

6.1.2 Collaborative WiFi-based A-GPS acquisition

Based on the thesis work on integrating WiFi with GPS for a faster acquisition in an A-GPS structure, the ability to use WiFi signals to provide fine-time assistance for GPS acquisition has been investigated using the 802.11g standard with OFDM signaling. It has been proposed to monitor 802.11g OFDM signals in the physical layer in a collaborative A-GPS scheme where reference time information can be communicated from WiFi users currently tracking GPS to WiFi users attempting to acquire GPS signals. This has been accomplished by monitoring WiFi and GPS signals at the physical layer, and decoding and estimating high accuracy relative timing between receivers. It has been shown that estimated timing along with position approximation can be used as assistance data in an A-GPS framework to reduce the search space and speed up acquisition of satellites in weak signal environments. The proposed scheme can be deployed in places where WiFi coverage is available and where there is no or limited access to other synchronized systems. WiFi enabled mobile devices deployed on university campuses, hospitals, shopping malls and similar public areas are good examples where this method could be applied. Another example could be tablet computers being used on public WiFi networks. Based on the application, communication between users can be established in a centralized or non-centralized manner. The main conclusions can be summarized as

- The proposed system has been developed using existing lab equipment and experimental hardware design. The developed system should be able to perform synchronized sampling of WiFi and GPS. The performance of the proposed WLAN-based A-GPS has been evaluated primarily in a dominant LOS indoor environment. The time offset between collaborative WiFi

users has been estimated using two practical low complexity methods i.e. the CP-based correlation technique and the minimum difference technique. The methods are implemented in the time domain. Different factors contributing to achievable time estimation accuracy in the proposed method have been considered and test results have demonstrated that the accuracy of estimated timing from the WiFi is at the microsecond level, which satisfies the accuracy requirements for fine time A-GPS applications.

- The proposed system has been then tested in real situations under multipath conditions. The performance of conventional low complexity OFDM timing methods was assessed for NLOS multipath environments. Several practical time-domain OFDM timing techniques were considered based on signal structure namely CP-based LTS-based and STS-based correlation methods. The performance analysis and test results demonstrated that multipath may result in large errors in terms of timing accuracy which necessitated improving the OFDM timing techniques for enhanced accuracy and robustness in NLOS multipath environments.

- In order to maintain low complexity for the timing method, an algorithm for relative time estimation was developed by the effective combination of time domain correlation-based techniques. By conducting several experiments, the method proved to be sufficient to enable an effective WiFi-based A-GPS acquisition system with fine time assistance in NLOS multipath environments. However, it was shown that the accuracy of relative timing between the two users degrades to about 14 μs in a realistic multipath NLOS environment with low SNR values.

- In order to achieve high accuracy timing in NLOS multipath environments with low SNRs, a constrained GM method was proposed based on the properties of the 802.11g OFDM CP structure. Performance analysis of the proposed method demonstrated considerable improvements in terms of timing accuracy and the ability to detect non-dominant direct path in multipath channels. The GM method proved to maintain its robustness in different NLOS environments and under low SNR conditions. The method was then applied to the WiFi-based A-GPS scheme and tested for two different indoor environments. Experimental results showed that the method was able to provide timing estimation with accuracy of about 2 μs for low SNR multipath environments to provide fine time for A-GPS acquisition and achieve similar results as in dominant LOS conditions.

6.2 Recommendations for Future Work

Based on the work presented in this thesis the following recommendations are made for further enhancements and possible continuations:

- In the field of navigation domain integration of WiFi and GPS, the contexts were identified based on WiFi features using simple and practical threshold setting methods. The method could be further improved in terms of robustness by adding threshold setting algorithms to the context identification system based on mathematical modeling of the WiFi signal features. Another option would be to develop adaptive threshold setting methods to maintain performance in highly dynamic situations and time variant parameters.

- In this thesis the contexts identifiers are developed for indoor/outdoor and static/kinematic mode determinations. Extracting other contexts such as the type of the motion could also be investigated using WiFi signals. Different other WiFi features such as receiver parameters could be explored as well to identify different contexts.

- In the context-aware WiFi-based KF, the bank of Kalman filters could be modified to include a wider range of motions along the trajectory, depending on the application.

- In the field of integration of WiFi with GPS to increase acquisition speed, the proposed WiFi-based A-GPS scheme was developed and tested for 802.11g OFDM signaling. Development of the system using other 802.11 protocols such as 802.11b and 802.11n could be investigated. Especially for the 802.11n protocol, which enables MIMO communication between users, time and space diversity techniques can also be explored to further enhance the results. Also the method could be modified to work in places where different 802.11 protocols are used for communication between the users.

- In the proposed WiFi-based A-GPS method, an interesting research would be investigating and evaluating the effects of APs geometry and the number of APs on performance.

- The developed WiFi-based A-GPS system was tested for static users. The problem of moving users should be addressed to broaden the application of the developed method. An example can be deploying the system on mobile devices carried by walking individuals.

- The GM based method can be exploited as a channel estimation technique to estimate channel impulse response. By iterating the algorithm for different number of paths, fitting errors can be used to determine the most probable channel delay spreads. Moreover, the developed timing method combined with any post-FFT timing algorithm could achieve higher resolution timing estimations and further improve the performance of the system. Also, any modifications in the algorithm that reduce the complexity will result in improvements in terms of computational load.

REFERENCES

Ai B., Z. Yang, C. Pan, J. Ge, Y. Wang, and Z. Lu (2006), "On the Synchronization Techniques for Wireless OFDM Systems", IEEE Transactions On Broadcasting, Vol. 52, No. 2

Amidi S. (2010), "Method and Apparatus for Location Detection Using GPS and WiFi/WIMAX", US Patent 2010/0026569

Au, A., Chen Feng, S. Valaee, S. Reyes, S. Sorour, S. Markowitz, D. Gold, K. Gordon, and M. Eizenman (2012): "Indoor tracking and navigation using received signal strength and compressive sensing on a mobile device." 1-1.

Bagdonas K., K. Borre (2008), "Ubiquitous WiFi/GNSS Positioning System – TOA Based Distance Estimation", ION GNSS 21st International Technical Meeting of the Satellite Division, pp. 16-19

Bahl, P., and Padmanbhan, V. (2000),"RADAR: An In- Building RF-based User Location and Tracking System". In Proc. IEEE INFOCOM, Tel-Aviv, Israel, Mar

Bhattacharya T. (2006), "Estimating the Location of a Wireless Terminal Based on Assisted-GPS and Pattern Matching", US Patent 2006/0240841

Brown R.G., P. Y. Hwang (1997), "Introduction to Random Signals and Applied Kalman Filtering", John Wiley & Sons, 3rd Edition

Cacopardi S., M. Femminella, G. Reali, A. Sedini (2010),"WiFi Assisted GPS for Extended Location Services", In PSATS, pp. 191-202

Cao X., X. Guo (2007),"Partially Observable Markov Decision Processes with Reward Information: Basic Ideas and Models", IEEE Transactions on Automatic Control, Vol. 52, No.4, pp. 677-680

Cardoso J. F. (1998), “Blind Signal Separation: Statistical Principles”, Proc. IEEE, Vol.86, No.10, pp. 2009-2025

Carlson H., H. Koorapaty (2006), “Systems and Methods for Providing GPS Time and Assistance in a Communication Network”, US Patent 7009948 B1

Carver, C. (2005), “Myths and Realities of Anywhere GPS”, GPS-World, No. 16.9, pp. 30-41.

Cavalieri S. (2007), “WLAN-based outdoor localization using pattern matching algorithm,” International Journal of Wireless Information Networks, vol. 14, no. 4, pp. 265-279

Cheung K. W., W. K. Ma and H. C. So (2004), “Accurate approximation algorithm for TOA-based maximum likelihood mobile location using semidefinite programming,” in Proc. IEEE Int. Conf. Acoust., Speech, Signal Process. (ICASSP), vol. 2, pp. 145–148

Cho Y., J. Kim, W. Yang, C.G. Kang (2010),” MIMO-OFDM Wireless Communications”, Wiley-IEEE Press

Ciurana M., F., Barcelo-Arroyo, and F. Izquierdo (2007), "A ranging system with IEEE 802.11 data frames," in IEEE Radio and Wireless Symposium, p. 133-138

Cook B., G. Buckberry, I. Scowcroft, J. Mitchell, T. Allen (2005), “Indoor Location Using Trilateration Characteristics”, London Communications Symposium, London, England

Courcoubetis C., M. Yannakakis (1998),”Markov Decision Processes and Regular Events”, IEEE Transactions on Automatic Control, Vol. 43, No.10, pp. 1399-1418

CSRIC III Report (2012), http://www.fcc.gov/encyclopedia/communications-security-reliability-and-interoperability-council-iii, last accessed on Jul 4, 2013

Cypriani, M., Lassabe, F., Canalda, P., & Spies, F. (2010), “Wi-Fi-based indoor positioning: Basic techniques, hybrid algorithms and open software platform”, IEEE International Conference on Indoor Positioning and Indoor Navigation (IPIN) 2010, pp. 1-10

Deric W., A.E. Xhafa, R. Vedantham and K. Ramasubramanian (2011), “Fine-Time Assistance for GNSS using WiFi”, International Conference on Indoor Positioning and Indoor Navigation (IPIN), 21-23 September, Guimarães, Portugal

Dick C., F. Harris (2003), “FPGA Implementation of an OFDM PHY”, 37th Asilomar Conference on Signals, Systems and Computers, vol. 1, pp. 905-909.

di Flora C. and M. Hermersdorf (2008) “A practical implementation of indoor location-based services using simple WiFi positioning”, Journal of Location Based Services

Duffett-Smith P. J. and P. Hansen (2005), “Precise time transfer in a mobile radio terminal,” Proceedings of ION ITM 2005, Jan 24-26, San Diego, California, pp. 1101-1106

El-Sheimy, N., K. P. Schwarz, M. Wei, and M. Lavigne (1995), VISAT: A Mobile City Survey System of High Accuracy, Proceedings of ION GNSS 1995, pp. 1307–1315.

Fakatselis J., IEEE 802.11-97/157-r1, November 1997.http://grouper.ieee.org/groups/802/11/Documents/DocumentArchives/1997_docs/97novp.zip

FCC Report, The Communications Security, Reliability and Interoperability Council III Working Group 3 (2013), “Indoor Location Test Bed Report”, http://transition.fcc.gov/bureaus/pshs/advisory/csric3/CSRIC_III_WG3_Report_March_%202013_ILTestBedReport.pdf

Gelb A. (1974), “Applied Optimal Estimation”, MIT Press

Geng Y.,J. Wang (2008),”Adaptive Estimation of Multiple Fading Factors in Kalman filter for Navigation Application”, Springer GPS Solution , vol.12 , pp.273-279

Godha, S. (2006), Performance Evaluation of Low Cost MEMS-Based IMU Integrated With GPS for Land Vehicle Navigation Application, MSc Thesis, Department of Geomatics Engineering, University of Calgary, Canada, UCGE Report No. 20239

Golden S.A., S.S.Bateman (2007), “Sensor Measurements for WiFi Location with Emphasis on Time-of-Arrival Ranging”, IEEE Transactions on Mobile Computing, Vol.6, N. 10

Goldsmith A. (2005), “Wireless Communications”, First Edition, Cambridge University Press

Goran M., R. E. Richton (2001), “Geolocation and Assisted GPS”, IEEE Computer Society Press, Vol. 34, Issue 2, pp 123-125

Grejner-Brzezinska, D. A., R. Da, and C. Toth (1998), GPS error modeling and OTF ambiguity resolution for high-accuracy GPS/INS integrated system. Journal of Geodesy, Vol. 72, pp. 626–638

Grewal M. S., A. P. Andrews (2001), “Kalman Filtering: Theory and Practice Using MATLAB”, John Wiley & Sons, Second Edition

Guffey J., A. M. Wyglinski, G. J. Minden (2007), “Agile RadioImplementation of OFDM Physical Layer for DynamicSpectrum Access Research”, GLOBECOM, pp.4051-4055

Hahm M. D., Z. Mitrovski, E. Titlebaum (1997), “Deconvolution in the presence of Doppler with application to specular multipath parameter estimation”, IEEE Transactions on Signal Processing, Vol. 45, pp. 2203-2219

Hatami A. & K. Pahlavan (2006), “Comparative Statistical Analysis of Indoor Positioning Using Empirical Data and Indoor Radio Channel Models”, IEEE CCNC 2006

Hayward R.C. (1997), “Inertially Aided GPS Based Attitude Heading Reference System (AHRS) for General Aviation Aircraft”, Proceeding of ION GNSS 97, Kansas City, MO, pp. 289-298

Hertz D. (1986), “Time delay estimation by combining efficient algorithms and generalized cross correlation methods”, IEEE Trans. Acoust. Speech Signal Process, Vol. 34, No. 1, pp. 1-7

Ho K. C. and Y. T. Chan (1993), “Solution and performance analysis of geolocation by TDOA,” IEEE Trans. Aerosp.Electron. Syst., vol. 29, no.4, pp. 1311–1322

Huang Y.-L., C.-R. Sheu, and C.-C. Huang (1999), “Joint synchronization in Eureka 147 DAB system based on abrupt phase change detection,” IEEE Journal on Selected Areas in Communications, vol. 17, no. 10, pp. 1770–1780

Iannello J. P. (1986), “Large and small error performance limits for multipath time delay estimation”, IEEE Trans. Acoust. Speech Signal Process, Vol. ASSP-34, pp. 245-251

Inside GNSS, Gibsons Media and Research LLC (2013), “Indoor Location Market Studies, Product Releases Seek to Extend GNSS Mobile Applications”, June 27

Institute of Electrical and Electronics Engineers, 802.11a, Wireless LAN MediumAccess Control (MAC) and Physical Layer (PHY) Specifications: High-SpeedPhysical Layer Extension in the 5 GHz Band, 16 September 1999

Institute of Electrical and Electronics Engineers, 802.11b, Wireless LAN MediumAccess Control (MAC) and Physical Layer (PHY) Specifications: Higher-SpeedPhysical Layer Extension in the 2.4 GHz Band, 16 September 1999

Institute of Electrical and Electronics Engineers, 802.11g, Wireless LAN MediumAccess Control (MAC) and Physical Layer (PHY) Specifications Amendment 4:Further Higher Data Rate Extension in the 2.4 GHz Band, 12 June 2003.ISO/IEC standard 7498-1:1994

Institute of Electrical and Electronics Engineers, P802.11 Wireless LANs, “TGn Channel Models”, IEEE 802.11-03/940r4, 2004-05-10

Jakobsson A., A. L. Swindlehurst, P. Stocia (1998), “subspace-based estimation of time delays and Doppler shifts”, IEEE Transactions on Signal Processing, Vol. 46, pp. 2472-2483

Jami I., M. Ali, R. F. Ormondroyd (1999), “Comparison of Methods of Locating and Tracking Cellular Mobiles”, IEE Colloquium on Novel Methods of Location and Tracking of Cellular Mobiles and Their System Applications (Ref. No. 1999/046), pp. 1/1-1/6

Kaemarungsi K. and P. Krishnamurthy (2004), “Modeling of indoor positioning systems based on location fingerprinting,” IEEE Infocom, pp. 76-79.

Kalman, R. E. (1960), “A New Approach to Linear Filtering and Prediction Problems”
ASME Journal of Basic Engineering, vol. 82

Kay S. M. (1993), “Fundamentals of Statistical Signal Processing”, Volume 1: Detection Theory, First Edition, Prentice Hall

Knapp C. H. & C. G. Carter (1976), “The generalized correlation method for estimation of time delay”, IEEE Trans. Acoust. Speech Signal Process, Vol. ASSP-21, pp. 320-327

Kotanen A., M. Hännikäinen, H. Leppäkoski, T. Hämäläinen (2003), “Positioning with IEEE 802.11b wireless LAN”, IEEE Personal, Indoor and Mobile Radio Communications, vol.3, pages 2218- 2222, 7-10

Lassabe F., P. Canalda, P. Chatonnay, and F. Spies (2009) "Indoor Wi-Fi positioning: techniques and systems." annals of telecommunications-annales des télécommunications 64, No. 9-10, pp. 651-664.

Lee D. L., Q. Chen (2007), ‘’A model-based WiFi localization method’’, ACM International Conference Proceeding Series; Vol. 304, pp.1-7

Lee J. K., D. Grenjer-Brzezinska, C. Toth (2012), “Network-based Collaborative Navigation in GPS-Denied Environments”, The Journal of Navigation, Vol. 65, pp. 445–457

Li J. and A. Barron (2000), “Mixture Density Estimation”, in Solla, Leen, and Mueller (eds.) Advances in Neural Information Processing Systems 12, The MIT Press

Li X. and K. Pahlavan (2004), “Super resolution TOA estimation with diversity for indoor geolocation” IEEE Transactions on Wireless Communications, Vol.3 , No. 1, pp. 224-234

Lim C., Y. Wan, B. Neg , and S. See (2007),“A real-time indoor WiFi localization system using smart antennas,” IEEE Trans. Consum. Electron. 53(2), pp. 618–622

Martin R. K., C. Yan, H. Fan, C. Rondeau (2011), “Algorithms and bounds for distributed TDOA-based positioning using OFDM signals”, IEEE transactions on signal processing, vol. 59, No. 3, pp. 1255-1268

Maybeck, P. S. (1994), Stochastic Models, Estimation and Control, vol. 1, Navtech GPS

Mautz R. (2012), “Indoor Positioning Technologies”, PhD Thesis, ETH Zurich, February 2012

Mehra R. K. (1970), “On the identification of variances and adaptive Kalman filtering”, IEEE Transactions on Automatic Control, Vol.AC-15, No. 2, pp. 175-184

Misra P. and P. Enge (2001), “Global Positioning System: Signals, Measurements, and Performance” Ganga-Jamuna Press, Lincoln, Mass

Mohammed A. H., Schwarz K. P. (1999), “Adaptive Kalman filtering for INS/GPS”, Journal of Geodesy, Vol.73, pp. 193-203

Mok E. & G. Retscher (2007), “Location determination using WiFi fingerprinting versus WiFi trilateration”, Journal of Location Based Services Vol. 1, No. 2, 145–159

Monnerat M. (2007), “Method for the Accelerated Acquisition of Satellite Signals”, US Patent 20070194985A1

Moon T.K. (1996), “The Expectation-Maximization Algorithm,” IEEE Signal Processing Magazine, pp. 47-59

Moreno V. M., A. Pigazo (2009), “Kalman Filter: Recent Advances and Applications”, Vienna, Austria: I-Tech

Murphy C. K.(2000), “Combining Belief Functions When Evidence Conflicts” , Decision Support Systems, vol. 12, no.1 , pp. 1-9

Muthukrishnan, K., Koprinkov, G. T., Meratnia, N., & Lijding, M. E. M. (2006), “Using time-of-flight for WLAN localization: feasibility study”, Technical Report

Nasir A., S. Durrani, R. A. Kennedy (2010), “Performance of Coarse and Fine Timing Synchronization in OFDM Receivers”,2nd International Conference on Future Computer and Communication

Nelder, J. A., & Mead, R. (1965), “A simplex method for function minimization”, The computer journal, 7(4), 308-313.

Oguz-Ekim P., J. Gomes, P. Oliveira, M. R. Gholami, E. G. Strom (2013), “TW-TOA Based Cooperative Sensor Network Localization with Unknown Turn-Around Time”, ICASSP 2013, Vancouver, Canada

O’Hara B. and A. Petrick, IEEE 802.11 Handbook: A Designer’s Companion, Standards Information Network IEEE Press, New York, 1999

Orlov Y., J. Bentsman (2000), “Adaptive distributed parameter systems identification with enforceable identifiability conditions and reduced-order spatial differentiation”, IEEE Transactions on Automatic Control, Vol. 45, No.2, pp. 203-215

Pahlavan K. , P. Krishnamurthy, and J. Beneat (1998), "Wideband radio propagation modeling for indoor geolocation application," IEEE Communications Magazine, vol. 36, no. 4, pp. 60-65

Pahlavan K., F. Akgul, F. Dovis, Y. Ye, T. Morgan, F. Alizadeh-Shabdiz ,M. Heidari and C. Steger (2010) “Taking Positioning Indoors WiFi Localization and GNSS” Inside GNSS, May , pp. 40-47

Palin A., J. Pikkarainen, and J. Rinne, “Improved symbol synchronization method in OFDM system in channels with large delay spreads,” in Proceedings of the 1st International Symposium on Communication Systems and Digital Signal Processing (CSDSP ’98), pp. 309–312, Sheffield, UK, April 1998

Palin A. and J. Rinne (1998), “Enhanced symbol synchronization method for OFDM system in SFN channels,” in Proceedings of IEEE Global Telecommunications Conference (GLOBECOM ’98), vol. 5, pp. 2788–2793, Sydney, Australia

Pan X., Y. Zhou, Sh. Ma and T. Sang Ng (2007),“An Improved Derivative Method for Symbol Synchronization in OFDM Systems”, In the Proceedings of IEEE WCNC

Papandrea M., S. Vanini, S. Giordano (2009) “A Lightweight Localization Architecture and Application for Opportunistic Networks”. WoWMoM 2009

Papoulis, A. and A. Pillai (2002), Probability, Random Variables and Stochastic Processes, 4th ed. McGraw-Hill, New York, NY

Petovello, M. (2003), “Real-time Integration of a Tactical-Grade IMU and GPS for High Accuracy Positioning and Navigation”, PhD Thesis, Department of Geomatics Engineering, University of Calgary, Canada, UCGE Report No. 20173

Petovello M.G., C. O'Driscoll, G. Lachapelle, D. Borio, H. Murtaza (2008), “Architecture and Benefits of an Advanced GNSS Software Receiver, International Symposium on GPS/GNSS”, Tokyo, Japan, 11 pages

Petovello M. (2011), Estimation for Navigation, Lecture Notes for ENGO 620

Press W.H., Teukolsky S.A., Vetterling W.T. & Flannery B.P. (1992), “Numerical Recipes in Fortran”, Cambridge University Press, Cambridge

Progri F. (2010), "Wireless-enabled GPS indoor geolocation system," in Proc. IEEE/ION-PLANS 2010, Palm Spring, CA, pp. 526 – 538

Quinten M. (2012), “Practical Guide to Optical Metrology for Thin Films”, First Edition, Wiley-VCH Verlag GmbH & Co. KGaA

Richards J. A., X. Jia (2007), ”A Dempster-Shafer Approach to Context Classification” , IEEE Transactions on Geoscience and Remote Sensing, vol. 45, no.5 , pp. 1422-1431

Saarnisaari H. (1996), “ML time delay estimation in a multipath channel”, IEEE ISSTA, pp.1007-1011

Saarnisaari H. (1997), “TLS-ESPRIT in a time delay estimation”, Proc. of IEEE Vehiculat Technology Conference, pp. 1619-1623

Salychev O. S. (1998), Inertial Systems in Navigation and Geophysics, Bauman MSTU Press, Moscow

Sayed A. H., A. Tarighat, and N. Khajehnouri (2005), “Network-based wireless location: Challenges faced in developing techniques for accurate wireless location information,” IEEE Signal Process. Mag., vol. 22, no. 4, pp. 24–40

Schmidl T. M. and D. C. Cox (1997), “Robust Frequency and Timing Synchronization for OFDM,” IEEE Trans. Comm., vol. 45, pp.1613 -1621

Shin, E. (2005), “Estimation Techniques for Low-Cost Inertial Navigation”, PhD Thesis, Department of Geomatics Engineering, University of Calgary, Canada, UCGE Report No. 20219

Stocia P. & Moses R. (2005), “Spectral Analysis of Signals”, Upper Saddle River, NJ: Prentice Hall

Sundaramurthy M., S. N. Chayapathy, A.Kumar, D. Akopian (2011), “WiFi Assistance to SUPL-based Assisted-GPS Simulators for Indoor Positioning”, The 8th Annual IEEE Consumer Communications and Networking Conference - Special Session on Location Aware Technologies and Applications on Smartphones

The Economist Technology Quarterly (2012), “Indoor Positioning: Finding the Way Inside”, Q4 2012

Tseng C., C. Chang, D. Jwo (2011),”Fuzzy Adaptive Interacting Multiple Model Nonlinear Filter for Integrated Navigation Sensor Fusion”, sensors2011, vol. 11, pp. 2090-2111

Van de Beek J. J. ,M. Sandell, and P. O. Borjesson (1997), “ML estimation of time and frequency offset in OFDM systems,” IEEE Trans. Signal Process.,vol. 45, no. 7, pp. 1800–1805

Vanderveen A. J., M. C. Vanderveen, A. J. Paulraj (1997), “joint angle and delay estimation using shift invariant properties”, IEEE Signal Processing Letters, Vol. 4, No. 5, pp. 142-145

Vanderveen, M. C., Van der Veen, A. J., & Paulraj, A. (1998), “Estimation of multipath parameters in wireless communications”, Signal Processing, IEEE Transactions on, 46(3), 682-690

Van Dierendonck, A.J., J.B. McGraw and R.G. Brown (1984), “Relationship Between Allan Variances and Kalman Filter Parameters”, Proceedings of Applications and Planning Meeting, NASA Goddard Space Flight Center, Precise Time and Time Interval, 273-293.

Van Diggelen F. (2009), “A-GPS, Assisted GPS, GNSS, and SBAS”, First edition, Artech House

Wang K., M. Faulkner, J. Singh, I. Tolochko (2003), "Timing Synchronization for 802.1 la WLAN under Multipath Channels", ATNAC 2003, Melbourne, Australia

Wang Y., J. T. Chen, W. H. Fang (2001), “TST-MUSIC for joint DOA delay estimation”, IEEE Transactions on Signal Processing, Vol. 49,No.4, pp. 721-729

Wang Y., G. Jian-hua, B. Ai, L. Zong-qiang, and N. Yuan-fei (2005), “A Novel Scheme for Symbol Timing in OFDM WLAN Systems”, ECTI Transactions On Electrical Engineering, Electronics and Communications, Vol.3, No.2, pp. 86-91,August 2005

Weyn M., F. Schrooyen (2008), “A WiFi Assisted GPS Positioning Concept”, ECUMICT, Gent, Belgium

Wibowo, S. B., Klepal, M., & Pesch, D. (2009), “Time of Flight Ranging using Off-the-self IEEE802. 11 WiFi Tags”, POCA, Antwerp, Belgium

Williams C., M. A. Beach and S. McLaughlin (2005), “Robust OFDM timing synchronisation”, Electronics Letters, vol. 41, pp. 751-752

Xiang, Z., S. Song, J. Chen, H. Wang, J. Juang, and X. Gao (2004), ‘’A Wireless LAN-based Indoor Positioning Technology’’, IBM Journal of Research and Development, Vol. 48, No. 5/6

Zandbergen P. A. (2009), “accuracy of iPhone locations: A comparison of assisted GPS, WiFi and cellular positioning”, transactions in GIS, Vol. 13(s1), pp. 5-26

Zekavat S. A. & Buehrer R. M. (2012), “Handbook of Position Location Theory, Practice and Advances”, John Wiley and Sons, First Edition